

Ferroptosis-induced Secretomes promote Macrophage priming

Inaugural-Dissertation
zur
Erlangung des Doktorgrades
Dr. rer. nat.
der Mathematisch-Naturwissenschaftlichen Fakultät
der Universität zu Köln



vorgelegt von
Fatma Işıl Yapıcı
aus İstanbul, die Türkei

Köln, 2024

First reviewer and examiner:

Prof. Dr. Silvia von Karstedt
Department of Translational Genomics and
CECAD Research Center
University of Cologne

Second reviewer and examiner:

Prof. Dr. Guenter Schwarz
Institute of Biochemistry
University of Cologne

Chair of the thesis defence committee:

Prof. Dr. Kay Hofmann
Institute of Genetics
University of Cologne

Table of Contents

List of Figures	4
List of Tables	6
Abbreviations	7
Abstract	17
1 Introduction	18
1.1. Regulated cell death	18
1.1.1. Intrinsic Apoptosis.....	18
1.1.2. Extrinsic Apoptosis.....	20
1.1.3. Necroptosis.....	22
1.1.4. Pyroptosis.....	23
1.1.5. Ferroptosis (adapted from Yapici and Bebbber 2024).....	25
1.1.5.1. GPX4-dependent regulation of ferroptosis.....	27
1.1.5.2. Regulation of ferroptosis via the synthesis of endogenous radical trapping agents (RTAs).....	28
1.1.5.3. Metabolic checkpoints of ferroptosis regulation.....	29
1.1.5.3.1. Iron metabolism.....	29
1.1.5.3.2. Lipid metabolism.....	31
1.1.5.3.3. Non-lipid metabolism.....	32
1.1.5.4. Ferroptosis-inducing agents (FINs) and sensitizers.....	34
1.1.5.5. Ferroptosis relevance <i>in vivo</i>	35
1.2. Inflammation and immune response	36
1.2.1. Necroinflammation.....	42
1.2.2. Ferroptosis and DAMP release.....	46
1.2.3. Ferroptosis associated immune response.....	47
1.3. Aims of the study	50
2 Results	52
2.1. Characterisation of proteomes released from ferroptotic cells	52
2.1.1. Experimental system for the generation of ferroptotic secretome analysis.....	52
2.1.2. Quantitative secretome analysis of precipitated supernatants by SILAC.....	56
2.1.3. Ferroptosis induces the production and release of inflammatory oxylipins.....	60
2.1.4. Ferroptotic cells release small metabolites.....	65
2.2. Ferroptotic supernatants induce macrophage reprogramming	70
2.2.1. Ferroptotic supernatants induce transcriptional reprogramming of macrophages.....	70
2.2.2. Ferroptotic supernatants prime macrophages.....	73
2.2.3. Ferroptotic secretome-exposed macrophages also show signs of trained immunity.....	77
2.2.4. Ferroptosis <i>in vivo</i>	80
3 Discussion	84
3.1. Investigating the protein fraction of ferroptotic secretome	84
3.2. Ferroptotic oxylipins and metabolites can influence macrophage phenotype	86
3.3. Priming of macrophages is linked to the non-protein fraction of ferroptotic secretomes	89
3.4. Ferroptosis and inflammation in tissue pathology	92

3.5. Concluding remarks and future perspectives	93
4 Materials and Methods	95
4.1. Animals	95
4.1.1. Tissue harvest	95
4.1.2. Inhalations	95
4.2. Chemicals and reagents	95
4.3. Nucleic acid techniques	97
4.3.1. RNA isolation and cDNA synthesis.....	97
4.3.2. Determination of DNA concentration	98
4.3.3. Quantitative real-time PCR analysis (qRT-PCR)	98
4.4. Cell culture techniques	101
4.4.1. Cell lines and culture conditions.....	102
4.5. Protein analysis techniques	102
4.5.1. Cell lysis and protein isolation from cells	102
4.5.2. SDS – Polyacrylamide gel electrophoresis (PAGE)	103
4.5.3. Western blot analysis	103
4.5.4. Enzyme-linked immunoabsorbent assay (ELISA).....	104
4.6. Fluorescence activated cell sorting (FACS)	104
4.6.1. BODIPY C11 staining	105
4.6.2. Propidium iodide (PI) staining	105
4.6.3. pBMDM staining.....	105
4.6.4. Immune cell analysis from murine lungs.....	106
4.7. Cell death assays	107
4.7.1. Live cell imaging (IncuCyte)	107
4.7.2. LDH release assay	107
4.8. Quantification of proteins in ferroptotic supernatants.....	107
4.9. Quantification of oxylipins in ferroptotic supernatants.....	109
4.10. Quantification of intracellular and supernatant metabolites.....	110
4.11. RNA sequencing.....	112
5 References	114
6 Publications	140
7 Acknowledgements.....	141
8 Erklärung zur Dissertation	142

List of Figures

Figure 1. Different types of regulated cell death (RCD)

Figure 2. Schematic overview of extrinsic and intrinsic apoptosis

Figure 3. Schematic overview of necroptosis

Figure 4. Schematic overview of pyroptosis

Figure 5. Schematic overview of ferroptosis

Figure 6. Iron metabolism in ferroptosis

Figure 7. Metabolic regulators of ferroptosis

Figure 8. Mechanisms behind innate and adaptive immune system

Figure 9. Mechanisms of innate immunity

Figure 10. Mechanisms of adaptive immunity

Figure 11. Mechanisms of trained immunity

Figure 12. Overview of eicosanoid biosynthesis

Figure 13. Effect of DAMPs and SAMPs/iDAMPs released from dying cells on macrophage differentiation.

Figure 14. Immunomodulatory roles of ferroptosis

Figure 15. Inducible *Gpx4* deletion to ferroptosis.

Figure 16. Constitutive *Gpx4* deletion leads to ferroptosis.

Figure 17. Ferroptotic cells release a passive proteomics secretome.

Figure 18. Ferroptotic proteomics secretome includes MIF but lacks *bona-fide* chemo- and cytokines.

Figure 19. *Ptgs2* is induced in a lipidROS-dependent manner.

Figure 20. LPS-induced *Ptgs2* induction is independent of ferroptosis.

Figure 21. Ferroptotic cells release different types of prostaglandins.

Figure 22. Ferroptosis induces the production and release of inflammatory oxylipins.

Figure 23. Ferroptotic cells release nucleotides.

Figure 24. Ferroptotic cells shows different metabolic profiles at different time points.

Figure 25. Early ferroptotic cells activate nucleotide synthesis and release metabolites of active anabolism.

Figure 26. Exposure to supernatants from ferroptotic cells triggers a transcriptional reprogramming in macrophages.

Figure 27. Inducible ZBP1 overexpression leads to necroptotic cell death.

Figure 28. Ferroptotic supernatants prime macrophages.

Figure 29. Non-protein fraction of ferroptotic supernatants is responsible for priming.

Figure 30. Necroptotic supernatants fail to prime macrophages.

Figure 31. Ferroptotic-exposed macrophages also show signs of trained immunity.

Figure 32. Ferroptosis induction *in vivo* via *Gpx4* deletion induces T cell recruitment.

Figure 33. *Gpx4* deletion in the lungs shows signs of inflammation.

List of Tables

Table 1-1. List of ferroptosis-inducing agents (FINs).

Table 1-2. List of DAMPs, origins and receptors

Table 4-1. Chemicals, peptides, and recombinant proteins

Table 4-2. Critical commercial assays

Table 4-3. cDNA reaction components

Table 4-4. cDNA synthesis thermocycler protocol

Table 4-5. qPCR reaction components

Table 4-6. qPCR primer sequences

Table 4-7. Cell culture reagents

Table 4-8. Cell lines

Table 4-9. SDS-PAGE composition

Table 4-10. Western blot antibodies

Table 4-11. ELISAs

Table 4-12. FACS antibodies

Abbreviations

α-KG	Alpha-ketoglutarate (also referred as 2-oxoglutarate)
4-HNE	4-hydroxynonenal
4-OHT	4-hydroxytamoxifen
7-DHC	7-dehydrocholesterol
8-OHdG	8-hydroxy-2'-deoxyguanosine
AA	Arachidonic acid
AdA	Adrenic acid
ACD	Accidental cell death
ACSL3	Acyl-CoA synthetase long chain family member 3
ACSL4	Acyl-CoA synthetase long-chain family member 4
ADCD	Autophagy-dependent cell death
AIM2	Absent in melanoma 2
AKI	Acute kidney injury
ALI	Acute lung injury
AP-1	Activator protein-1
APAF-1	Apoptotic protease activating factor 1
APC	Antigen-presenting cell
APS	Ammonium persulfate
ARE	Antioxidant response element
ATP	Adenosine triphosphate
BAD	Bcl-2-associated death promoter
BAK	Bcl-2 homology antagonist/killer
BAL	Bronchoalveolar lavage
BAX	Bcl-2 associated X protein
BMDC	Bone marrow-derived dendritic cell
BMDM	Bone marrow-derived macrophage
BCL-2	B-cell lymphoma 2
BCL-XL	B-cell lymphoma-extra-large
BCG	Bacillus Calmette-Guérin
BH2	Dihydrobiopterin

BH₄	Tetrahydrobiopterin
BID	BH3 interacting domain death agonist
BIM	Bcl-2-like protein 11
BIRC2/c-IAP1	baculoviral IAP repeat containing 2
BIRC3/c-IAP2	baculoviral IAP repeat containing 3
BOK	Bcl-2 related ovarian killer
BSO	Buthionine sulfoximine
CAD	Caspase activated DNase
CASP	Caspase
CASP1	Caspase 1
CASP4	Caspase 4
CASP5	Caspase 5
CASP11	Caspase 11
CARD	Caspase recruitment domain
CBS	Cystathionine beta-synthase
CCL2	Chemokine C-C motif ligand 2
CCL7	Chemokine C-C motif ligand 7
CD4+ T cells	T helper cells
CD8+ T cells	Cytotoxic T cells
CDO1	Cysteine dioxygenase 1
CGAS	Cyclic guanosine monophosphate–adenosine monophosphate synthase
cFLIP	FLICE-like inhibitory protein
cFLIP_L	cFLIP long
cFLIP_S	cFLIP short
CMA	Chaperon-mediated autophagy
CoA	Coenzyme A
COPD	Chronic obstructive pulmonary disease
CoQ10	Coenzyme Q10
CoQH₂	Ubiquinol
COX	Cyclooxygenase
cPLA₂	Cytoplasmic phospholipase A ₂

CPR	C-type lectin receptors
CSF2	Colony stimulating factor 2
CXCL1	Chemokine C-X-C motif ligand 1
CXCL2	Chemokine C-X-C motif ligand 2
CYLD	Cylindromatosis
CYP	Cytochrome P450
D-PUFAs	Deuterated polyunsaturated fatty acids
DAI	DNA-dependent activator of IFN regulatory factors
DAMP	Damage-associated molecular pattern
DFO	Deferoxamine
DGLA	Dihomo- γ -linolenic acid
DHCR7	7-Dehydrocholesterol reductase
DHFR	Dihydrofolate Reductase
DHODH	Dihydroorotate dehydrogenase
DIABLO	direct IAP binding protein with low pI
DISC	Death-inducing signalling complex
DLBCL	Diffuse large B-cell lymphoma
DMT1	Divalent metal transporter 1
DNA	Deoxyribonucleic acid
DR	Death receptor
dsRNA	Double-stranded RNA
DTT	Dithiothreitol
ECM	Extracellular matrix
ERASTIN	Eradicator of RAS and ST-expressing cells
ELISA	Enzyme-linked immunoabsorbent assay
EPA	Eicosapentaenoic acid
FA	Formic acid
FACS	Fluorescent activated cell sorting
FADD	Fas-associated death domain protein
FATP2	Fatty acid transport protein 2
FCS	Fetal calf serum

Fe⁺²	Ferrous iron
Fe⁺³	Ferric iron
Fer-1	Ferrostatin-1
FIN	Ferroptosis inducing agent
fMLF	fMet-Leu-Phe
FSP1	Ferroptosis suppressor protein 1
FPN1/SLC40A1	Ferroportin
FPR	N-formyl peptide receptor
FTH1	Ferritin heavy chain
FTL	Ferritin light chain
GCH1	GTP cyclohydrolase 1
GCHFR	GTP Cyclohydrolase 1 Feedback Regulator
GCL	Glutamate-cysteine ligase
GLS2	Glutamine synthase 2
GPX4	Glutathione peroxidase 4
GSDMD	Gasdermin D
GSDMD-C	C-Terminal Gasdermin D
GSDMD-N	N-terminal Gasdermin D
GSDME	Gasdermin E
GSDME-C	C-Terminal Gasdermin E
GSDME-N	N-terminal Gasdermin E
GSH	Reduced glutathione
GSS	Glutathione synthetase
GSSG	Oxidized glutathione
H₂O₂	Hydrogen peroxide
HMGB1	High mobility group box 1 protein
HO·	Hydroxyl radical
HO-1	Heme oxygenase-1
HOIL-1	RANBP2-type and C3HC4-type zinc finger containing 1
HOIP	Ring finger protein 31
HRP	Horseradish peroxidase

HPSC	Hematopoietic stem cell
IAP	Inhibitors of apoptosis
iBMDM	Immortalized bone marrow-derived macrophages
ICD	Immunogenic cell death
IκBα	NF- κ B inhibitor alpha
IKKα	Component Of Inhibitor Of Nuclear Factor Kappa B Kinase Complex
IKKβ	Inhibitor Of Nuclear Factor Kappa B Kinase Subunit Beta
IFN	Interferon
IFN-γ	Interferon gamma
IL-1	Interleukin-1
IL-4	Interleukin-4
IL-6	Interleukin-6
IL-8	Interleukin-8
IL-1β	Interleukin 1 beta
IL-10	Interleukin-10
IL-13	Interleukin-13
IL-15	Interleukin-15
IL-17	Interleukin-17
IL-18	Interleukin-18
IL-23	Interleukin-23
IL-33	Interleukin-33
iNOS	Nitric oxide synthase
IRE	Iron regulatory element
IRF3	Interferon regulatory factor 3
IRI	Ischaemia/reperfusion injury
IRP1/2	Iron regulatory proteins 1 and 2
JAK	Janus kinase
KEAP1	Kelch-like ECH-associated protein 1
KO	Knock out
LA	Linoleic acid
LDGD	Lysosome-dependent cell death

LIP	Labile iron pool
Lip-1	Liproxstatin-1
lipidROS	Lipid reactive oxygen species
LOX	Lipoxygenase
LPCAT3	Lysophosphatidylcholine acyltransferase 3
LPS	Lipopolysaccharide
LT	Leukotriene
LX	Lipoxin
LUBAC	Linear ubiquitin chain assembly complex
MAPK	Mitogen-activated protein kinase
MBOAT1/2	Membrane-bound O-acyltransferase domains containing 1 and 2
MCL-1	Myeloid cell leukemia-1
MDA	Malondialdehyde
MEF	Mouse embryonic fibroblast
MIF	Macrophage migration inhibitory factor
MLKL	Mixed lineage kinase domain like pseudokinase
MNA	1-methylnicotinamide
MOMP	Mitochondrial outer membrane permeabilization
MPT	Mitochondrial permeability transition
MRP1	Multidrug resistance protein 1
MyD88	Myeloid differentiation factor-88
MUFA	Monounsaturated fatty acids
MUFA-CoA	Monounsaturated fatty acid-coenzyme A
MUFA-PL	Monounsaturated fatty acid phospholipid
NAC	N-acetyl cysteine
NADH	Nicotinamide adenine dinucleotide
NADPH	Nicotinamide adenine dinucleotide phosphate
NAFLD	Nonalcoholic fatty liver disease
NASH	Nonalcoholic steatohepatitis
NCOA4	Nuclear receptor coactivator 4
Nec-1	Necrostatin-1

NET	Neutrophil extracellular trap
NF-κB	Nuclear factor kappa-light-chain-enhancer of activated B cells
NINJ1	Ninjurin-1
NLR	Nucleotide-binding domain leucine-rich receptor (also referred to NOD-like receptors)
NLRC4	NLR family CARD domain containing 4
NLRP1	NLR family pyrin domain containing 1
NLRP3	NLR family pyrin domain containing 3
NLRP6	NLR family pyrin domain containing 6
NLRP7	NLR family pyrin domain containing 7
NLRP12	NLR family pyrin domain containing 12
NOX	NADPH oxidases
NOXA	Phorbol-12-myristate-13-acetate-induced protein 1
NRF2	Nuclear factor erythroid 2-related factor
NSCLC	Non-small cell lung cancer
OXPHOS	Oxidative phosphorylation
oxPL	Oxidized phospholipid
OTULIN	OTU Deubiquitinase With Linear Linkage Specificity
P53	Cellular tumour antigen p53
PAGE	Polyacrylamide gel electrophoresis
PAMP	Pathogen-associated molecular pattern
PARL	Presenelin-associated rhomboid-like protein
pBMDM	Primary bone marrow-derived macrophage
PDAC	Pancreatic ductal adenocarcinoma
PE	Phosphatidylethanolamine
PFA	Paraformaldehyde
PG	Prostaglandin
PGE2	Prostaglandin E2
PI	Propidium iodide
PMLF	Primary lung fibroblast
PMN-MDSC	Polymorphonuclear myeloid-derived suppressor cell

POR	Cytochrome P450 oxidoreductase
PPP	Pentose phosphate pathway
PPR	Pattern recognition receptor
PROM2	Prominin 2
PS	Phosphatidylserine
PTS	6-Pyruvoyltetrahydropterin Synthase
PUFA	Polyunsaturated fatty acid
PUFA-CoA	Polyunsaturated fatty acid-coenzyme A
PUFA-PE/PC	Polyunsaturated fatty acid-phosphatidylethanolamine/phosphatidylcholine
PUMA	p53 upregulated modulator of apoptosis
PYD	Pyrin domain
PYCARD/ASC	Apoptosis-associated speck-like protein containing a CARD
RAGE	Advanced glycation end product-specific receptor
RCD	Regulated cell death
RHIM	RIP homotypic interaction motif
RIG	Retinoic acid-inducible gene
RILF	Radiation-induced lung fibrosis
RIPK1	Serine/threonine-protein kinase 1
RIPK3	Serine/threonine-protein kinase 3
RLR	RIG-I-like receptors
RNA	Ribonucleic acid
ROS	Reactive oxygen species
RTA	Radical trapping agent
RSL3	Ras-selective lethal 3
SAH	S-adenosylhomocysteine
SAM	S-adenosylmethionine
SAMPs/iDAMPs	Suppressing/inhibiting DAMPs
SAPE-OOH	1-stearoyl-2-15-HpETE-sn-glycero-3-phosphatidylethanolamine
SCID	Severe combined immunodeficient
SCLC	Small cell lung cancer
SDS	Sodium dodecyl sulphate

SHARPIN	SHANK associated RH domain interactor
SILAC	Stable isotope labelling in cell culture
SLC3A1	Solute carrier family 3 member 1
SLC7A11/xCT	Solute carrier family 7 member 11
SMAC	Second mitochondria-derived activator of caspases
SPATA2	Spermatogenesis Associated 2
SPR	Sepiapterin Reductase
STAT	Signal transducer and activator of transcription
STARD7	StAR-related lipid transfer domain protein 7
STEAP3	Six-transmembrane epithelial antigen of prostate 3
STING	Stimulator of interferon genes
T3SS	Type III secretion systems
TAB2/3	Mitogen-Activated Protein Kinase Kinase Kinase 7-Interacting Protein 2/3
TAK1	Mitogen-Activated Protein Kinase Kinase Kinase 7
tBID	Truncated BID
TCA	Tricarboxylic acid
TCR	T-cell receptor
TEMED	Tetramethylethylenediamine
TfR1	Transferrin receptor 1
TLR	Toll-like receptor
TLR2	Toll-like receptor 2
TLR3	Toll-like receptor 3
TLR4	Toll-like receptor 4
TME	Tumour microenvironment
TNF	Tumor necrosis factor
TNFR1	TNF receptor member 1
TNFR2	TNF receptor member 2
TRADD	TNFR1-associated death domain protein
TRAF2	TNF receptor associated factor 2
TRAF5	TNF receptor associated factor 5
TRAIL	TNF-related apoptosis-inducing ligand

TRAILR1	TRAIL receptor 1
TRAILR2	TRAIL receptor 2
T_{reg}	Regulatory T cell
TRIF	TIR-domain-containing adapter-inducing interferon- β
TRP14	Thioredoxin-related protein of 14 kDa
TXNRD1	Thioredoxin reductase 1
VDAC2	Voltage-dependent anion channel 2
WT	Wild type
XIAP	X-linked inhibitor of apoptosis protein
UTP	Uridine triphosphate
ZBP1	Z-DNA-binding protein

Abstract

Cells undergoing regulated cell death communicate with the immune system by releasing various protein and non-protein secretomes. Ferroptosis, a recently identified iron-dependent form of regulated cell death characterized by extensive lipid peroxidation, involves membrane rupture. However, a detailed analysis of ferroptotic secretomes and their biological activity has been lacking. In this study, we used a multi-omics approach to create an atlas of secretomes induced by ferroptosis and discovered a novel role in macrophage priming. Proteins known to function as damage-associated molecular patterns (DAMPs) and innate immune system components, such as MIF, heat shock proteins (HSPs), and chaperones, were released from ferroptotic cells. Non-protein secretomes with inflammatory functions included oxylipins and metabolites from the tricarboxylic acid (TCA) cycle and methionine cycles. Notably, when bone marrow-derived macrophages (BMDMs) were incubated with ferroptotic supernatants, they underwent transcriptional reprogramming indicative of priming. Exposure to ferroptotic supernatants also enhanced cytokine production in response to LPS. These findings provide a comprehensive catalogue of ferroptosis-induced secretomes and reveal their role in macrophage priming, which has significant implications for modulating inflammatory processes.

1. Introduction

1.1. Regulated cell death

Cell death is an essential part of homeostasis and development of organisms. Accidental cell death (ACD) is a spontaneous event that occurs as a result of exposure to external factors like chemicals (e.g. pH changes, carcinogens) or physical changes (e.g. high pressure, temperature) driving the cell into a state of cellular senescence and loss of plasma membrane integrity. In contrast to this, regulated cell death (RCD) involves different signalling cascades with diverse effector molecules¹. Initially cell death was categorised into three major subgroups based on the morphological alterations: type I cell death or apoptosis, type II cell death or autophagy and type III cell death or necrosis. However, a great deal of new signalling pathways that coordinate regulated cell death have further been identified to date¹.

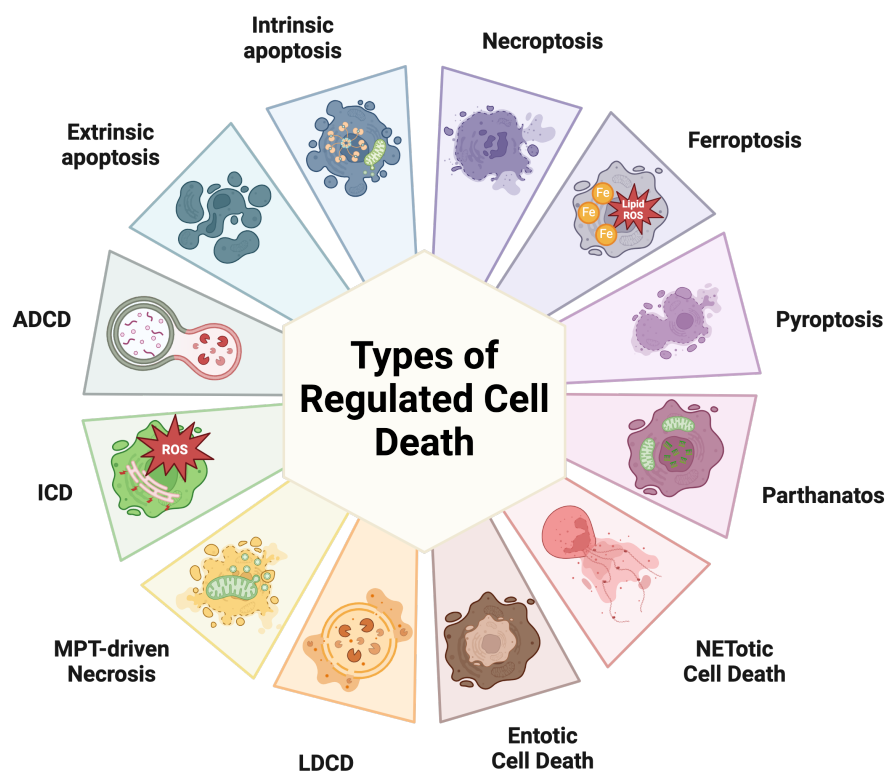


Figure 1. Different types of regulated cell death (RCD)

Schematic illustration of different types of regulated cell death. ADCD: autophagy-dependent cell death, ICD: immunogenic cell death, NET: neutrophil extracellular trap, LDCD: lysosome-dependent cell death, MPT: mitochondrial permeability transition. Adapted from Galluzzi et al. 2018¹. The figure has been created using Biorender.

1.1.1. Intrinsic Apoptosis

Apoptosis is the first type of regulated cell death that has been described in the literature by Kerr et al. in 1972². Various morphological changes occur during apoptosis such as cell

shrinkage, chromatin condensation (pyknosis), nuclear fragmentation (karyorrhexis) and plasma membrane blebbing with the formation of small intact vesicles referred to as apoptotic bodies^{2,3}. Apoptosis is coordinated by a group of cysteine proteases called 'caspases'⁴ where a cysteine in their active site can nucleophilically attack and cleave the target amino acid following an aspartic acid residue⁵. Apoptosis can be induced extrinsically by the binding of death ligands to their respective receptors and intrinsically by intracellular triggers such as DNA damage or stress signals⁶.

Intrinsic apoptosis is the response to negative signals such as the absence of certain growth factors, hormones and cytokines or positive signals such as radiation, toxins and hypoxia⁷. Intrinsic apoptosis is a non-receptor mediated pathway where apoptotic signals are transmitted via the B-cell lymphoma 2 (BCL-2) protein family which consists of pro-apoptotic and anti-apoptotic members⁸. Anti-apoptotic factors include proteins such as BCL-2⁹, B-cell lymphoma-extra-large (BCL-xL)¹⁰ and myeloid cell leukemia-1 (MCL-1)¹¹. Death promoting factors include proteins such as Bcl-2-associated X protein (BAX)¹², Bcl-2 homologous antagonist/killer (BAK)¹³, Bcl-2 related ovarian killer (BOK)^{14,15}, Bcl-2-associated death promoter (BAD)¹⁶, BH3 interacting-domain death agonist (BID)¹⁷ and Bcl-2-like protein 11 (BIM)¹⁸. Cellular tumour antigen p53 (P53) upregulated modulator of apoptosis (PUMA) and phorbol-12-myristate-13-acetate-induced protein 1 (NOXA) are also members of the BCL-2 family that are involved in P53-mediated apoptosis^{19,20}. The BCL-2 protein family shares homology in one to four different Bcl-2 homology domains (BH)⁸. These stimuli can result in mitochondrial outer membrane permeabilization (MOMP) leading to loss of mitochondrial membrane potential and release of cytochrome c, and direct inhibitor of apoptosis (IAP) binding protein with low pI (DIABLO) also known as second mitochondria-derived activator of caspases (SMAC) into the cytoplasm^{21,22}. Heterodimers formed by BAX and BAK further activate the other BH3-only proteins and their oligomerization results in a rapid opening of pores in the mitochondrial outer membrane^{23,24}. Cytochrome c then binds and activates the cytosolic apoptotic protease activating factor 1 (APAF-1) and procaspase-9 to form the apoptosome^{25,26}. Activated caspase-9 further cleaves and activates executioner caspase-3 and caspase-7⁴. However, caspase-3/7/9 may be bound and inhibited by protein X-linked inhibitor of apoptosis (XIAP)²⁷⁻²⁹. The release of Smac inactivates XIAP leading to activation of caspases³⁰. Activation of the executioner caspases drives the apoptotic stimuli ultimately resulting in DNA fragmentation, morphological changes and cell death⁴.

1.1.2. Extrinsic Apoptosis

Extrinsic apoptosis is initiated by interaction between the death receptors (DRs) on the plasma membrane and their ligands³¹. These death receptors belong to the tumour necrosis factor (TNF) superfamily with cysteine-rich extracellular domains and an intracellular cytoplasmic domain known as the 'death domain'^{32,33}. Death ligands and DRs include TNF and TNF receptor 1 (TNFR1)/TNF receptor 2 (TNFR2)³⁴, Fas/Fas ligand (FasL)/CD95 ligand (CD95L) and Fas receptor/CD95³⁵, TNF-related apoptosis-inducing ligand (TRAIL) and TRAIL receptor 1 (TRAILR1)/TRAIL receptor 2 (TRAILR2)^{36,37}. Binding of FasL and TRAIL to their respective receptors induces a conformational change leading to the recruitment of the Fas-associated death domain protein (FADD)^{38,39}. FADD further recruits the initiator procaspase-8 to form death-inducing signalling complex (DISC), resulting in active caspase-8 via cross-activation and autocatalysis^{40,41}.

Caspase-8 activation following DISC and complex I formation upon CD95 and TRAILR activation is tightly regulated by FLICE-like inhibitory protein (cFLIP). This protein is present in two major isoforms referred to as either cFLIP long (cFLIP_L) or cFLIP short (cFLIP_S)^{42,43}. cFLIP_S blocks DISC-dependent procaspase-8 activation by disrupting the death-effector domain mediated procaspase-8 oligomer assembly. cFLIP_L resembles the procaspase-8 protein but lacks proteolytic activity due to the absence of a catalytic cysteine^{44,45}. High levels of cFLIP_L can reduce the activity of procaspase-8, possibly by disrupting procaspase-8 homodimer filaments to suppress apoptosis⁴⁶ whereas active caspase-8 can cleave c-FLIP_L favouring caspase-8 oligomerization and consequent activation of apoptotic signaling^{47,48}. On the other hand, TNFR1 signalling includes the association of the TNFR1-associated DEATH domain protein (TRADD) leading to the formation of complex I⁴⁹ with other adaptor proteins such as receptor-interacting serine/threonine-protein kinase 1 (RIPK1)⁵⁰, TNF receptor associated factor 2 (TRAF2)⁵¹, TRAF5⁵², baculoviral IAP repeat containing 2 (BIRC2/c-IAP1) and baculoviral IAP repeat containing 3 (BIRC3/c-IAP2)⁵³⁻⁵⁵. Eventually the linear ubiquitin chain assembly complex (LUBAC), a supramolecular entity consisting of SHANK associated RH domain interactor (SHARPIN), RANBP2-type and C3HC4-type zinc finger containing 1 (HOIL-1), and ring finger protein 31 (HOIP)⁵⁶ is also recruited.

TNFR1-induced activation differs from the CD95 and TRAILR1/TRAILR2 activation in which TNFR1 can induce apoptosis via caspase-8 activation but simultaneously can inhibit apoptosis via nuclear factor kappa-light-chain-enhancer of activated B cells (NF- κ B)-induced expression of cFLIP⁵⁷. Upon ligand binding to TNFR1, RIPK1 is recruited to complex I and ubiquitinated by c-IAP1, c-IAP2, and LUBAC^{58,59}. Polyubiquitination of RIPK1 can unfold a scaffolding function leading to mitogen-activated protein kinase (MAPK) signalling or I κ B kinase (IKK)-dependent NF- κ B activation leading to pro-inflammatory cytokines and pro-survival genes, including cFLIP^{60,61}. Thus, RIPK1 ubiquitylation controls whether cells undergo apoptosis or survive.

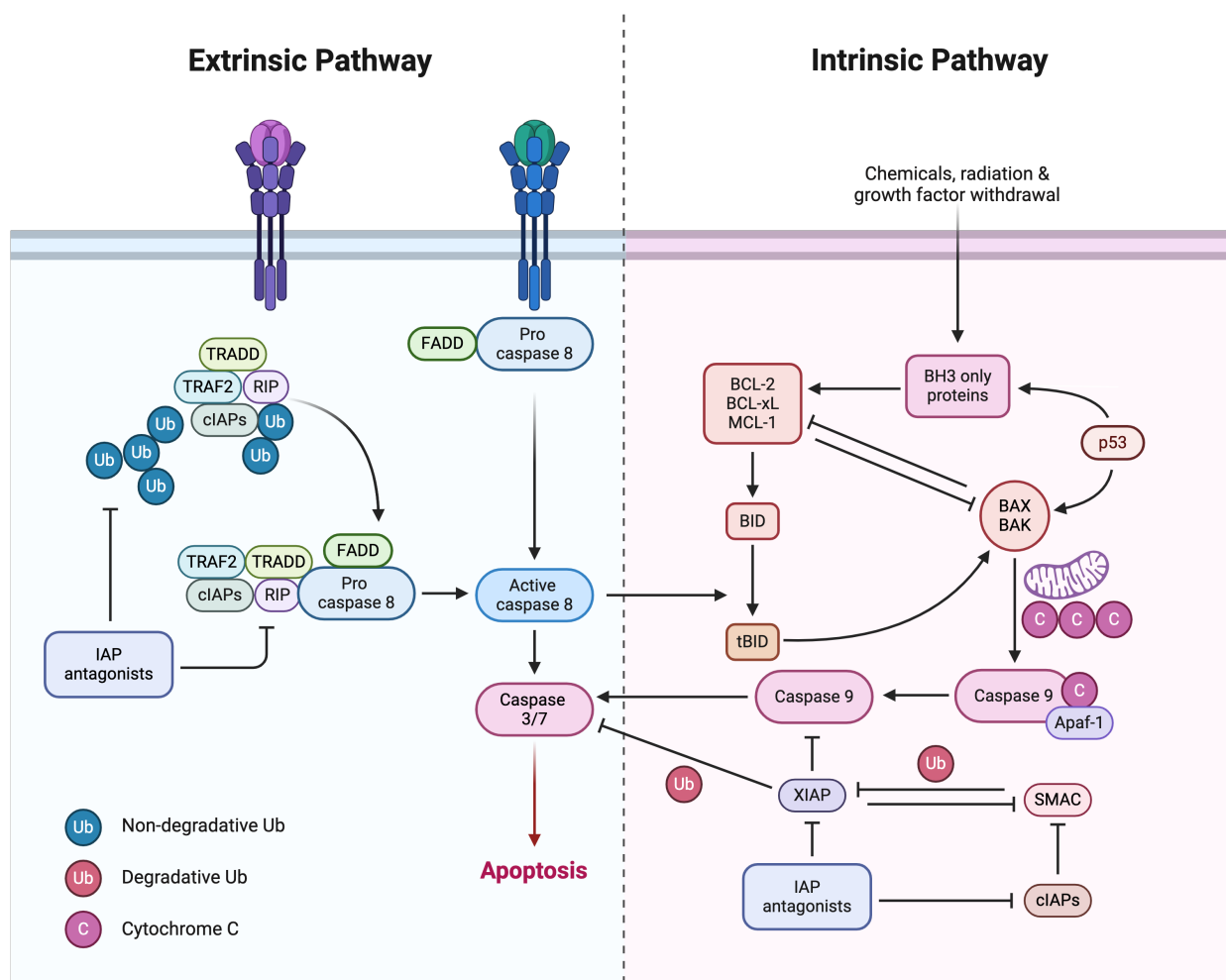


Figure 2. Schematic overview of extrinsic and intrinsic apoptosis

The extrinsic pathway is activated by death receptor ligands such as FasL, TNF α or TRAIL. The binding of FasL to Fas recruits FADD and procaspase-8 to form DISC complex leading to activation of caspase-8 and downstream executioner caspases. The binding of TNF α or TRAIL to TNFR1 recruits TRADD, RIP, TRAF2/5 and cIAP1/2 forming complex I leading also to activation of caspase-8. The intrinsic pathway is activated by apoptotic stimuli such as intracellular stress. Inhibition of BH3-only proteins and Bcl-2 leads to activation of BAK and BAX. The activated BAK and BAX promotes the release of cytochrome c and Smac. Association of cytochrome c with APAF-1 and procaspase-9 results in apoptosome formation which activates caspase-9 and downstream executioner caspases leading to apoptosis. APAF-1: apoptotic protease activating factor 1, BAK: Bcl-2 homologous antagonist/killer, BAX: Bcl-2-

associated X protein, BCL-2: B-cell lymphoma 2, BCL-xL: B-cell lymphoma-extra-large, BID: BH3 interacting-domain death agonist, cIAPs: baculoviral IAP repeat containing, FADD: Fas-associated death domain protein, MCL-1: myeloid cell leukemia-1, p53: cellular tumour antigen p53, RIP: receptor-interacting serine/threonine-protein, SMAC/DIABLO: direct IAP binding protein with low pI, tBID: truncated BID, TRADD: TNFR1-associated DEATH domain protein, TRAF2: TNF receptor associated factor 2, XIAP: X-linked inhibitor of apoptosis. Adapted from Elmore et al. 2007⁶. The figure has been created using Biorender.

1.1.3. Necroptosis

Necroptosis is a type of RCD that results from changes in the extracellular and intracellular environment that is detected by death receptors and/or pathogen recognition receptors respectively⁶². TNF α -mediated necroptosis is the classical necroptosis where upon ligand binding to TNFR1, the sequential activation of receptor-interacting serine/threonine-protein kinase 3 (RIPK3) and mixed lineage kinase domain like pseudokinase (MLKL) initiated by RIPK1 leads to the necrotic type of cell death⁶³. Complex I formation upon ligand binding further proceeds to complex II (a formation that can result in apoptosis). However, if caspase-8 is inhibited, a shift from extrinsic apoptosis to necroptosis induction is facilitated⁶⁴. Inhibition of caspase-8, due to the absence of IAPs or cFLIP, or absence of LUBAC components can lead to deubiquitylation of RIPK1 by cylindromatosis (CYLD), destabilizing complex I formed upon ligand binding leading to the formation of complex II⁶⁵. Active RIPK3 phosphorylates MLKL, resulting in the formation of MLKL oligomers that translocate to the plasma membrane and trigger plasma membrane permeabilization⁶⁶⁻⁶⁸.

RIPK3 activation via RIPK1 happens through the physical interaction between their respective RIP homotypic interaction motif (RHIM) domains and RIPK1 catalytic activity^{69,70}. RIPK3 can also be activated through the RHIM domain interaction of TIR-domain-containing adapter-inducing interferon- β (TRIF) downstream of toll-like receptor 3 (TLR3) activation by double-stranded RNA (dsRNA) within endosomes, toll-like receptor 4 (TLR4) activation by lipopolysaccharide (LPS), or various danger-associated molecular patterns (DAMPs) at the plasma membrane⁷¹. Alternatively, Z-DNA-binding protein 1 (ZBP1) activation by dsRNA⁷² can interact with RIPK3 through its RHIM domains, facilitating the execution of RIPK1-independent, RIPK3-mediated necroptosis^{73,74}.

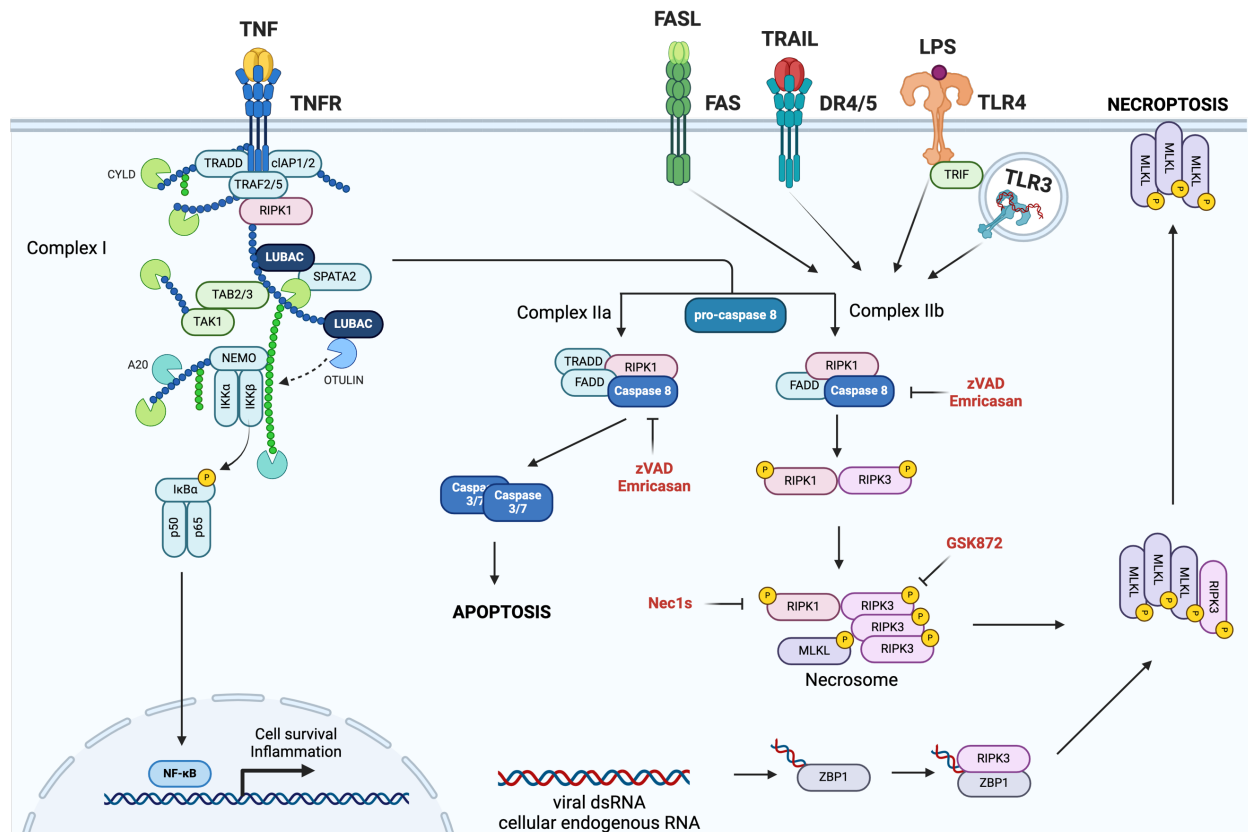


Figure 3. Schematic overview of necroptosis

Ligand binding to TNFR1 start the signalling cascade to form complex I, inhibition of NF- κ B mediated protein synthesis leads to formation of Complex IIa. Inhibition of RIPK1 ubiquitination in the early steps of TNF signalling, results or activation of other DRs as well as TLR4 result in the formation of Complex IIb. Inhibition or caspase 8, leads to a shift from apoptosis to necroptosis. RIPK1 further phosphorylates RIPK3, forming the and subsequently phosphorylate and activate MLKL. Oligomerization and translocation of MLKL to the plasma membrane leads to pore formation and lysis of the cell. DR4/5: Death receptor 4/5, FADD: Fas-associated death domain protein, FASL: Fas ligand, I κ B α : NF- κ B inhibitor alpha, IKK α : Component Of Inhibitor Of Nuclear Factor Kappa B Kinase Complex, IKK β : Inhibitor Of Nuclear Factor Kappa B Kinase Subunit Beta, LPS: Lipopolysaccharide, LUBAC: linear ubiquitin chain assembly complex, MLKL: mixed lineage kinase domain like pseudokinase, NEMO: Inhibitor Of Nuclear Factor Kappa B Kinase Regulatory Subunit Gamma, NF- κ B: nuclear factor kappa-light-chain-enhancer of activated B cells, OTULIN: OTU Deubiquitinase With Linear Linkage Specificity, RIPK1: interacting serine/threonine-protein kinase 1, RIPK3: interacting serine/threonine-protein kinase 3, SPATA2: Spermatogenesis Associated 2, TAB2/3: Mitogen-Activated Protein Kinase Kinase 7-Interacting Protein 2/3, TAK1: Mitogen-Activated Protein Kinase Kinase 7, TLR3: Toll-like receptor 3, TLR4: Toll-like receptor 4, TNF: Tumour necrosis factor, TNFR: TNF receptor, TRADD: TNFR1-associated DEATH domain protein, TRAF2: TNF receptor associated factor 2, TRAIL: TNF-related apoptosis-inducing ligand, TRIF: Toll like receptor adaptor molecule 1, ZBP1: Z-DNA-binding protein 1. Adapted from Seo et al. 2021⁷⁵. The figure has been created using Biorender.

1.1.4. Pyroptosis

Pyroptotic cell death was initially referred to as apoptosis, despite the fact that it was shown to induce a lytic type of cell death in *Shigella flexneri*-infected macrophages⁷⁶ due to sharing similarities including DNA fragmentation, nuclear condensation and caspase activation. Later on, it was proposed to be a caspase-1-dependent non-apoptotic cell death induced in

macrophages as in the case of *Salmonella typhimurium* infection⁷⁷. Large multi-protein complexes called inflammasomes assemble in response to detecting pathogens, leading to caspase-1 (CASP1) proteolytic activity and subsequent pore formation in the plasma membrane⁷⁸. Recognition of the inflammatory ligands by pattern-recognition receptors (PPRs) results in activation of inflammasomes via Nod-like receptors (NLRP1, 3, 6, 7, 12, NLRC4), interferon-inducible protein, or absent in melanoma 2 (AIM2). Notably, these proteins all have caspase activation and recruitment domains (CARD) or a pyrin domain (PYD)⁷⁹. NLRP3 recognizes various agonists⁷⁹, whereas NLRC4 is specific for cytosolic flagellin⁸⁰ and the components of type III secretion systems (T3SS)^{81,82}, and AIM2 can sense cytosolic DNA^{83,84}. Inflammasomes recruit apoptosis-associated speck-like protein containing a CARD (PYCARD or ASC) adaptor in which the additional CARD-CARD or PYD-PYD interactions leads to the recruitment of pro-CASP1 and formation of active CASP1 via autocatalytic cleavage⁸⁵. Active CASP1 cleaves gasdermin D (GSDMD), and processes pro-interleukin-1 β (pro-IL-1 β) and pro-interleukin-18 (pro-IL-18) to their mature forms^{86,87}. The cleavage of GSDMD produces an N-terminal domain (GSDMD-N) and a C-terminal domain (GSDMD-C) where GSDMD-N can oligomerize and form transmembrane pores with the inner diameter of 10-14 nm⁸⁸. The pores allow the release of IL-1 β and IL-18 and other cytosolic content into the extracellular space while the water influx from the pore causes cell swelling and osmotic lysis⁷⁸. Canonical pyroptosis relies on CASP1, whereas the non-canonical pyroptosis happens independent of CASP1 via caspase-11 (CASP11) in murine cells and caspase-4 (CASP4) and caspase-5 (CASP5) in human cells, processing IL-1 β by NLRP3-ASC-CASP1 pathway⁸⁹. LPS within the cytosol works as an agonist for CASP11 and CASP4/5 by promoting oligomerization and activation independent from TLR4^{90,91}. CASP11 needs to be activated prior to LPS sensing either by type I interferon⁹²⁻⁹⁴ or interferon gamma (IFN- γ)⁹⁴⁻⁹⁶. GSDMD cleavage to GSDMD-N by these caspases results in pyroptosis^{97,98}. Another alternative pathway is through gasdermin E (GSDME) cleavage by caspase-3, one of the executioner caspases in apoptosis, to produce a N- and C-terminal fragment similar to GSDMD cleavage leading to formation of pores on the cellular membrane^{99,100}.

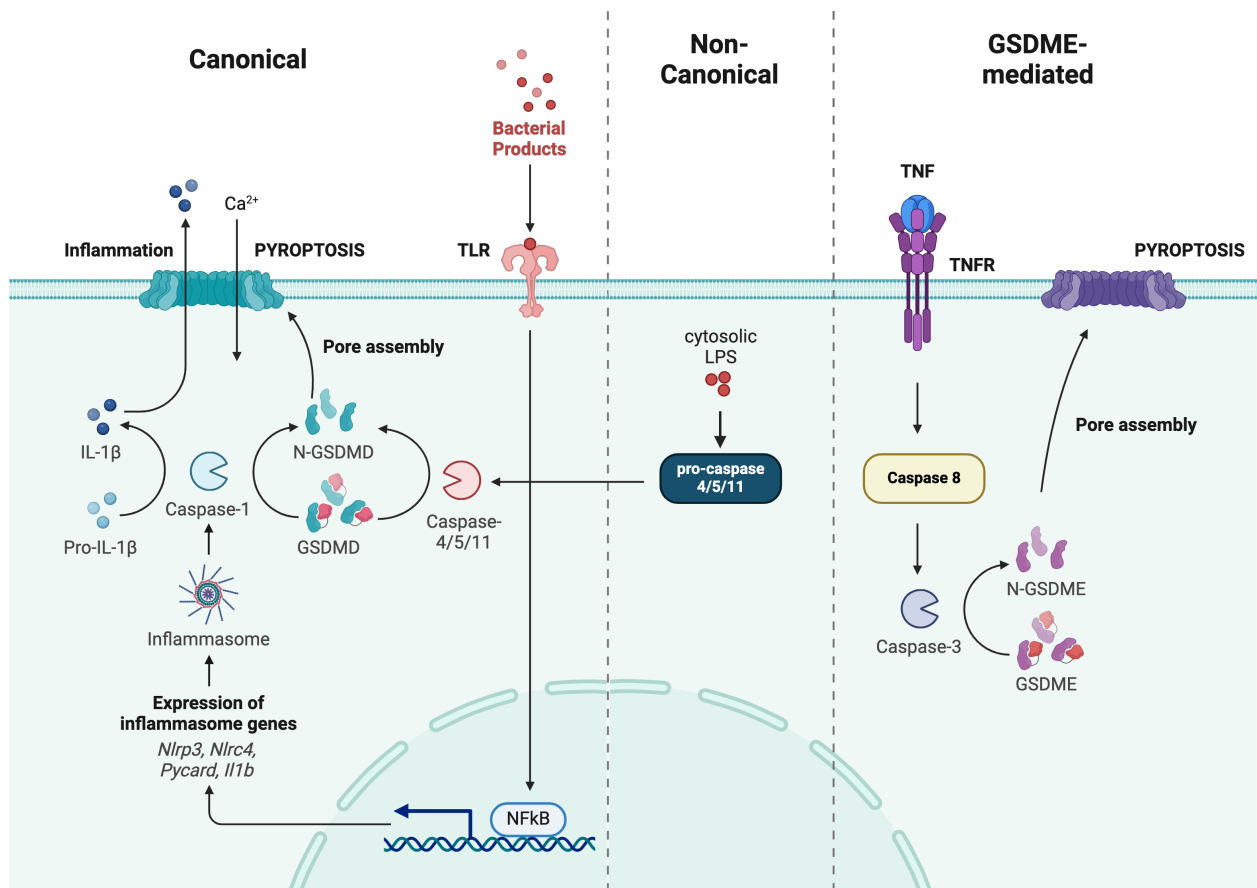


Figure 4. Schematic overview of pyroptosis

In canonical pathway, multiple stimuli can activate pattern recognition receptors leading to inflammasome activation within the cell. Inflammasome activated caspase-1 can cleave pro-IL-1 β into mature IL-1 β and GSDMD into N-GSDMD. N-GSDMD can form pores on the plasma membrane resulting in secretion through the pore leading to cell swelling and bursting. In non-canonical pathway, cytosolic LPS activated caspase-4/5/11 N-GSDMD mediated pyroptosis. In addition to GSDMD, GSDME can also activated upon death receptor mediated activation of caspase 8 and caspase 3 and form membrane pores upon cleavage into N-GSDME. GSDMD: Gasdermin D, GSDME: Gasdermin E, IL-1 β : Interleukin 1 beta, LPS: Lipopolysaccharide, N-GSDMD: N-terminal Gasdermin D, N-GSDME: N-terminal Gasdermin E, TLR: Toll-like receptor. Adapted from Yu et al. 2021¹⁰¹. The figure has been created using Biorender.

1.1.5. Ferroptosis (adapted from Yapici and Bebbler 2024)

Ferroptosis, although not named at the time, was discovered as the result of a lethality drug screen for targeting cancer cells. The Stockwell Lab initiated a screening effort which ultimately lead to the discovery of a set of compounds that can trigger a distinct form of oxidative cell death which does not involve the apoptosis or necroptosis molecular machinery¹⁰². Follow-up studies revealed that when exposed to eradicator of RAS and ST-expressing cells (ERASTIN), a small molecule that targets the solute carrier family 7 member 11 (SLC7A11 or xCT), cells with Ras-pathway activation underwent a selective type of cell death with necrosis-like morphological features which were distinct from apoptosis, necrosis or autophagy¹⁰³. Due to its dependence on iron, the term ‘ferroptosis’ was coined in 2012 by

Dixon et al¹⁰⁴. Ferroptotic cells also displayed mitochondrial failure, cytoplasmic swelling, and a loss of plasma membrane integrity^{105,106}. Upon depletion of intracellular glutathione (GSH) and subsequent inactivation of glutathione peroxidase 4 (GPX4) lipid hydroperoxides can no longer be reduced to their corresponding lipid alcohols. This leads to significantly higher levels of lipid reactive oxygen species (lipidROS), which ultimately leads to ferroptosis¹⁰⁷. Lipid peroxides subsequently produce secondary toxic aldehydes such as 4-hydroxy-2-noneal (4-HNE) and malondialdehyde (MDA) that can react with DNA bases, proteins and other nucleophilic molecules¹⁰⁸. Lipid peroxidation also changes the shape and curvature of lipid membranes, promoting the access of oxidants, which further accelerates the destruction of membranes and triggers the final cell death¹⁰⁹. Several lipophilic antioxidants with radical-trapping properties such as ferrostatin-1 (Fer-1), liproxstatin-1 (Lip-1) and iron chelating compounds such as deferoxamine (DFO) were shown to be effective in reversing this kind of cell death in further screening tests¹⁰³. Other compounds such as vitamin E, trolox, deuterated polyunsaturated fatty acids (D-PUFAs) and butylated hydroxytoluene can also block lipid peroxidation directly¹¹⁰. Ultimately, ferroptotic cells form small nanopores before cell burst¹¹¹, making ferroptosis a lytic and potentially inflammatory type of cell death with the potential release of DAMPs.

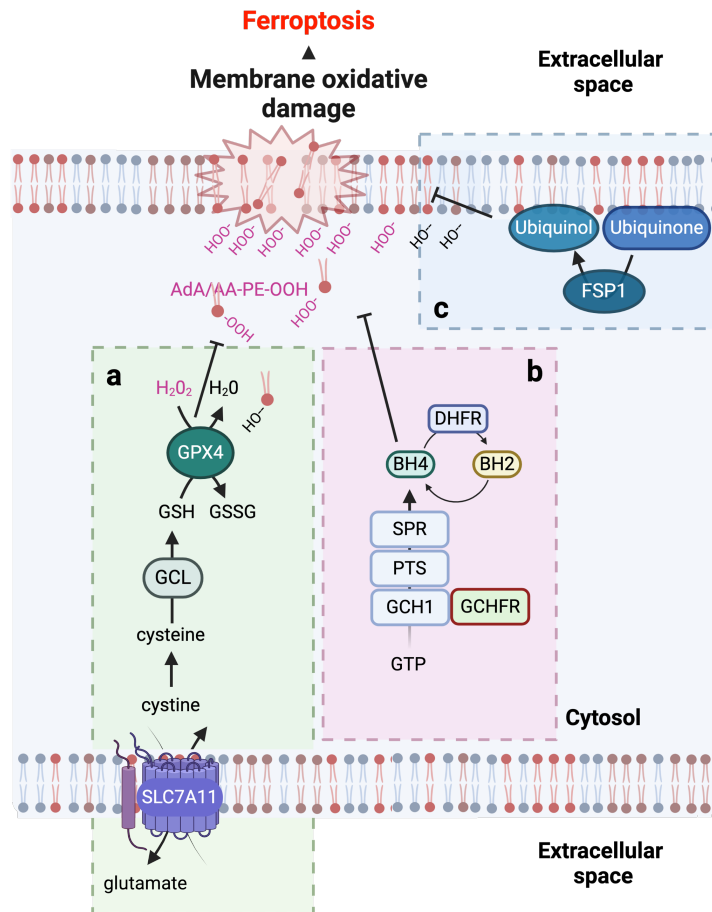


Figure 5. Schematic overview of ferroptosis

Cellular mechanisms modulating the sensitivity of cells to ferroptosis are divided into GPX4-dependent **(a)** and GPX4-independent **(b, c)** regulation. **(a)** Inhibition of system xc- or GPX4 leads to accumulation of lipidROS in the cell resulting in ferroptotic cell death. Radical-trapping agents mediated by GCH1 **(b)** or FSP1 **(c)** serves as protection mechanisms from ferroptosis. BH2: Dihydrobiopterin, BH4: Tetrahydrobiopterin, FSP1: Ferroptosis suppressor protein 1, DHFR: Dihydrofolate Reductase, GCH1: GTP Cyclohydrolase 1, GCHFR: GTP Cyclohydrolase 1 Feedback Regulator, GCL: Glutamate cysteine ligase, GPX4: Glutathione peroxidase 4, GTP: Guanosine triphosphate, PTS: 6-Pyruvoyltetrahydropterin Synthase, SLC7A11: solute carrier family 7 member 11, SPR: Sepiapterin Reductase. Adapted from Yapici and Bebbler, 2024¹¹². The figure has been created using Biorender.

1.1.5.1. GPX4-dependent regulation of ferroptosis

Ferroptosis is fundamentally caused by the peroxidation of specific membrane lipids. Polyunsaturated fatty acids (PUFAs) have been shown to be the most susceptible lipid class to undergo peroxidation during ferroptosis¹¹³. Arachidonic acid (AA) and adrenic acid (AdA)-containing phospholipids, particularly phosphatidylethanolamine (PE) species, have been identified as important lipid sources of *in vivo* ferroptosis¹¹⁴. In addition, ether-linked phospholipids have recently been identified as specific targets of lipid peroxidation during ferroptosis¹¹⁵. GPX4, a selenoprotein, is the major enzyme that catalyses the reduction of these phospholipid hydroperoxides¹¹⁶. GPX4 activity depends upon its co-factor and substrate

glutathione (GSH) as an electron donor¹¹⁷. GSH is a tripeptide synthesized from cysteine, glutamate, and glycine. Cells take up cystine via the cystine/glutamate antiporter (system xc) that consists of two subunits: solute carrier family 3 member 2 (SLC3A2 or 4F2) and solute carrier family 7 member 11 (SLC7A11 or xCT)¹⁰⁴. Once within the cell, thioredoxin reductase 1 (TXNRD1) or thioredoxin-related protein of 14 kDa (TRP14) converts cystine to cysteine¹¹⁸. Glutamate cysteine ligase (GCL) combines cysteine with glutamate to generate γ -glutamylcysteine. GSH synthase then adds glycine to γ -glutamylcysteine to form GSH^{118,119}. Similarly, directly interrupting the synthesis of GSH by inhibiting GCL using buthionine sulfoximine (BSO) also induces ferroptosis¹²⁰. An alternative source for intracellular cysteine used for GSH synthesis is the transsulfuration pathway, which can compensate for cystine-deprivation^{121,122}. Sensitization to ferroptosis can also occur through the depletion of glutathione via alternative mechanisms. The multidrug resistance protein 1 (MRP1) has been shown to cause a glutathione efflux¹²³ and the cysteine dioxygenase 1 (CDO1) increases the sensitivity to ferroptosis by depleting cysteine and consequently glutathione levels¹²⁴. The main protection mechanisms from ferroptosis therefore involve regulation of expression and activity of GPX4 through GSH synthesis, recovery and localization.

1.1.5.2. Regulation of ferroptosis via the synthesis of endogenous radical trapping agents (RTAs)

Recent studies have also shown additional pathways that can protect the cells from ferroptosis. First, ferroptosis suppressor protein 1 (FSP1), formerly known as AIFM2, has been identified as an antioxidant regulator of ferroptosis by two different working groups^{125,126}. FSP1 functions as an oxidoreductase to reduce coenzyme Q10 (CoQ10) to ubiquinol (CoQH₂) upon recruitment to the cellular membrane from mitochondria, while also functioning as a lipophilic radical trapping antioxidant. Myristoylation of FSP1 in the N-terminus is needed in order to achieve its cell membrane localization¹²⁶. The substrate of FSP1, CoQ10, is synthesized at the inner mitochondrial membrane and is shuttled to the plasma membrane by the cytosolic form of StAR-related lipid transfer domain protein 7 (STARD7) upon cleavage by the mitochondrial membrane protease presenilin-associated rhomboid-like protein (PARL)¹²⁷. In addition to mitochondria, the mevalonate pathway can also play a crucial role in the synthesis of coenzyme Q10¹²⁸. Of note, the availability of NADPH also plays a role for FSP1's ability to suppress ferroptosis¹²⁹. In line with this, cellular levels of NADPH have been

shown to correlate with ferroptosis resistance amongst human cell lines¹³⁰. Dihydroorotate dehydrogenase (DHODH) was also described as a mitochondrial suppressor of ferroptosis through its function to reduce CoQ10 to CoQH₂ in the inner mitochondrial membrane¹³¹. The role of DHODH has recently been put in question as the DHODH inhibitor used in the original study can also cause inhibition of FSP1 rather than DHODH itself¹³². In addition to CoQ10, FSP1 can also reduce vitamin K to its hydroquinone form, thereby protecting cells from ferroptosis¹³³. GTP cyclohydrolase 1 (GCH1) was also recently reported as critical regulator of ferroptosis. The downstream product of GCH1 tetrahydrobiopterin (BH₄) prevents ferroptosis as a radical trapping antioxidant, but also proposed to be involved in the production of CoQ10 and lipid remodeling^{134,135}. Another study just recently revealed that hydropersulfides scavenge free radicals and thereby prevent cells from lipid peroxidation and ferroptosis¹³⁶. Thus, endogenous radical trapping agents can protect cells from ferroptotic cell death induced by the disruption of lipid ROS detoxification.

1.1.5.3. Metabolic checkpoints of ferroptosis regulation

Polyunsaturated fatty acids (PUFAs) such as AA, linoleic acid (LA) and docosahexaenoic acid, as well as unsaturated lipids like cholesterol, can undergo oxidation to form hydroperoxides, which can disrupt the integrity of cellular membranes¹³⁷. Additionally, lipid peroxides can interact with redox-active metals like iron, leading to the generation of various lipid hydroperoxides. Lipid ROS and dependence on iron serve as markers of ferroptosis. Therefore lipophilic antioxidants as described above and iron-chelating agents can inhibit ferroptosis¹³⁸.

1.1.5.3.1. Iron metabolism

Iron plays a vital role in ferroptosis, as it has the potential to generate highly reactive hydroxyl radicals through the Fenton reaction, which in turn initiate a chain reaction of lipid peroxidation¹³⁹. In addition, iron functions as a cofactor of lipoxygenases (LOXs) and cytochrome P450 family (CYPs), which have been implicated in the direct generation of oxygenated lipids in an event called autoxidation¹⁴⁰. Ferric iron (Fe⁺³), ferritin and heme are the most common forms of iron absorbed throughout the tissues. Macrophages provide the daily source of iron to the tissues by phagocytosing aged erythrocytes. Upon lysis of red blood cells, iron is released from hemoglobin by heme oxygenase-1 (HO-1)^{141,142}. Iron import into the cell occurs upon binding of transferrin-bound Fe⁺³ to transferrin receptor 1 (TfR1)

followed by endocytosis. Fe^{+3} is then reduced to ferrous iron (Fe^{+2}) by six-transmembrane epithelial antigen of prostate 3 (STEAP3). Fe^{+2} is then released into the cellular labile iron pool (LIP) by the divalent metal transporter 1 (DMT1) and Tfr1 is recycled to the cell membrane¹⁴³. During iron-deficient conditions iron-regulatory proteins (IRPs) can bind to iron-regulatory elements (IREs) on the *TfR1* mRNA to induce increased expression¹⁴⁴. The pool of redox active iron complexes comprises the LIP. Due to its reactivity it is stored within the cell bound to ferritin, which consists of two subunits: ferritin light chain (FTL) and ferritin heavy chain (FTH1). The nuclear receptor co-activator 4 (NCOA4) can directly bind to FTH1 to degrade ferritin via lysosomes to increase free iron levels in the cell, a process known as “ferritinophagy”^{145,146}. Iron can also be exported from the cell by the iron-efflux pump ferroportin (FPN1/SLC40A1)¹⁴⁷ or through exosome-dependent iron export mediated by prominin 2 (PROM2), which involves the formation of ferritin-containing multivesicular bodies¹⁴⁸. An antimicrobial peptide called hepcidin that is synthesised and secreted by the liver can act as a negative regulator of FPN1, causing iron overload in different tissues and contributing to ferroptosis¹⁴⁹. Diminished iron uptake and iron chelation blocks ferroptosis^{103,107}. While removal of transferrin from serum also prevents ferroptotic cell death¹⁵⁰. On the contrary, *TfR1* upregulation increases ferroptosis sensitivity, silencing IRP2 leads to a decrease in ferroptosis sensitivity^{104,107}. Lipid peroxidation can occur spontaneously in the presence of free redox-active Fe^{+2} to promote the Fenton reaction, which generates hydroxyl radicals ($\text{HO}\cdot$) from hydrogen peroxide (H_2O_2). These radicals can then react directly with PUFAs in membrane phospholipids.¹⁵¹ The intracellular iron pool therefore serves as an important requisite for many of the biochemical processes leading to lipid peroxidation.

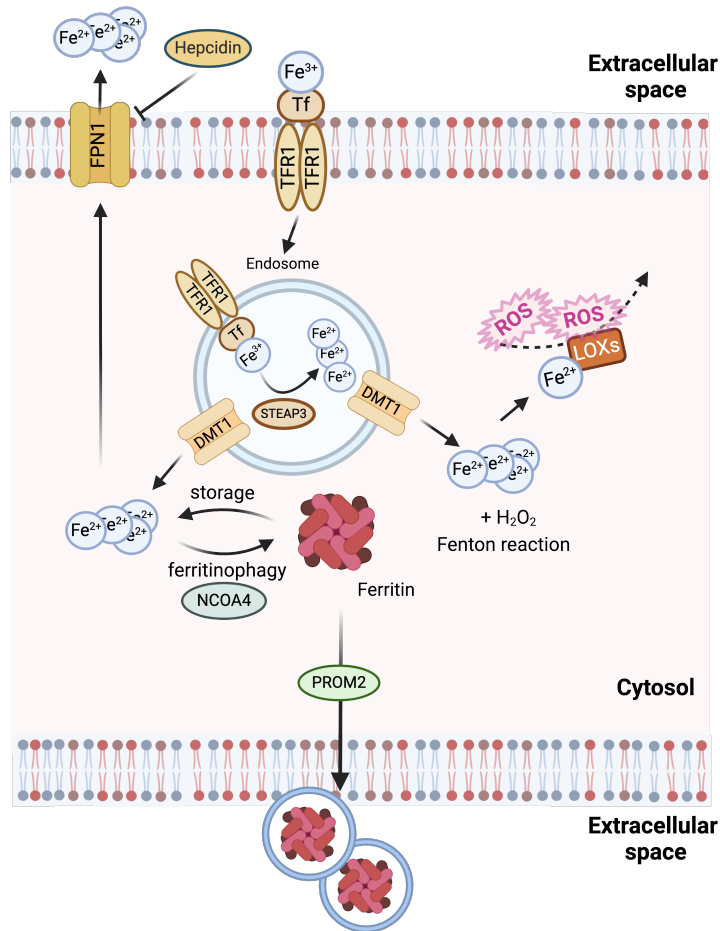


Figure 6. Iron metabolism in ferroptosis

Iron metabolism that modulates the sensitivity of cells to ferroptosis is the depicted. Iron export and import contributes to the Fenton reaction facilitating the labile iron pool. DMT1: Divalent metal transporter 1, FPN1: Ferroportin, LOXs: Lipoxygenases, NCOA4: Nuclear receptor coactivator 4, PROM2: Prominin 2, ROS: Reactive oxygen species, STEAP3: Six-transmembrane epithelial antigen of prostate 3 metalloredutase, Tf: Transferrin, TFR1: Transferrin receptor 1. Adapted from Yapici and Bebbler, 2024¹¹². The figure has been created using Biorender.

1.1.5.3.2. Lipid metabolism

PUFAs are particularly vulnerable to peroxidation due to their highly reactive hydrogen atoms in their methylene double bonds. Cell membranes are rich in AA- and AdA-containing phosphatidylethanolamine phospholipids, which are predominantly peroxidised during ferroptosis¹⁵². The lipid target pool for peroxidation is generated with a cascade of enzymes starting by acyl-CoA synthetase long-chain family member 4 (ACSL4)¹⁵³. ACSL4 facilitates the formation of acyl-CoA from AA or AdA with CoA to further undergo catabolic fatty acid oxidation or anabolic PUFA biosynthesis¹⁵⁴. Further downstream, lysophosphatidylcholine acyltransferase 3 (LPCAT3) provides the pool of PUFAs targeted by peroxidation by incorporating acyl-AA into the phospholipids of cellular membranes, thereby contributing to ferroptosis^{155,156}. In ferroptosis-sensitive cells ACSL4 and LPCAT3 levels are significantly

enriched^{153,154,156}. Further oxidation of PUFA-phospholipids can be catalysed by cytochrome P450 oxidoreductase (POR), cyclooxygenases (COXs) and LOXs¹⁰⁸. POR and CYPs play an important role in redox homeostasis; even though POR has been shown to facilitate lipid peroxidation¹⁵⁷ there were no specific CYPs found in partner catalysing lipid peroxidation¹⁵⁸. Besides the upregulation in *Ptgs2* gene upon ferroptosis induction, which encodes for COX-2, there is no direct link between COXs with lipid peroxidation and ferroptosis execution¹²⁰. LOXs directly oxidize the AA-PE and AdA-PE into lipid hydroperoxides^{113,159–161}. The tumour suppressor gene *TP53* has also been shown to induce ferroptosis through different LOXs¹⁶¹ and through suppression of SLC7A11 expression which in turn depletes GSH¹⁶².

Monounsaturated fatty acids (MUFAs) are less inclined to lipid peroxidation, therefore the proportion of MUFAs to PUFAs determines the speed at which lipid peroxidation spreads within membranes. Exogenous MUFAs when fed to cells decrease the sensitivity to ferroptosis by raising the MUFA/PUFA ratio and hindering lipid peroxidation on membranes both *in vitro* and *in vivo*¹³⁷. Membrane-bound O-acyltransferase domains containing 1 and 2 (MBOAT1/2) are lysophospholipid acyltransferases specific to MUFAs that alter the lipidome to increase the amounts of MUFA-phospholipids and resistance to ferroptosis¹⁶³. 7-dehydrocholesterol (7-DHC) has been shown in two recent independent studies to prevent excessive lipid peroxidation during ferroptosis by capturing peroxy radicals and protecting phospholipids from autoxidation^{164,165}. Both studies reveal a novel protective function for B-ring unsaturated sterols against ferroptosis and phospholipid peroxidation. They also suggest that phospholipid truncation can cause the nanopores seen during ferroptosis. The PUFA- and MUFA-composition of cell membranes is a strong determinant of susceptibility to ferroptosis, subject to tight metabolic regulation.

1.1.5.3.3. Non-lipid metabolism

Mitochondria are crucial for adenosine triphosphate (ATP) production due to their role in oxidative phosphorylation (OXPHOS). However, this process comes at the cost of reactive oxygen species production (ROS) as a by-product¹⁶⁶. The majority of antioxidant defence proteins are transcriptionally induced by the master antioxidant transcription factor nuclear factor erythroid 2-related factor 2 (NRF2, also called NFE2L2). Under basal conditions, NRF2 is kept in the cytoplasm by kelch-like ECH-associated protein 1-cullin3-ring box protein 1 (KEAP1-

CUL3-RBX1), an E3 ubiquitin ligase complex causing its ubiquitination and transport to the proteasome followed by degradation^{167,168}. However, increased oxidative stress conditions can disrupt the KEAP1-CUL3 ubiquitination system of NRF2, which allows translocation to the nucleus and leads to the transcription of target antioxidant genes¹⁶⁷. Still, high levels of ROS can overwhelm the cellular antioxidant defence system, resulting in oxidative stress in the form of free radicals directly oxidising cysteines within proteins, as well as lipids and DNA.

Within the mitochondrial lumen tricarboxylic acid (TCA) is converted to NADH with the contribution of various metabolites such as acetyl-CoA from glycolysis and β -oxidation¹⁶⁹. Members of the electron transport chain in the inner mitochondrial membrane transport electrons from nicotinamide adenine dinucleotide (NADH) to the terminal electron acceptor oxygen (O_2), which is thereby reduced to water (H_2O). Glutamine also plays an important role in ferroptosis¹⁵⁰. It has been shown that glutamine synthase 2 (GLS2), which regulates glutaminolysis, can also facilitate ferroptosis. GLS2 also aids in the degradation of glutamine, supplying the TCA cycle with GLS2 in the breakdown of glutamine, and supplying the TCA cycle with alpha-ketoglutaric acid (α -KG)¹⁷⁰. α -KG and its downstream metabolites including succinic acid, fumaric acid, and malic acid, can replace the function of glutamine in the accumulation of lipid ROS and cystine starvation induced or system Xc^- inhibition induced ferroptosis¹⁷¹. Fumarate, an intermediate in the TCA cycle, has also been described to influence ferroptosis sensitivity. Dimethyl-fumarate induces ferroptosis in diffuse large B-cell lymphoma (DLBCL) by depleting GSH and inhibiting GPX4¹⁷². These data suggest a strong connection between metabolic regulation and ferroptosis.

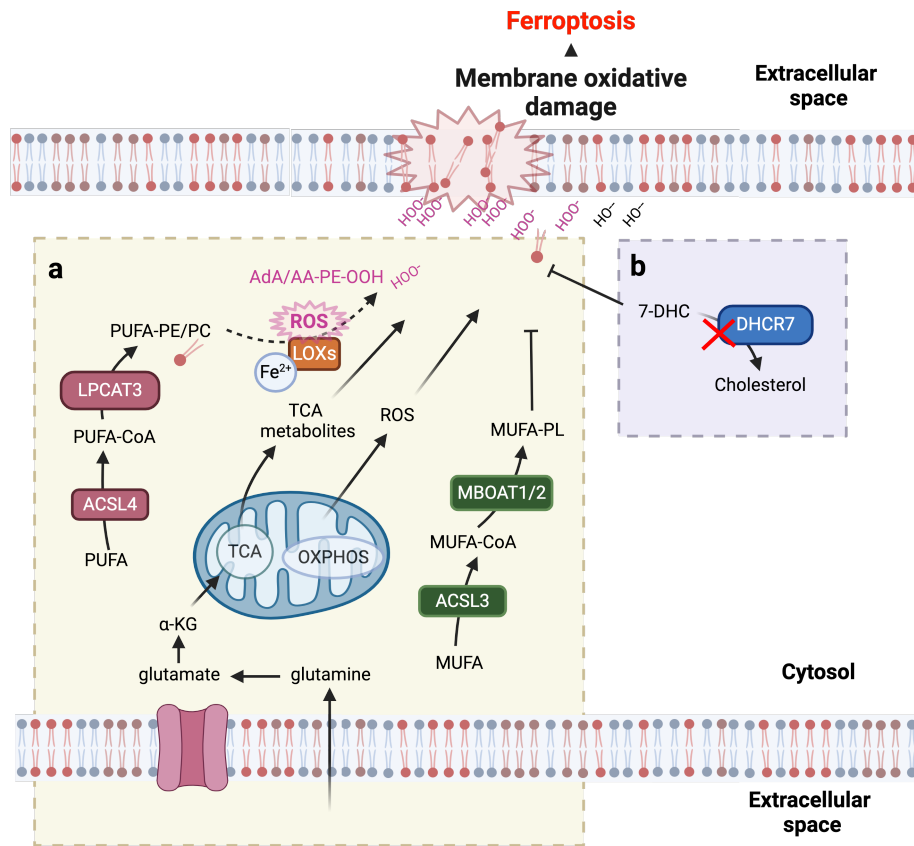


Figure 7. Metabolic regulators of ferroptosis

Ferroptosis sensitivity of the cells depends on lipid and non-lipid metabolisms. 7-DHC: 7-Dehydrocholesterol, ACSL3: Acyl-CoA synthetase long chain family member 3, ACSL4: Acyl-CoA synthetase long chain family member 4, DHCR7: 7-Dehydrocholesterol reductase, LPCAT3: Lysophosphatidylcholine acyltransferase 3, MBOAT1/2: Membrane bound O-acyltransferase domain containing 1/2, MUFA: Monounsaturated fatty acids, MUFA-CoA: Monounsaturated fatty acid-coenzyme A, MUFA-PL: Monounsaturated fatty acid phospholipid, OXPHOS: Oxidative phosphorylation, PUFA: Polyunsaturated fatty acids, PUFA-CoA: Polyunsaturated fatty acid-coenzyme A, PUFA-PE/PC: Polyunsaturated fatty acid-phosphatidylethanolamine/phosphatidylcholine, ROS: Reactive oxygen species, TCA: Tricarboxylic acid cycle, α -KG: Ketoglutaric acid. Adapted from Yapici and Bebbler, 2024¹¹². The figure has been created using Biorender.

1.1.5.4. Ferroptosis-inducing agents (FINs) and sensitizers

Ferroptosis inducing small molecules that have been described in the literature can be divided to 4 different subgroups: class I FINs decrease GPX4 activity through depletion of GSH, class II FINs inhibit GPX4 directly, class III FINs lead to GPX4 degradation and class IV FINs lead to iron oxidation¹⁷³. Although different FINs have already been characterized with respect to their effects on the ferroptosis pathway, recent studies have revealed new players in the pathway which necessitates updating the current classification system. GPX4 was initially identified as the main protein playing a role in ferroptosis and a binding target for RSL3 using an affinity pulldown assay and subsequent proteomics¹²⁰. RSL3 inhibits GPX4 by the alkylation of its

selenocysteine residue¹⁷⁴. In another study ML210 was also described as a GPX4 inhibitor, binding to the selenocysteine residue¹⁷⁵. Of note, a recent publication found that RSL3, ML210 and ML162 are rather direct robust inhibitors of TXNRD1, but they are not able to inhibit recombinant GPX4 in cell free settings¹⁷⁶. Erastin, even though described as a system xc⁻ inhibitor, was shown to directly bind to mitochondrial voltage-dependent anion channel 2 (VDAC2) using purified VDAC2 in a cell-free affinity assay and also cause ROS production through an NADPH-dependent pathway via mitochondrial damage¹⁰³. In some cases GPX4 inhibition is not be sufficient to induce ferroptosis due to high levels of FSP1^{125,126,177}. The first inhibitor identified for FSP1, iFSP1, can bind to quinone-binding pocket of FSP1 but is only human-selective^{125,126}. Whereas the newly defined viFSP1 binds the NAD(P)H binding pocket in a species independent manner¹⁷⁸, icFSP1 inhibits FSP1 by inducing condensation and the formation of droplet-like structures of FSP1¹⁷⁹. FINs and their proposed mechanisms of action are summarized in Table 1-1.

Table 1-1. List of ferroptosis-inducing agents (FINs).

	Compound name	Mechanism of action
FIN I	Erastin ^{102,180} Imidazole Ketone Erastin ¹⁸¹ Sulfalazine ^{182–184} Sorafenib ^{185–187} Cysteinase ¹⁸⁸ BSO ^{120,189,190} Artesunate ¹⁹¹	System xc ⁻ inhibitor System xc ⁻ inhibitor System xc ⁻ inhibitor System xc ⁻ inhibitor Cysteine depletion GCL inhibitor Glutathione S transferase
FIN II	RSL3 ¹⁰⁷ ML210 ¹²⁰ ML162 ^{120,192} Withaferin A ^{193,194} Altretamine ¹⁹⁵	GPX4 inhibitor GPX4 inhibitor GPX4 inhibitor GPX4 inhibitor GPX4 inhibitor
FIN III	iFSP1 ¹²⁵ , icFSP1 ¹⁷⁹ , viFSP1 ¹⁷⁸ FSEN ¹²⁹ , Brequinar ¹³² FIN56 ^{128,196} Statins ^{197–199}	FSP1 inhibitor FSP1 inhibitor GPX4 degradation, squalene synthase inhibition Blocks CoQ10 synthesis
FIN IV	Artemisinin ²⁰⁰	Lysosomal degradation of ferritin

1.1.5.5. Ferroptosis relevance *in vivo*

Recent studies on ferroptosis shows its essential role in developmental processes. GSH availability is essential for cells to be protected against ferroptosis as it's vital as a cofactor for

GPX4. While xCT-deficient mice are viable and fertile, xCT-deficient mouse embryonic fibroblasts (MEFs) rapidly die in culture due to a lack of intracellular cysteine. They are only able to survive when either 2-mercaptoethanol or N-acetyl cysteine (NAC) is supplemented, since both serve as alternative cysteine sources²⁰¹. The full-body knockout of *Gpx4* leads to lethality between E7.5 and E8.5 in mice and implicates the role of *Gpx4* in mouse development^{202,203}, whereas the inducible *Gpx4* knockout were shown to develop spontaneous acute renal failure and hepatic ischemia/reperfusion injury- induced damage via ferroptosis¹⁰⁵. Conditional deletion of *Gpx4* was also shown to be catastrophic *in vivo* in several different tissues. Mice lacking *Gpx4* in neurons display selective and rapid motor neuron degeneration via ferroptosis²⁰⁴. In addition, conditional deletion of *Gpx4* in T cells in mice resulted in T cell ferroptosis, resulting in a lack of an immune response to infection²⁰⁵.

1.2. Inflammation and immune response

The fundamental purpose of the immune system is to serve as the body's first line defence against harmful stimuli, including pathogens, tissue injury and toxins. The complex biological response of inflammation is triggered by the immune system in order to shield the body and promote healing²⁰⁶. It can be divided into two different categories: innate and adaptive immunity. Innate immunity refers to the first line of defence that is involved in an antigen-independent (non-specific) mechanism used by the host upon encountering the antigen²⁰⁷. The innate immune response was thought to have no immunologic memory and therefore be incapable of recognizing the same pathogen should the body be exposed to it in the future. However, this was recently proven to be incorrect²⁰⁸. On the other hand, adaptive immunity is antigen-dependent and specific, allowing for the mounting of a more rapid and efficient immune response upon exposure to an antigen²⁰⁹.

Innate immunity (quick, non-specific)



Adaptive immunity (long-term, specific)

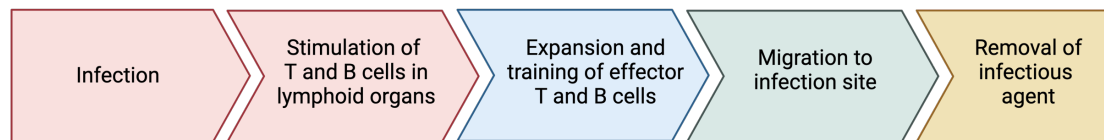


Figure 8. Mechanisms behind innate and adaptive immune system

Adapted from Janeway et al. 2001²¹⁰. The figure has been created using Biorender.

During acute inflammatory responses, cellular and molecular processes minimize the advancing injury or infection and, in the meantime, contribute to the restoration of tissue homeostasis and resolution of acute inflammation. In some cases, uncontrolled acute inflammation can lead to various chronic inflammatory diseases²¹¹. Inflammation is characterised by redness, swelling, heat, pain and loss of tissue function, all resulting from the local immune cell responses to infection or injury²¹². Upon detecting an injury or pathogens, immune cells such as macrophages and dendritic cells recognize the danger signals and release pro-inflammatory cytokines such as TNF, interleukin 1 (IL-1) and interleukin 6 (IL-6)²¹³. The inflammatory response initiated by these cytokines includes vascular permeability changes allowing the leukocyte recruitment and accumulation from the bloodstream to the site of injury or infection^{211,214}. Accumulation of immune cells at the site of inflammation allows them to engulf and digest the pathogens, dead cells and debris via phagocytosis in order to clear the site of infection or injury and prevent further spread of pathogens²¹⁵.

Innate immunity to pathogens starts with the recognition of ligands by the cell surface pattern receptors which further activate the inflammatory pathways to release and recruit immune cells. Pathogen-associated molecular patterns (PAMPs) originating from microbial structures can bind to PRRs on immune and non-immune cells²¹². PRRs can also recognize the signals from host-originating DAMPs and initiate non-infection inflammatory response²¹⁶. PRRs include Toll-like receptors (TLRs), C-type lectin receptors (CLR), retinoic acid-inducible gene (RIG)-I-like receptors (RLRs) and nucleotide-binding oligomerization domain (NOD)-like receptors (NLRs)²¹². Signalling through TLRs upon PAMP or DAMP sensing is mediated by

myeloid differentiation factor-88 (MyD88) or TRIF and leads to nuclear translocation of transcription factors such as NF- κ B, activator protein-1 (AP-1), or interferon regulatory factor 3 (IRF3)²¹⁷. Upon translocation, important cellular signalling pathways are triggered including NF- κ B, MAPK, Janus kinase (JAK)-signal transducer and activator of transcription (STAT)^{218–220}. Deregulation in the pathways are linked to conditions like autoimmune disorders, metabolic diseases and cancer²²¹. A variety of cell types are involved in the innate immune response including macrophages, neutrophils, dendritic cells, mast cells, basophils, eosinophils, natural killer (NK) cells and innate lymphoid cells²¹³. Dendritic cells act as the link between innate and adaptive immunity. They take up a pathogen in the infected tissue, become activated and mature into a highly effective antigen-presenting cell (APC), which can activate pathogen specific lymphocytes in the nearby lymph node²¹⁰. The concept of classic^{222,223} and alternative^{224,225} activation of macrophages to M1 or M2 states can happen at any point in the inflammatory process. The M1 polarization refers their ability to induce pro-inflammatory responses and markers such as CD16, CD32, CD86, CD64 and nitric oxide synthase 2 (iNOS) while M2 polarization refers to their ability to induce anti-inflammatory responses and markers such as CD163 and CD206. LPS, IFN- γ and TNF α can polarize macrophages towards the M1 phenotype, while M2 macrophage activation can be induced by interleukin-4 (IL-4) and interleukin-13 (IL-13)²²⁶. The imbalance of M1/M2 macrophages can contribute to various diseases.

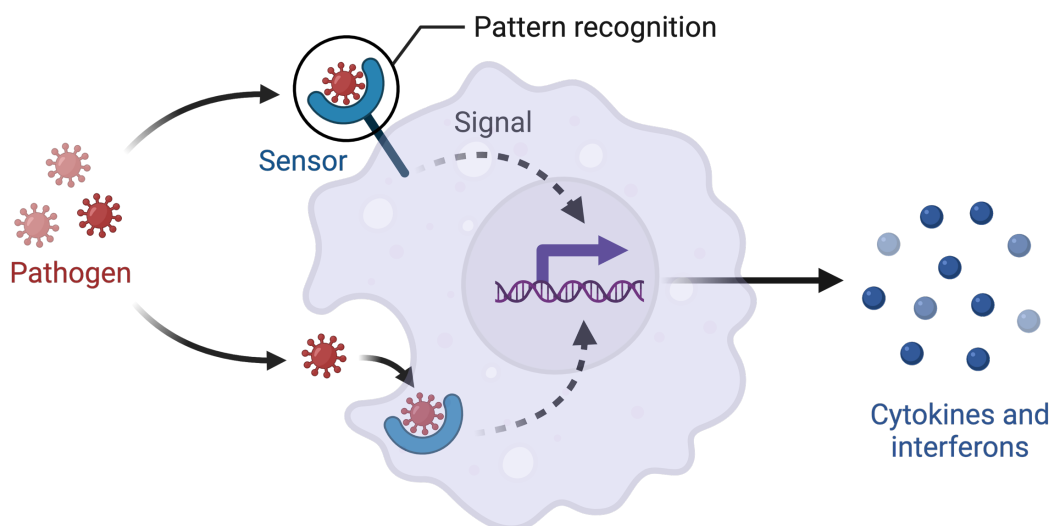


Figure 9. Mechanisms of innate immunity

The innate immune responses are the first line of defence against invading pathogens. Adapted from Janeway et al. 2001²¹⁰. The figure has been created using Biorender.

Adaptive immunity is critical in the cases when innate immunity is ineffective in the elimination of pathogens and for the establishment of an immunologic memory to quickly eliminate a specific pathogen²⁰⁹. The adaptive immune system is composed of antigen-specific T cells that are activated by APCs to proliferate and B cells that differentiate into plasma cells to produce antibodies²¹⁰. Each T cell expresses unique antigen binding receptors on the cell membrane called T-cell receptor (TCR) and can rapidly proliferate and differentiate upon receiving a stimulus from APCs. T cells possess different TCRs that can bind to specific foreign ligands. After antigen presentation, T cells differentiate into either cytotoxic T cells (CD8+ cells) or T-helper (Th) cells (CD4+ cells)²¹⁰. CD8+ cytotoxic T cells are involved in the destruction of cells infected by pathogens and the killing of tumour cells that express the corresponding antigens to the TCRs. After infection is resolved, most of the cells die and are cleared by macrophages. Nevertheless, a few can survive as memory cells and can differentiate into effector cells upon encountering the same antigen²²⁷. CD4+ Th cells have no cytotoxic activity but mediate the immune response by regulated cytokine release to control other cells. Most Th cells die upon resolution of infection like cytotoxic T cells with a few remaining as memory cells²²⁸. B cells can recognise antigens directly through the antibodies expressed on their cell surface and upon activation they undergo proliferation and differentiate into antibody-secreting plasma cells or memory B cells. Plasma cells produce large amounts of antibodies and provide the tissue with protection against pathogens, they usually die when the infection is resolved. On the other hand, memory B cells survive the infection and continue to express antigen-binding receptors to be called upon to respond quickly by producing antibodies²²⁹.

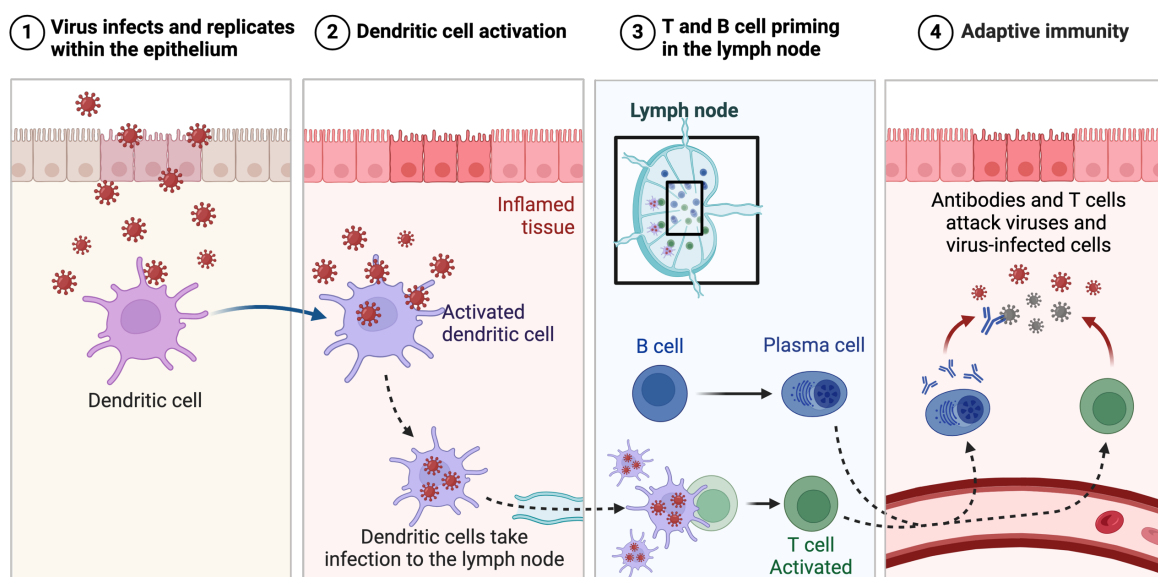


Figure 10. Mechanisms of adaptive immunity

The adaptive immunity, involves antigen-specific lymphocytes reacting to antigens and forming immunological memory. These responses are created through the clonal selection of lymphocytes. Adapted from Janeway et al. 2001²¹⁰. The figure has been created using Biorender.

For a long time, the absence of immunological memory in innate immunity was used to distinguish it from adaptive immunity. Initial studies showed a prior infection can provide protection against infection with unrelated pathogens dependent on macrophages and pro-inflammatory cytokine production^{230,231}. The term 'trained immunity' was first introduced in 2011 and describes the immunological memory response of the innate immune cells²³². After an initial stimuli the cells return to an inactivated state but the epigenetic changes and metabolic rewiring enable a faster and stronger response upon repeated encounter with an antigen²³³. PAMPs and DAMPs are classic inducers of trained immunity in the circulation and tissues as well as in hematopoietic stem cells (HPSCs) in the bone marrow²³⁴. This concept was fully demonstrated when the non-specific protective effects of the Bacillus Calmette-Guérin (BCG) vaccine were reported. BCG vaccination in severe combined immunodeficient (SCID) mice, which lack T and B lymphocytes, against *Mycobacterium tuberculosis* showed protection and reduced mortality when exposed to lethal *Candida albicans* infection²³⁵. Monocytes trained *in vitro* with *C. albicans* cell wall component β -glucan can maintain the ability to produce pro-inflammatory cytokines after LPS re-exposure when compared to non-trained cells²³⁶. The magnitude and the duration of the stimulation can lead to different stages of trained immunity in monocytes with regard to activation, priming, training and tolerance. Priming occurs as a result of the first stimulus changing the functional state of the cells. As the cell does not return to basal level, the impact of the second challenge in the primed cell is often additive to the original stimuli. In contrast to primed cells, in trained cells the immune activation status returns to basal levels following removal of the stimulus while the epigenetic changes remain. In contrast to priming and training, innate immune tolerance can also occur at which point the cell is unable to activate gene transcription resulting in blunted innate immune function²³³.

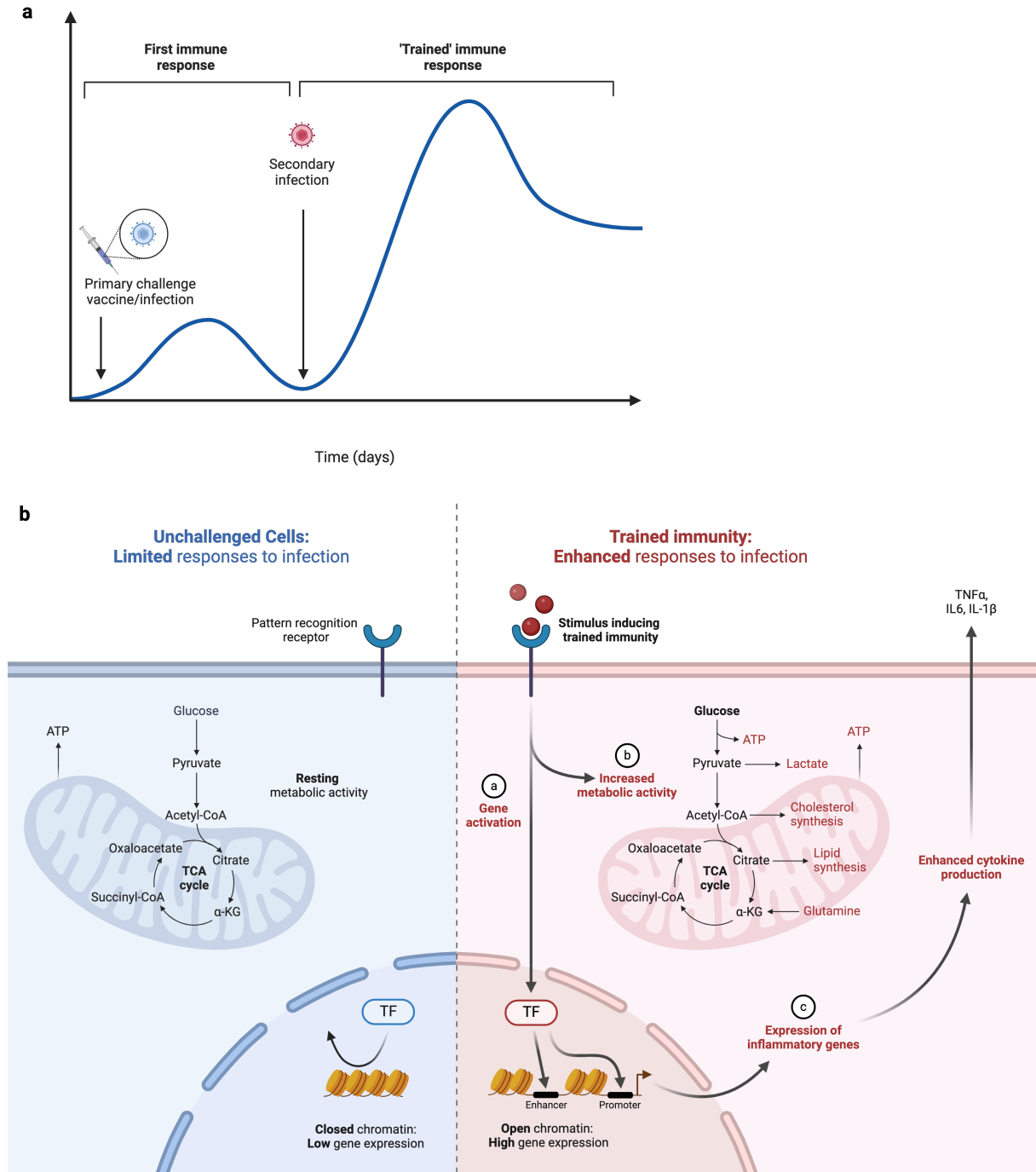


Figure 11. Mechanisms of trained immunity

Trained immunity is defined as an enhanced state of innate immune response to different pathogens after an initial challenge (a). Certain microbial ligands capable of binding to pattern recognition receptors can induce metabolic and epigenetic changes in innate immune cells (b) ATP: Adenosine triphosphate, TCA: Tricarboxylic acid cycle, α -KG: Ketoglutaric acid, TF: Transcription factor, $\text{TNF}\alpha$: Tumour necrosis factor, IL-6: Interleukin-6, IL-1 β : Interleukin-1 beta. Adapted from Netea et al. 2020²³⁷. The figure has been created using Biorender.

Levels of pro- or anti-inflammatory cytokines and chemokines (released mainly from immune cells) as well as growth factors, eicosanoids and proteins regulate inflammation²³⁸. Pro-inflammatory cytokines include IL-1, IL-6, interleukin-15 (IL-15), interleukin-17 (IL-17), interleukin-23 (IL-23), $\text{TNF-}\alpha$ and IFN- γ , anti-inflammatory cytokines include interleukin-4 (IL-

4), interleukin-10 (IL-10), interleukin-13 (IL-13) and transforming growth factor beta (TGF- β)²³⁸. Chemokines are small signalling peptides that play important roles in leukocyte recruitment. The major chemokines capable of influencing the activity of infiltrating immune cells belong to the CC and CXC families²³⁹. Eicosanoids, which function as lipid mediators, comprise an important category of inflammation mediators. They arise from oxidation of arachidonic acid (AA) and PUFAs by COX, LOX and CYP enzymes²⁴⁰. Even though AA serves as the primary precursor for eicosanoids, it is not freely available within the cell. Following activation by an inflammatory stimulus and subsequent Ca^{2+} influx, cytoplasmic phospholipase A₂ (cPLA₂) translocates to the membrane, resulting in free AA via cleavage from membrane phospholipids^{241,242}. AA can subsequently be converted into different eicosanoids which include prostaglandins (PGs), leukotrienes (LTs), lipoxins (LXs) and thromboxanes (TXs) generated by different enzymes. Other PUFAs such as eicosapentaenoic acid (EPA) and dihomo- γ -linolenic acid (DGLA) can serve use as eicosanoid precursors²⁴³. Prostaglandin E₂ (PGE₂) can cause vasodilation and stimulate hyperalgesia and fever²⁴⁴, in turn AA-derived lipoxins and dietary omega-3 fatty acid-derived resolvins and protectins and promote the resolution of inflammation and tissue repair^{245,246}.

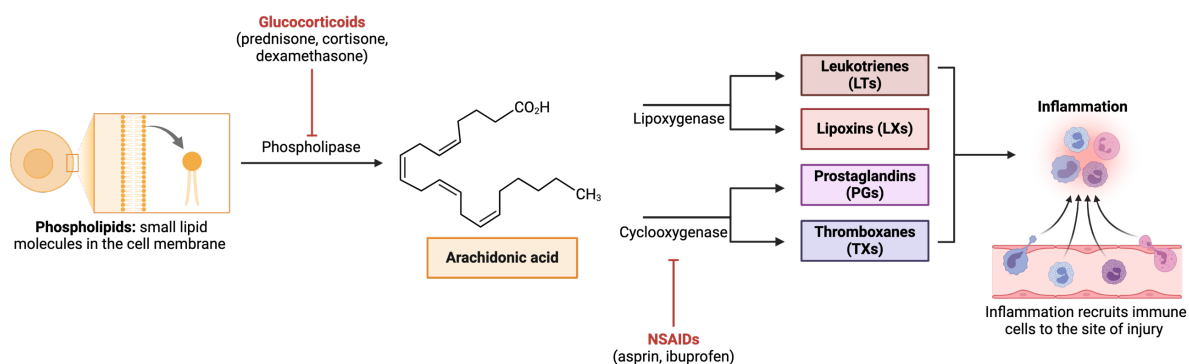


Figure 12. Overview of eicosanoid biosynthesis

Eicosanoid production from AA begins upon various stimuli, triggering the release cytosolic phospholipase A₂ (cPLA₂). The free AA can then be made into bioactive eicosanoids via the COX or LOX pathways. LOX enzymes facilitate the creation of LTs and LXs. COX enzymes, including the constitutive COX-1 and inducible COX-2, convert AA into PGs and TXs. Adapted from Dennis et al. 2020²⁴⁰. The figure has been created using Biorender.

1.2.1. Necroinflammation

Necroinflammation can be defined as the inflammatory response to necrotic cell death. Necrotic cell death occurs in both healthy and pathological conditions when highly immunogenic intracellular molecules and organelles are released into the microenvironment. Multiple regulated cell death modalities share the release of DAMPs or alarmins. The majority

of them also actively control the immune system through the production and/or maturation of pro- or anti-inflammatory cytokines/chemokines. Inflammation that occurs in the absence of any microorganisms has been termed 'sterile inflammation', with necroinflammation being the most common mechanism²⁴⁷.

At any time, a cell undergoes necrotic-type of cell death, DAMPs are released and can potentially bind to different molecules or receptors on various other cells in the microenvironment. At the same time, various suppressing/inhibiting DAMPs (SAMPs or iDAMPs) can be released²⁴⁸. DAMPs were initially referred to as endogenous ligands that can interact with TLRs on cells of the innate immune system^{216,249}. Constitutive DAMPs do not require protein synthesis and are rapidly released under certain conditions of major cell stress or tissue injury. DAMPs can be divided into different categories: i) detached molecules inside a cell under stress, ii) expressed molecules on the surface of a cell under stress, iii) secreted during early regulated necrosis, iv) released upon plasma membrane rupture or v) discarded from the extracellular matrix (ECM)²⁵⁰. Another category of DAMPs that are referred to as exogenous DAMPs are still yet to be identified and categorized. A clear distinction between PAMPs and exogenous DAMPs is difficult to make but for the time being the metal allergens are mainly regarded as exogenous DAMPs through innate immune activation via TLR4 stimulation²⁵¹. There is also evidence that DAMPs can act as triggers during bacterial and viral infections²⁵². Most studied DAMPs are summarized in Table 1-2.

Table 1-2. List of DAMPs, origins and receptors

	Origins	PPRs
<i>Intracellular</i>		
ATP ^{253,254}	Mitochondria	P ₂ Y ₂ , P ₂ X ₇
mtDNA ²⁵⁵	Mitochondria	TLR9
Mitochondrial transcription factor A ²⁵⁶	Mitochondria	TLR9, RAGE
mtROS ²⁵⁷	Mitochondria	NLRP3
Cyclophilin A ²⁵⁸	Nucleus	CD147
dsDNA ^{259–261}	Nucleus	cGAS, AIM2
RNA ²⁶²	Nucleus	TLR3
Histones ^{263,264}	Nucleus	TLR2, TLR4, NLRP3
HMGB1 ^{265–267}	Nucleus, autophagosome	TLR2, TLR4, TLR9, RAGE
Heat shock proteins (HSPs) ^{268–270}	Cytosol	TLR2, TLR4, CD91

S-100 ^{271,272}	Cytosol	TLR4, RAGE
Myosin ²⁷³	Cytosol	TLR2, TLR4, RAGE
Actin ²⁷⁴	Cytosol	DNGR-1
Uric acid ²⁷⁵	Cytosol	NLRP3
Calreticulin (CRT) ^{269,276}	Endoplasmic Reticulum (ER)	CD91
Extracellular		
Aggrecan ²⁷⁷	Proteoglycan	TLR2
Biglycan ^{278,279}	Proteoglycan	TLR2, TLR4, NLRP3
Decorin ²⁸⁰	Proteoglycan	TLR2, TLR4
Versican ²⁸¹	Proteoglycan	TLR2, TLR6, CD14
Heparan sulphate ^{282,283}	Glycosaminoglycan	TLR4, RAGE
Low-molecular-weight hyaluronan ^{284–287}	Glycosaminoglycan	CD44, TLR2, TLR4, NLRP3
Tenascin-C ²⁸⁸	ECM glycoprotein	TLR4
Fibrinogen ²⁸⁹	ECM glycoprotein	TLR4
Fibronectin ^{290–292}	ECM glycoprotein	TLR2, TLR4

DNGR-1: Dendritic cell NK lectin group receptor-1, NLRP3: NLR family pyrin domain containing 3, RAGE: Receptor for advanced glycation endproducts, TLR2: Toll-like receptor 2, TLR4: Toll-like receptor 4, TLR6: Toll-like receptor 6, TLR9: Toll-like receptor 9, P2X₇: P2X purinoceptor 7

Dying cells can release or expose DAMPs, providing potential adjuvants to promote antigen processing and presentation^{293,294}. Immunogenic cell death (ICD) can be regarded as a cell death modality that can elicit an immune response in the host¹ and different DAMPs mediate distinct immunostimulatory responses^{254,295}. Necrosis is the primary type of cell death that leads to the passive release of DAMPs, while necroptosis, apoptosis, pyroptosis, ferroptosis, and the formation of extracellular traps also contribute to the release of DAMPs²⁹⁶. As apoptosis is a regulated cell death without the loss of membrane, it is usually considered as immunotolerogenic, while necrotic type of regulated cell death is regarded as immunogenic²⁹⁷. In apoptosis, caspase activated DNase (CAD) causes the DNA fragmentation, producing shorter DNA fragments and weakening the immunostimulatory properties of cytosolic DNA, while in necroptosis much longer DNA fragments are released²⁹⁸. Of note, apoptotic cells release nuclear DNA in a time-dependent manner²⁹⁹. Similarly, the full length interleukin-33 (IL-33) released during necroptotic cell death undergoes caspase-dependent proteolysis into a nonimmunological form during apoptosis³⁰⁰. Caspase activation and ROS production in apoptosis oxidises high mobility group box 1 protein (HMGB1), one of the well-defined DAMPs and renders it immunologically silent contributing to an immunologically tolerant state³⁰¹. ATP can be released from apoptotic cells as a result of ER stress with the

combination of CRT expression on cell surface that facilitates the uptake of dying cells by APCs³⁰². Caspases are essential for pannexin 1- or autophagy-dependent ATP secretion^{303,304}. ATP as well as uridine triphosphate (UTP) were also shown to be essential “eat-me” signals released by apoptotic cells for phagocyte recruitment *in vivo*³⁰⁵. Even though TNF- or LPS-induced necroptosis significantly halts the cytokine and chemokine production³⁰⁶, release of ATP and several cytokines were also detected from cells undergoing necroptosis upon RIPK3 activation such as chemokine (C-X-C motif) ligand 1 (CXCL1), chemokine (C-X-C motif) ligand 2 (CXCL2) and chemokine (C-C motif) ligand 2 (CCL2) even after they’ve lost plasma membrane integrity influencing myeloid cell migration and CD8+ T cells³⁰⁷. Another study also showed interleukin-8 (IL-8 or chemokine (C-X-C motif) ligand 8, CXCL8) and granulocyte-macrophage colony-stimulating factor (GM-CSF) also known as colony stimulating factor 2 (CSF2) were released from necroptotic cells in addition to CXCL1 and CXCL2³⁰⁸. IL-6 release was also associated with necrotic but not with apoptotic cells³⁰⁹. Necroptotic tumour cells can lead to bone-marrow derived DC maturation and cross-prime CD8+ T cells³¹⁰. TRAIL-induced secretome has been shown to recruit M2-like immune cells supporting tumour growth³¹¹. Pyroptosis has been considered as one of the most inflammatory cell death modality, since in addition to the release of HMGB1³¹² upon cell rupture, cells release ATP³¹³ and the pro-inflammatory cytokine IL-1 β via the GSDMD pores without requiring cell rupture³¹⁴. Release of IL-1 β were shown to promote cancer development and progression, which can potentially make pyroptosis a pro-tumorigenic cell death modality³¹⁵. Ca²⁺ influx caused by pyroptosis can also mediate the generation of eicosanoids³¹⁶. PGE₂ is referred to as an inhibitory DAMP, as the necrotic cell supernatants containing it inhibit inflammatory responses³¹⁷. Independent of the canonical cell death machinery, oligomerization of the ninjurin-1 (NINJ1) protein can also disrupt membranes and lead to release of DAMPs in apoptosis, ferroptosis and pyroptosis but not in necroptosis^{318,319}. The clearance of necroptotic and pyroptotic cells by macrophages also depends on the exposed phosphatidylserine (PS) residues on the cell membrane that is normally present in the inner leaflet^{313,320,321}.

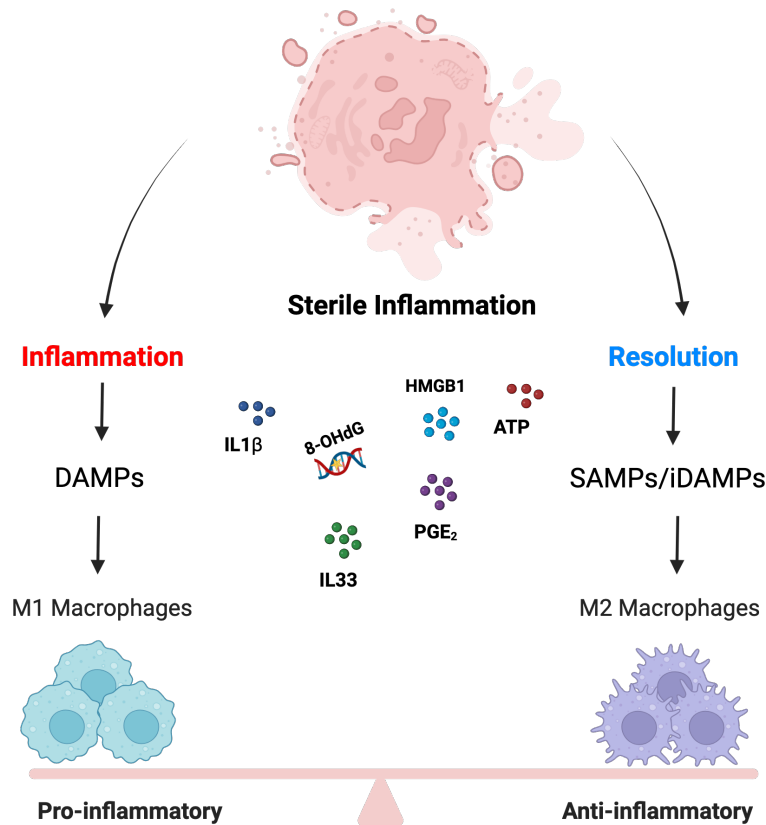


Figure 14. Effect of DAMPs and SAMPs/iDAMPs released from dying cells on macrophage differentiation

DAMPs, SAMPs/iDAMPs released during sterile inflammation, depending on the different forms of cell death can result in activation of many different receptors subsequently generating different stimuli. Adapted from Koncz et al. 2023³²². The figure has been created using Biorender.

1.2.2. Ferroptosis and DAMP release

Ferroptotic cell death is also capable of releasing DAMPs that promote sterile inflammation and the development of numerous inflammatory diseases. The release of oxidized phospholipids (oxPLs), the lipid peroxidation by-product 4-HNE, HMGB1 and ATP were reported as potential immune modulators released from ferroptotic cells³²³. Ferroptotic cells release HMGB1 through an autophagy-dependent process, which activates immune cells by binding to RAGE, rather than TLR4³²⁴. 4-HNE can inhibit stimulator of interferon genes (STING) activation by its direct carbonylation in mouse primary peritoneal macrophages³²⁵. In contrast, in a mouse model of pancreatic ductal adenocarcinoma (PDAC), it was suggested that ferroptotic cells release the oxidized nucleotide 8-hydroxy-2'-deoxyguanosine (8-OHdG) and activate the STING pathway, leading to macrophage infiltration and pro-tumour M2 polarization³²⁶. KRAS^{G12D} released by ferroptotic cells induces AGER-dependent M2 polarization of macrophages through the activation of STAT3-mediated fatty acid oxidation³²⁷.

Ferroptotic cells can also secrete CCL2 and chemokine (C-C motif) ligand 7 (CCL7) that can induce the recruitment of macrophages³²⁸. IL-33, an alarmin associated with necroptosis, was also shown to be released from ferroptotic cells³²⁹. oxPLs can also be regarded as immunomodulatory³³⁰, as 1-stearoyl-2-15-HpETE-sn-glycero-3-phosphatidylethanolamine (SAPE-OOH), can act as an eat-me signal on the surface of ferroptotic cells and recruit macrophages via binding to TLR2³³¹. Oxidized phosphatidylcholine can inhibit the maturation and activation of bone marrow derived dendritic cells (BMDCs)³³². Elevated levels of COX2, an enzyme crucial for producing the inflammatory mediator PGE₂ from AA, have been recognized as a characteristic feature of ferroptosis¹²⁰. Knockdown of *Gpx4* in NIH-3T3 cells led to the release of COX2-dependent PGE₂ and PGF_{2α}³³³. Additionally, increased levels of PGE₂ were noted in keratinocytes from *Gpx4*-deficient mice³³⁴.

Two studies have reported the kinetic release of key DAMPs from ferroptotic cancer cells and their associated potential, by comparing early and late stages of ferroptosis^{335,336}. Both studies have demonstrated that ferroptotic cancer cells release DAMPs such as HMGB1, ATP, and calreticulin on their surface. Efimova et al.³³⁵ argue that 'early' ferroptotic cancer cells can be effectively engulfed by BMDCs, promoting their maturation and activation, and can protect mice from tumour development when used as a prophylactic vaccine. However, this effect was not seen with 'late' ferroptotic cells. In contrast, Wiernicki et al.³³⁶ report that 'early' ferroptotic cells inhibit BMDC maturation and engulfment, reducing antigen cross-presentation and predominantly suppressing an antitumor immune response. While both studies used the same cell line model, the differences in the amount of cell death induced by RSL3 in Efimova et al.'s study and inducible knockdown in Wiernicki et al.'s study, or metabolic differences, likely account for the discrepancies in results.

1.2.3. Ferroptosis-associated immune response

As numerous DAMPs have been shown to be released from ferroptotic cells, it has long been argued whether ferroptosis is an inflammatory type of cell death. In many cases, the pro- and anti-tumour effects of ferroptosis were documented under different conditions. The anti-tumour response driven by CD8+ T cells can be reversed when combined with ferroptosis-selective inhibitor Lip-1³³⁷. Additionally, IFN-γ secretion from CD8 T-cells was found to synergize with free AA to enhance ACSL4-mediated AA lipid integration, thereby increasing

the sensitivity of tumour cells to ferroptosis³³⁸. Even though tissue ferroptosis can enhance an anti-tumour immune response, recent studies have shown that M2 macrophages are more susceptible to ferroptosis than M1 macrophages due to having lower levels of nitric oxide synthase (iNOS)³³⁹. Tumour-associated macrophages (TAMs) are highly plastic and can exhibit either an M1 or M2 phenotype, leading to tumour-attacking or tumour-protective activities, respectively. Conditional knockout of *Gpx4* in macrophages can lead to high levels of hydrogen peroxide, inducing DNA mutations and the development of intestinal tumours³⁴⁰. Pathologically activated neutrophils, known as polymorphonuclear myeloid-derived suppressor cells (PMN-MDSCs), can undergo ferroptosis and release immunosuppressive oxygenated lipids through fatty acid transport protein 2 (FATP2), resulting in overall immunosuppression³⁴¹. DCs that were exposed to ferroptotic cells showed reduced ability to cross-present cancer associated antigens³³⁶. The accumulation of oxidatively truncated lipids within lipid bodies causes the intracellular trapping of MHC complexes, further impairing the cross-presentation capability of DCs^{342,343}. The upregulation of CD36 on CD8+ T cells is another way of weakening the anti-tumour immunity as this upregulation promotes the uptake of PUFAs, leading to ferroptosis in CD8+ T cells^{344,345}. Additionally, activated regulatory T cells (T_{reg}) were vulnerable to T_{reg} -selective *Gpx4* deletion, which enhanced anti-tumour immunity³⁴⁶. Taken together, these studies highlight that the effect of ferroptosis on various cell types within the tumour microenvironment (TME) is highly diverse.

Ischemia is another condition in which ferroptosis was shown to play an important part. It occurs when the blood supply in tissues is highly reduced, resulting in deficiencies in oxygen and other essential molecules. Restoration of blood supply to the tissue (reperfusion) causes further damage accompanied with cell death, oxidative stress damage and ultimately results in tissue injury³⁴⁷. Linkermann et al. showed that ferroptosis mediates ischemia-reperfusion injury (IRI) induced immune cell infiltrations of the cremaster muscle where Fer-1 inhibited leukocyte transmigration³⁴⁸. Several other studies have shown that ferroptosis is involved in IRI in the liver¹⁰⁵, brain³⁴⁹ and heart¹⁵⁰. Additionally, the use of ferrostatins and lipoxstatins can protect mice used in these studies. Furthermore, in IRI following heart transplantation ferroptosis was shown to regulate neutrophil recruitment by promoting adhesion of neutrophils to coronary vascular endothelial cells through a TLR4-mediated signalling pathway³⁵⁰. In both IRI and acute kidney injury (AKI), Fer-1 treatment was shown to reduce

immune cell infiltrations and decreased expression levels of inflammatory cytokines and chemokines^{329,348}. In the severe form of nonalcoholic fatty liver disease (NAFLD) called nonalcoholic steatohepatitis (NASH), the protein levels of proinflammatory cytokines, including TNF α , IL-1 β and IL-6 were significantly increased upon RSL3 treatment, exacerbating the NASH-related biomarkers in a process that can be reversed upon iron chelation, liprostatins or activation of GPX4^{351,352}. In Crohn's disease PUFAs but not MUFAs can trigger ACSL4-mediated lipid peroxidation and the GPX4-repressible induction of cytokines intestinal epithelial cells³⁵³. In vivo experiments have demonstrated that Fer-1 has a therapeutic effect on numerous lung diseases including LPS-induced acute lung injury (ALI)³⁵⁴, chronic obstructive pulmonary disease (COPD)³⁵⁵ and radiation-induced lung fibrosis (RILF)³⁵⁶. Fer-1 reduces the levels of proinflammatory cytokines IL-6 and TNF- α in bronchoalveolar lavage (BAL) fluid, thereby alleviating ferroptosis.

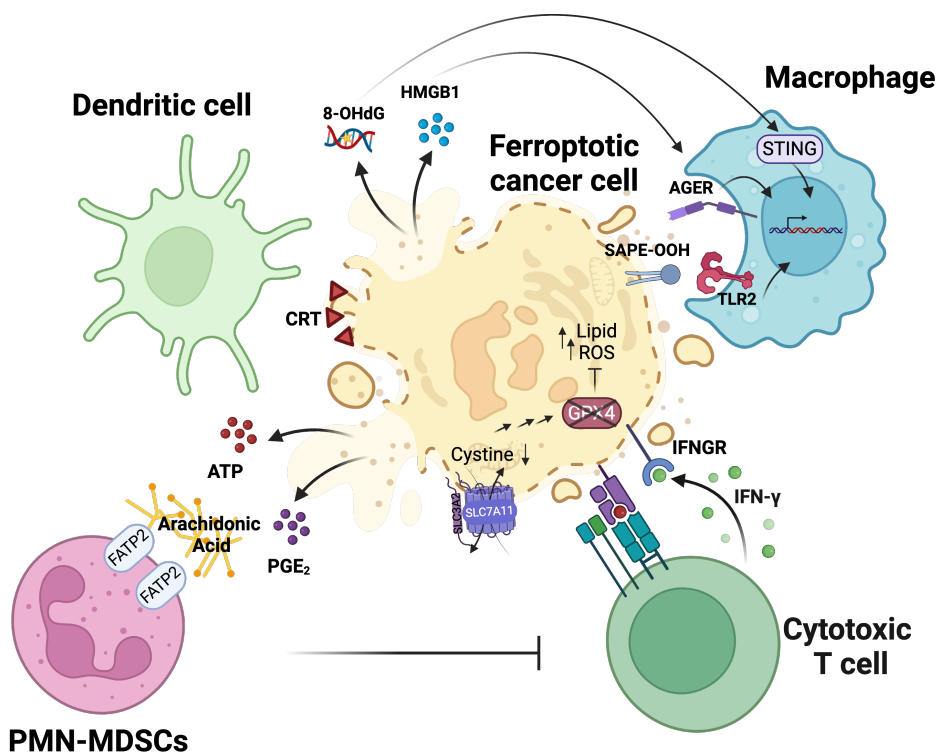


Figure 15. Immunomodulatory roles of ferroptosis

Ferroptosis triggers the release of various types of danger-associated molecular patterns (DAMPs), influencing the responses of dendritic cells and macrophages. The oxidized phospholipid SAPE-OOH can be identified by TLR2 on macrophages, facilitating phagocytosis. Additionally, released 8-OHdG can interact with cGAS, activating STING-mediated macrophage responses that support tumours progression. Polymorphonuclear myeloid-derived suppressor cells (PMN-MDSCs) that suppress the antitumor immune response can undergo ferroptosis, releasing immunosuppressive oxidized lipids into the tumor microenvironment (TME), which promotes tumor growth. The antitumor activity of CD8+ T cells can be influenced by ferroptosis. IFN- γ secreted by activated CD8+ T cells can reduce the expression of system Xc- (SLC7A11/SLC3A2), making tumor cells more susceptible to ferroptosis. Adapted from Yapici and Bebbler, 2024¹¹². The figure has been created using Biorender.

1.3. Aims of this study

Ferroptosis is characterized by the accumulation of lipid reactive oxygen species (ROS), causing irreparable oxidative damage within the cell and the lipid bilayer³⁵⁷. Oxidation of lipids can either happen by Fenton reaction with iron in a non-enzymatic manner or by oxygenation and esterification of phosphatidylethanolamine (PE) containing polyunsaturated fatty acids (PUFAs)¹¹⁷. The enzyme-dependent production of lipid peroxides is controlled by acyl-CoA synthetase long-chain family 4 (ACSL4), lysophosphatidylcholine acyltransferase 3 (LPCAT3) and lipoxygenases (LOXs)¹¹⁷. More importantly, ACSL4 was identified as an essential pro-ferroptotic gene where lipid peroxidation upon GPX4 inhibition requires its presence¹⁵³. Generation of lipid ROS is prevented by glutathione peroxidase 4 (GPX4) through reduction of the toxic lipid peroxides to their corresponding nontoxic lipid alcohols in the presence of reduced glutathione (GSH) in which GSH works as a cofactor¹²⁰. GSH synthesis within the cell depends on the availability of intracellular cysteine³⁵⁷. Cysteine can either be synthesized from methionine via the transsulfuration pathway¹²¹ or by transporting its precursor cystine into the cell via the glutamate-cysteine antiporter system xc-¹⁸⁰. Ferroptosis can be induced by small molecule inhibition of GPX4 using RSL3¹⁰⁷ or ML210¹²⁰ or by inhibiting system xc- using erastin¹⁰². Vice versa, lipophilic anti-oxidants such as Fer-1 and Lip-1 as well as iron chelators were shown to inhibit ferroptosis¹⁰³. Recently, the ferroptosis suppressor protein 1 (FSP1) was found to prevent lipid peroxidation and suppress ferroptosis through a mechanism that is independent of GPX4. Myristoylation of FSP1 mediates its recruitment to the plasma membrane where it reduces coenzyme Q10 (CoQ) to the lipophilic radical scavenger ubiquinol that prevents the propagation of lipid peroxides^{125,126}.

Programmed necrosis can result in the release of cytosolic damage-associated molecular patterns (DAMPs) and alarmins that ultimately result in the initiation of inflammation referred to as “necroinflammation”³⁵⁸. Several studies revealed the set of proteins expressed and secreted into the extracellular space, otherwise known as secretome, of pyroptotic and necroptotic cells^{359,360} yet the class of released agents released from ferroptotic cells remains elusive. Interestingly, ferroptosis inhibitors exhibited significant anti-inflammatory effects in numerous disease models. However, it is unknown if and how the contents of ferroptotic cells directly elicit an inflammatory response. Based on the evidence so far, ferroptosis is likely to play an important role in inflammation. Nevertheless, it is as yet uncharacterized how exactly

ferroptosis plays a role in normal tissue homeostasis and regulation of inflammation. It is also still unresolved whether ferroptosis alone is sufficient to directly initiate inflammation or whether it contributes to the induction of other secondary inflammatory pathways or inflammatory types of cell death. Therefore, this project aims to understand how ferroptosis might trigger inflammation and its potential implications for human diseases.

Therefore, the following study aims were defined:

1. Identifying inflammatory molecules released from ferroptotic cells
2. Elucidating signalling cascades inducing cytokine production in macrophages exposed to ferroptotic cells
3. Determining the influence of ferroptosis induced by GPX4 deletion *in vivo*

2. Results

2.1. Characterisation of proteomes released from ferroptotic cells

2.1.1. Experimental system for the generation of ferroptotic secretome analysis

The nature of possible DAMPs directly released from ferroptotic cells, the mechanisms underlying the inflammatory response triggered in immune cells, and whether or not ferroptosis actually causes inflammation are unknown. In order to investigate these aspects, mouse embryonic fibroblasts (MEFs) named Pfa1³⁶¹ cells, in which *Gpx4* can be deleted with tamoxifen (4-OHT) treatment, were employed to produce ferroptotic supernatants that do not include ferroptosis-inducing small molecules for the investigation of the ferroptotic secretome¹⁰⁵. The fact that only Fer-1 as opposed to the necroptosis inhibitors nec1s/GSK872 and the pan-caspase inhibitor zVad was able to completely rescue cell death, confirms that *Gpx4* deletion causes ferroptotic cell death (Figure 15A, 15B). In order to show that efficient knockout of GPX4 had taken place, a kinetic experiment was performed at 24-hour intervals. As seen in Figure 15C, already after 48 hours of tamoxifen treatment, GPX4 was indeed efficiently deleted. Ferroptotic cell death was accompanied by release of lactate dehydrogenase (LDH) into the media (Figure 15D) while FSP1 overexpression in the presence of *Gpx4* deletion (Pfa1-mFSP1 OE¹²⁵ cells) can revert this phenotype and the cell death (Figure 15E). Furthermore, cell death was accompanied by the accumulation of lipid ROS confirming the induction of ferroptotic cell death in a 72-hour time period (Figure 15F). In live-cell imaging experiments using the IncuCyte, kinetics of lipid ROS accumulation and cell death can be monitored simultaneously and quantification shows that cell death starts around 40 hours post 4-OHT treatment with cells completely dying after 72 hours (Figure 15B, 15G) with lipidROS accumulation increasing (Figure 15H). These data confirm that inducible deletion of *Gpx4* is a valuable experimental model to study ferroptotic cell death.

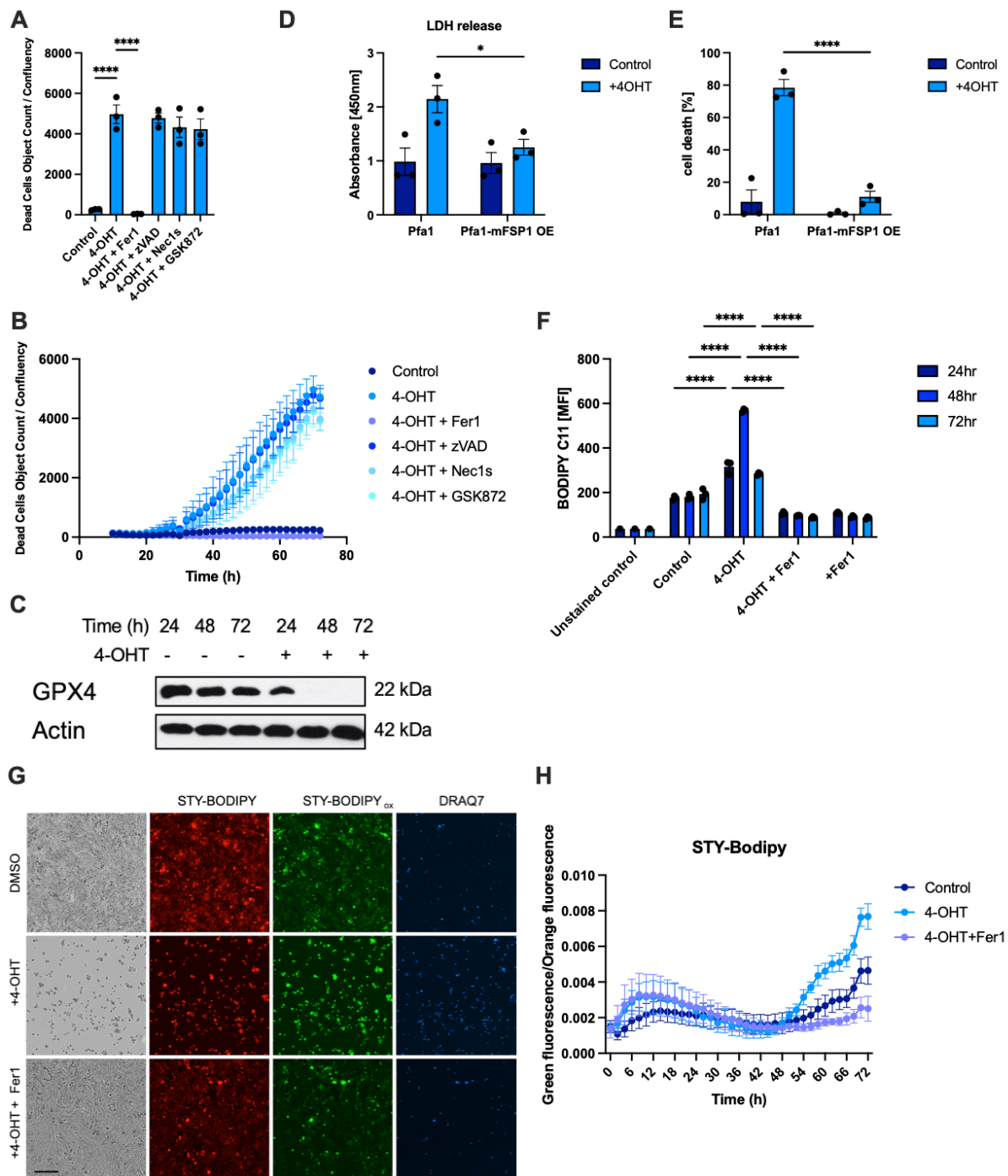


Figure 15. Inducible *Gpx4* deletion leads to ferroptosis.

A) Pfa1 cells treated with +/- 4OHT [1 μ M] +/- Ferrostatin-1 (Fer1) [1 μ M] +/- zVAD [20 μ M] +/- Nec1s [10 μ M] +/- GSK872 [3,33 μ M] for 72h, cell death was measured with by IncuCyte live cell imaging. Images were acquired every 2h using the IncuCyte SX5 bioimaging platform. **B**) Time kinetic of the cells treated in (A) also measured for cell death using DRAQ7 [100nM] by IncuCyte live cell imaging. Images were acquired every 2h using the IncuCyte SX5 bioimaging platform. **C**) Pfa1 cells treated +/- 4OHT [1 μ M] were subjected to Western Blot analysis of the indicated proteins in a time kinetic. **D**) Parental Pfa1 or Pfa1 cells with stable FSP1 overexpression¹²⁵ were treated with 4OHT [1 μ M] for 72 h. Supernatants from cells and treatments were subjected to LDH quantification. **E**) Parental Pfa1 or Pfa1 cells with stable FSP1 overexpression¹²⁵ were stained with Draq7 [100nM] and treated with 4OHT [1 μ M] for 72 h. Cells were imaged for near-infrared (NIR) count as a measure of dead cells using the IncuCyte live cell imaging system and cell death was normalized to confluency. **F**) Pfa1 cells treated with +/- 4OHT [1 μ M] +/- Fer1 [1 μ M] were and stained for lipid ROS accumulation using BODIPY C11. Cells were analysed by flow cytometry. **G**) Pfa1 cells treated as in (F), and stained for lipid ROS

accumulation using STY-BODIPY [1 μ M] for 72h. Dead cells were visualized using DRAQ7 [100nM] Images were acquired every 2h using the IncuCyte SX5 bioimaging platform, n = 3 biological replicates. **H)** Quantification of cells treated in (G) and stained for lipid ROS accumulation using STY-BODIPY [1 μ M] for 72h. Levels of lipid peroxidation can be monitored by quantifying levels of co-oxidized STY-BODIPY (green, λ_{ex} = 488 nm, λ_{em} = 495–540 nm) emitting green signals over reduced STY-Bodipy (red, λ_{ex} = 561 nm, λ_{em} = 568–630 nm) emitting in the orange spectrum. Representative images are shown. Data are means +/- SEM of at least three independent experiments were applicable. One- or two-way ANOVA was used to calculate p-values. ns: not significant; *: p<0.05; **: p<0.01; ***: p<0.001; ****: p<0.0001. Incucyte experiment (G, H) contributed by Christina Bebbber.

To include an additional genetic system with ferroptosis induction, CRISPR/Cas9-mediated *Gpx4* deletion in RP252.7 mouse small cell lung cancer (SCLC) cells were generated in the laboratory and previously described³⁶². Because of GPX4's essential role, these cells can only be cultured and grown when Fer1 is present in the culture medium. Cells with GPX4 KO selectively died upon withdrawal of Fer1 whereas inhibitors of other cell death modalities weren't successful in preventing this cell death (Figure 16A). Live-cell imaging experiments showed that GPX4 KO cells start to die 3 hours after Fer1 withdrawal and that Fer1 can revert this cell death (Figure 16B, 16C). Deletion of GPX4 was also seen on protein level, confirming the constitutive knockout (Figure 16D). Of note, lipid peroxidation precedes the cell death, being detectable already 1-hour after Fer1 withdrawal (Figure 16E, 16F). These cells therefore can also be used as a second experimental system on which ferroptotic supernatants can be generated.

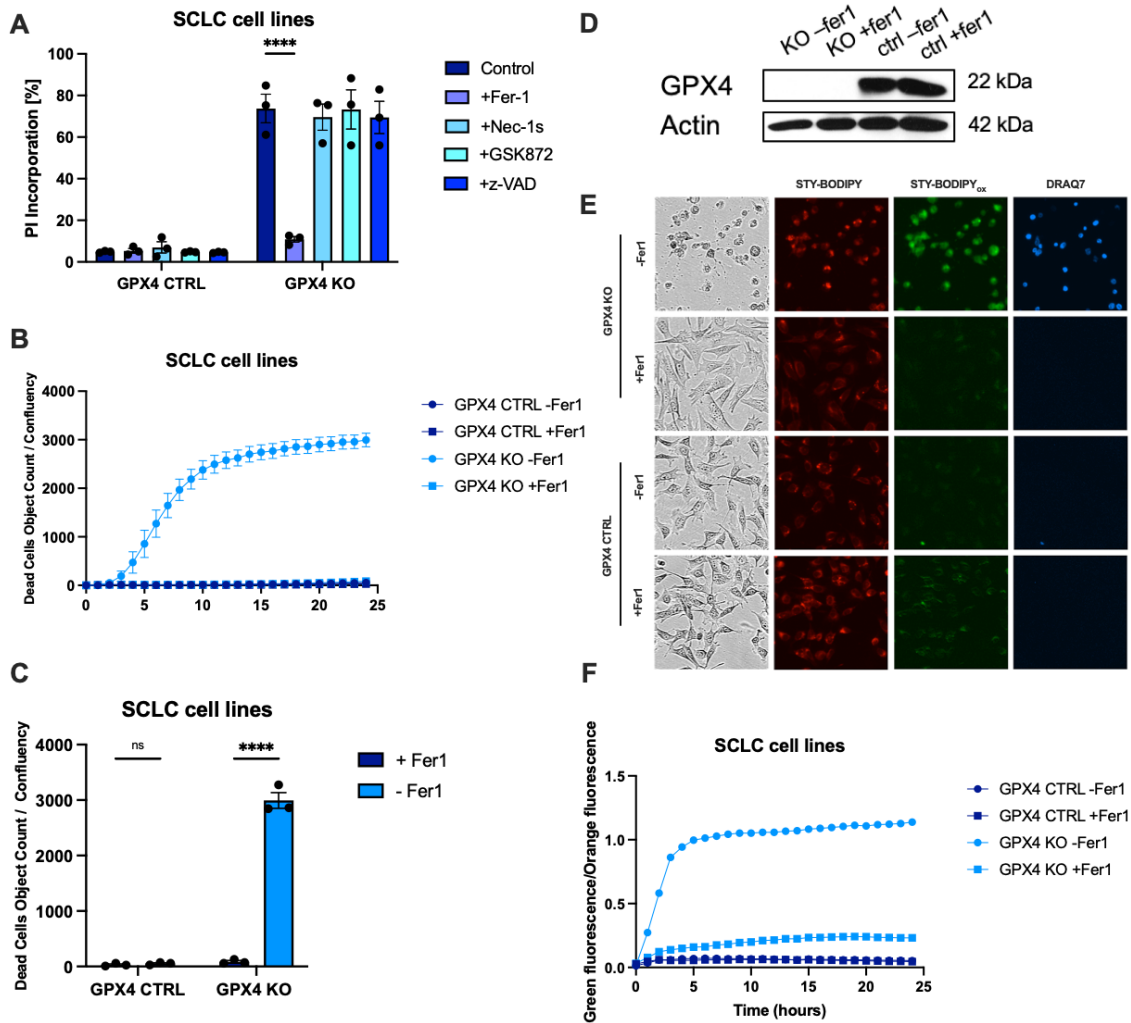


Figure 16. Constitutive *Gpx4* deletion leads to ferroptosis.

A) GPX4 control (GPX4 CTRL) or GPX4-deficient (GPX4 KO) SCLC cell lines³⁶² cultured with +/- Ferrostatin-1 (Fer1) [1 μ M] +/- zVAD [20 μ M] +/- Nec1s [10 μ M] +/- GSK872 [3,33 μ M] for 24h, cell death was measured with PI incorporation (%). Cells were analysed by flow cytometry. **B)** Time kinetic of the cells treated in (A) also measured for cell death using DRAQ7 [100nM] by IncuCyte live cell imaging. Images were acquired every 2h using the IncuCyte SX5 bioimaging platform. **C)** GPX4 CTRL and GPX4 KO cells were stained with DraQ7 [100nM] and culture +/- Fer1 [1 μ M] for 24 h. Cells were imaged for near-infrared (NIR) count as a measure of dead cells using the IncuCyte live cell imaging system and cell death was normalized to confluency. **D)** GPX4 CTRL and GPX4 KO cells treated +/- Fer1 [1 μ M] were subjected to Western Blot analysis of the indicated proteins. **E)** GPX4 CTRL and GPX4 KO cells treated as in (B), and stained for lipid ROS accumulation using STY-BODIPY [1 μ M] for 72h. Dead cells were visualized using DRAQ7 [100nM] Images were acquired every 2h using the IncuCyte SX5 bioimaging platform. **F)** Quantification of cells treated in (E) and stained for lipid ROS accumulation using STY-BODIPY [1 μ M] for 24h. Levels of lipid peroxidation can be monitored by quantifying levels of co-oxidized STY-BODIPY (green, λ_{ex} = 488 nm, λ_{em} = 495–540 nm) emitting green signals over reduced STY-Bodipy (red, λ_{ex} = 561 nm, λ_{em} = 568–630 nm) emitting in the orange spectrum. Data are means +/- SEM of at least three independent experiments were applicable. One- or two-way ANOVA was used to calculate p-values. ns: not significant; *: p<0.05; **: p<0.01; ***: p<0.001; ****: p<0.0001.

2.1.2. Quantitative secretome analysis of precipitated supernatants by SILAC

In order to fully characterize ferroptotic secretomes, mass spectrometry experiments were planned on supernatants from ferroptotic cells. Different experimental set-ups for mass spectrometry have been optimized as high fetal calf serum (FCS) concentrations in the media can affect label-free mass spectrometry³⁶³. However due to the requirement of transferrin that is present in FCS for ferroptosis to take place¹⁵⁰, stable isotope-labelled amino acids (SILAC) and a media supplement that contains insulin, transferrin and sodium selenite (ITS) was used to replace FCS in media during ferroptosis induction. Using Pfa1 cells, different supplement conditions were tested in order to mimic the effect of FCS (Figure 17A). The condition of seeding cells in 10% FCS and replacing media after 40 hours with 0% FCS + 1:100 ITS was chosen as it was the condition that had the highest similarity to normal culture conditions (Figure 17B). For proteomics sample preparation, Pfa1 cells were passaged 6 times with SILAC medium in order to incorporate the light and heavy amino acids³⁶⁴. Supernatants of Pfa1 cells +/- 4OHT were collected filtered, pooled, and concentrated above a molecular weight cut-off of 10 kDa for subsequent semi-quantitative mass spectrometry (Figure 17C). After data processing, 353 proteins were identified, 48 of which were significantly enriched in ferroptotic and 53 were uniquely enriched in live cells (Figure 17D). The 48 proteins were analysed further for functional association networks using STRING (Figure 17E), which revealed enrichment in MHC class II antigen presentation and innate immune system among others (Figure 17F).

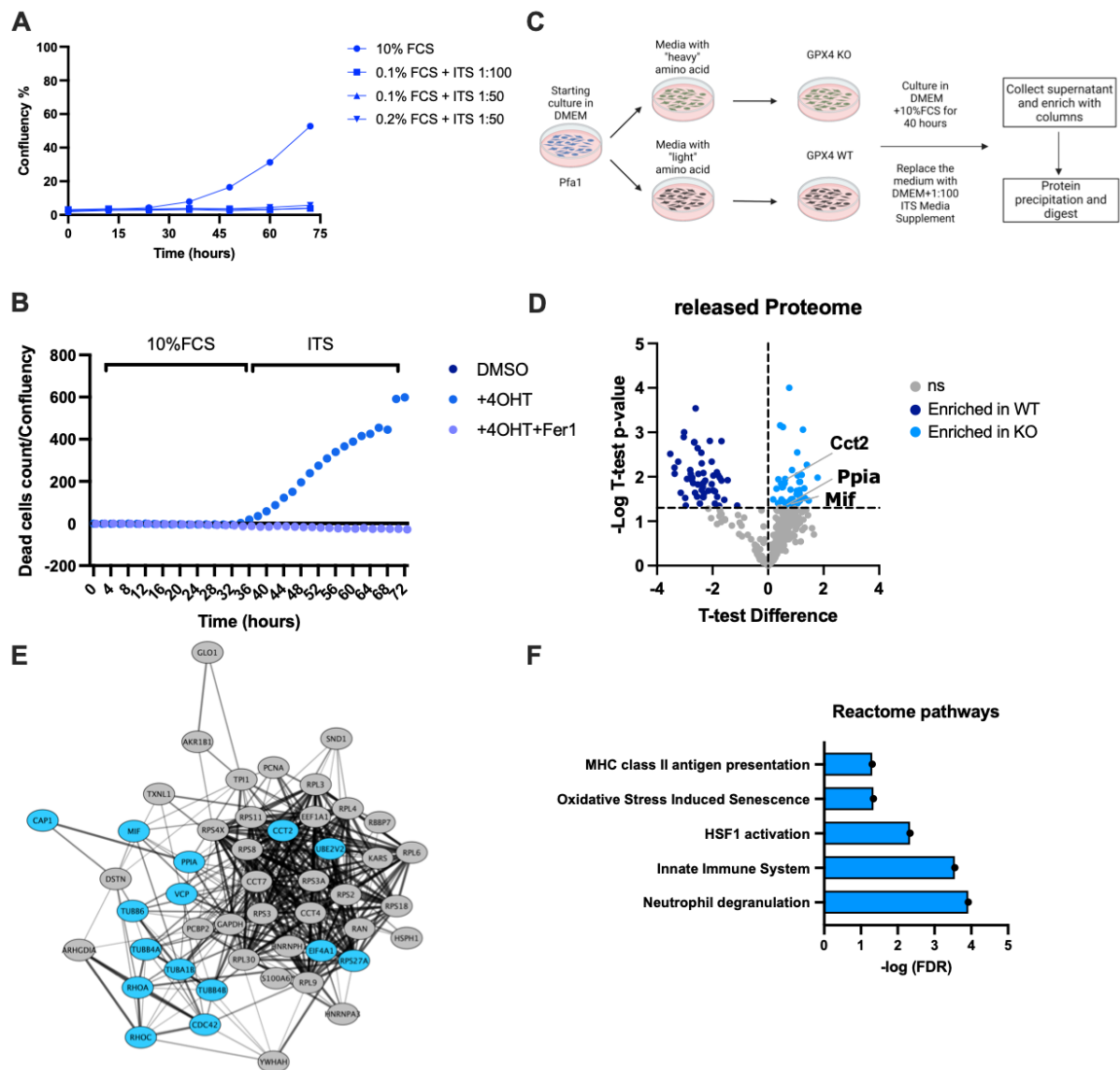


Figure 17. Ferroptotic cells release a passive proteomics secretome.

A) Time kinetic of cellular proliferation were determined with indicated different medium conditions by IncuCyte live cell imaging for 72 hours. Images were acquired every 2h using the IncuCyte SX5 bioimaging platform. **B)** Time kinetic of cells treated with indicated medium conditions were also measured for cell death using DRAQ7 [100nM] by IncuCyte live cell imaging. Images were acquired every 2h using the IncuCyte SX5 bioimaging platform. **C)** Schematic of amino acid labelling strategy by SILAC and experimental design to obtain ferroptotic secretomes (n=3 per condition). **D)** Volcano plot from the total proteomics mass spectrometry data demonstrates the significance of the proteins in WT and KO conditions. **E)** Proteins significantly enriched in ferroptotic secretomes were analysed for protein-protein interaction networks using STRING. **F)** Reactome pathways enriched within ferroptotic supernatants are plotted. All images were created with BioRender.com. One- or two-way ANOVA was used to calculate p-values. ns: not significant; *: p<0.05; **: p<0.01; ***: p<0.001; ****: p<0.0001. Proteomics experiment (D-F) was contributed by Eric Seidel and CECAD proteomics facility.

Macrophage migration inhibitory factor (MIF), which has been shown to play a role in immune system's activation in response to bacteria, as well as to be secreted upon necroptotic cell death, was found among the enriched proteins. Recombinant MIF stimulation of macrophages

results in TNF-alpha production³⁶⁵ and augments M1 polarisation in BMDM in vitro³⁶⁶. By raising cellular GSH levels, MIF has also been demonstrated to lessen oxidative stress and lipid peroxidation both in vitro and in vivo³⁶⁷. A unique feature of MIF is its abundant expression and the fact that it is stored within the cytoplasm pre-made³⁶⁵. The fact that the mRNA levels of MIF were stable (Figure 18A), intracellular protein levels of MIF were depleted upon induction of *Gpx4* deletion (Figure 18B) and extracellular MIF levels increased in supernatants simultaneously suggests that ferroptotic cells can release pre-made proteins passively. Strikingly, FSP1 overexpression was able to diminish MIF release upon ferroptosis induction (Figure 18C). Additionally, GPX4 KO but not control mouse SCLC cell lines (Figure 18D) and the RSL3-treated primary lung fibroblasts (PMLFs) (Figure 18E) showed significant levels of MIF release. MIF release was not unique to ferroptotic cell death as apoptosis induction slightly and necroptosis strongly induced the release of MIF from PMLFs (Figure 18F) supporting the hypothesis that pre-made MIF is preferentially released upon plasma membrane rupture. Of note, the total secretome released from ferroptotic cells lacks the *bona-fide* chemo-cytokines known to be released from cells undergoing apoptosis or necroptosis^{311,359}. For example, PMLFs that undergo apoptosis (TNF/Smac mimetic, TS) or necroptosis (TNF/Smac mimetic/Emricasan, TES) release significant levels of CXCL1 and CXCL2 (Figure 18G, 18H) where ferroptotic cells fails to do so (Figure 18I, 18J). Taken together, our data identify that ferroptotic cells release a secretome with potential for immune modulation.

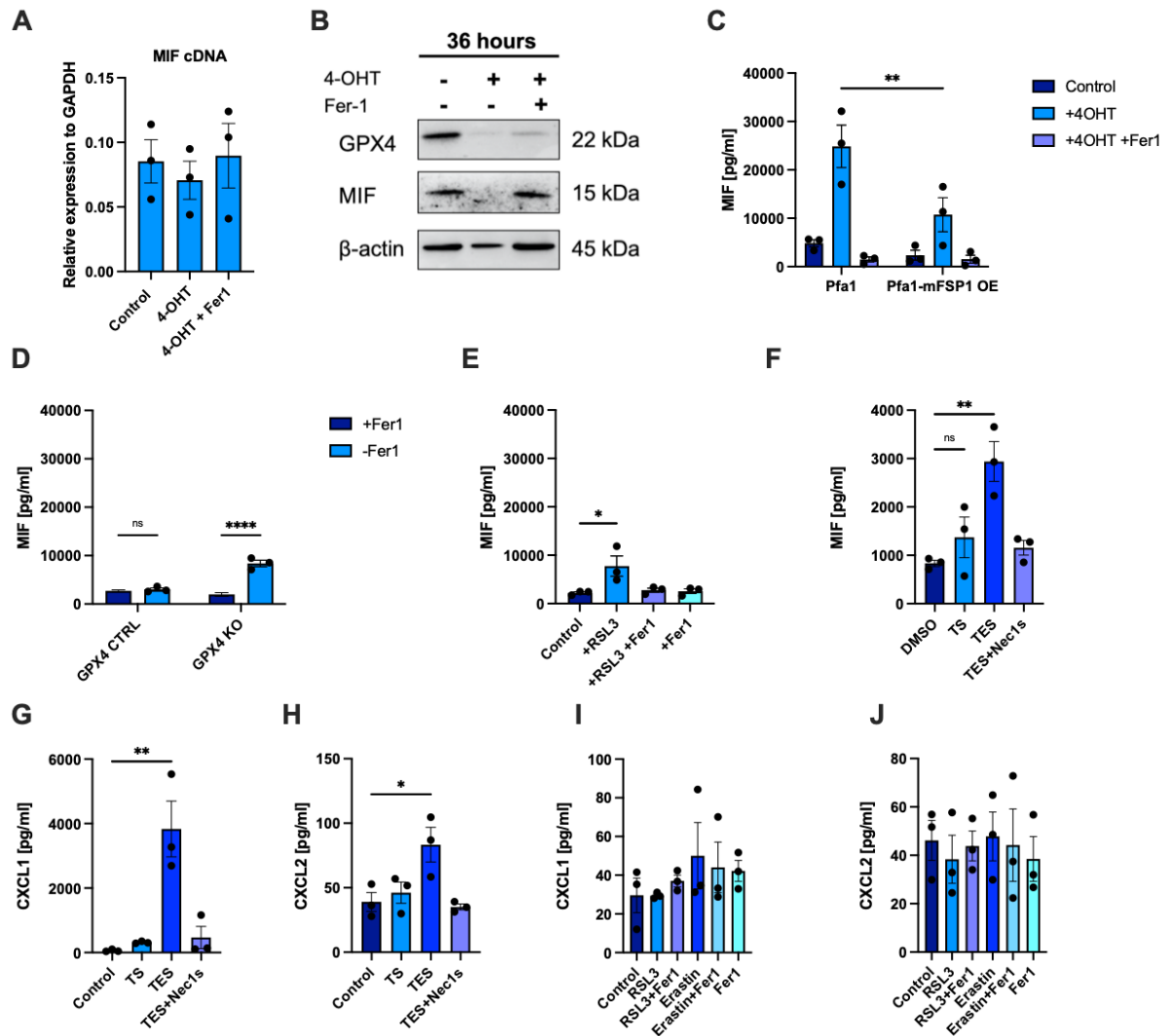


Figure 18. Ferroptotic protein secretomes include MIF but lack detection of *bona-fide* chemo- and cytokines.

A) Pfa1 cells treated with +/- 4OHT [1 μ M] +/- Ferrostatin-1 (Fer1) [1 μ M] for 24h. qPCR-mediated quantification of MIF cDNA is shown. **B)** Pfa1 cells treated +/- 4OHT [1 μ M] +/- Ferrostatin-1 [1 μ M] for 36 h were subjected to Western Blot analysis of the indicated proteins. **C)** Supernatant from Pfa1 and Pfa1-mFSP1 OE cells treated with +/- 4OHT [1 μ M] +/- Ferrostatin-1 (Fer1) [1 μ M] for 72h cells were subjected to MIF ELISAs. **D)** GPX4 control or GPX4-deficient SCLC cell lines were cultured in Ferrostatin-1 [1 μ M]. Supernatants were collected 16h after Ferrostatin-1 withdrawal and MIF was quantified using ELISA. **E)** Primary mouse lung fibroblasts (PMLFs) were treated with RSL3 [1 μ M] +/- Ferrostatin-1 [1 μ M] for 24 h. Supernatants were collected and subjected to MIF ELISAs. **F)** PMLFs treated with +/- TNF α [20ng/ml] +/- Birinapant [1 μ M] (TS) +/- Emricasan [2,5 μ M] (TES) for 24h. MIF was quantified using ELISA. **G)** PMLFs treated as in (F). CXCL1 was quantified using ELISA. **H)** PMLFs treated as in (F). CXCL2 was quantified using ELISA. **I)** PMLFs treated with +/- RSL3 [1 μ M] +/- Fer1 [1 μ M] +/- Erastin [1 μ M] for 24h. CXCL1 was quantified using ELISA. **J)** PMLFs treated as in (I). CXCL2 was quantified using ELISA. Data are means +/- SEM of at least three independent experiments were applicable. One- or two-way ANOVA was used to calculate p-values. ns: not significant; *: p<0.05; **: p<0.01; ***: p<0.001; ****: p<0.0001. qPCR and Western blot (A, B) were contributed by Ioanna Kotouza.

2.1.3. Ferroptosis induces the production and release of inflammatory oxylipins

Oxylipins are bioactive lipids generated by the oxidation of PUFAs and have potent pro- and anti-inflammatory roles. Oxylipins in animals are often referred as eicosanoids. COX2 is one of the essential enzymes that utilizes arachidonic acid (AA) to generate several different classes of eicosanoids³⁶⁸. They are synthesized *de novo* after cell activation through the release of phospholipids via phospholipase A₂ (PLA₂) and then further processed by lipoxygenases (LOXs) and cytochrome p450 (POR) to generate prostaglandins (PG) and thromboxanes (TB) or leukotrienes (LT)³⁶⁹. As upregulation of *Ptgs2*/COX2 has been shown as a ferroptotic marker¹²⁰, activation of these enzymes was investigated upon induction of ferroptosis using RSL3 and ML210. RSL3 treatment for 3 (Figure 19A) and 6 hours (Figure 19B) as well as ML210 treatment for 8 hours on PMLFs (Figure 19C) significantly upregulated *Ptgs2* which can be reversed by Fer1 co-treatment. Overexpression of FSP1 in Pfa1 cells was also able to revert the ferroptosis-induced induction of *Ptgs2* (Figure 19D). While *Por* was also slightly induced upon ferroptosis induction using RSL3 but not ML210, none of lipoxygenases (LOX5, LOX12 and LOX15) was altered upon ferroptosis induction (Figure 19E, 19F).

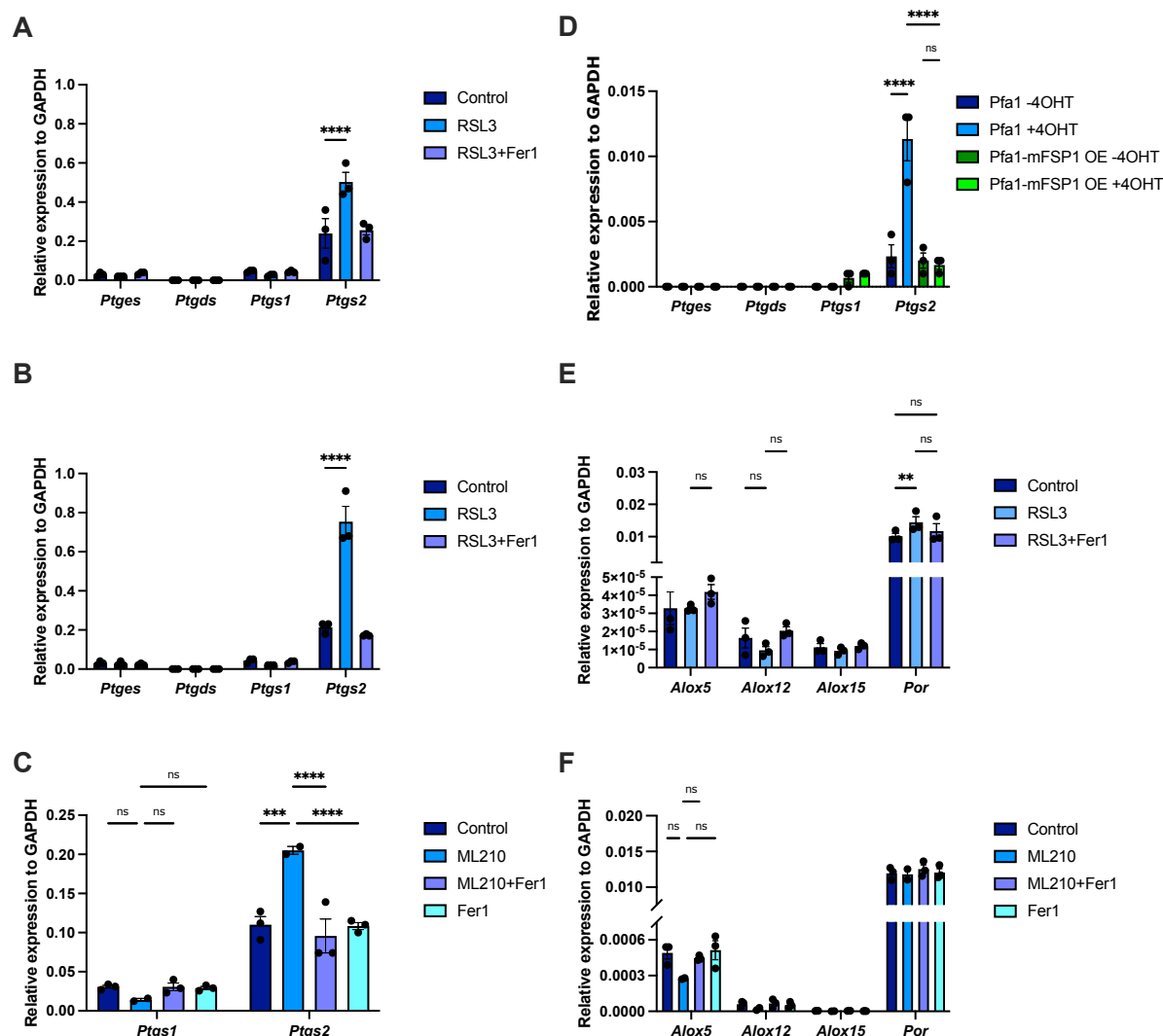


Figure 19. *Ptgs2* is induced in a lipid ROS-dependent manner.

A) Primary mouse lung fibroblasts (PMLFs) were treated with RSL3 [1 μ M] +/- Ferrostatin-1 [1 μ M] for 3h. qPCR of the indicated transcripts was performed. **B)** PMLFs were treated with RSL3 [1 μ M] +/- Ferrostatin-1 [1 μ M] for 6h. qPCR of the indicated transcripts was performed. **C)** PMLFs were treated with ML210 [0.5 μ M] +/- Ferrostatin-1 [1 μ M] for 8h. qPCR of the indicated transcripts was performed. **D)** Parental Pfa1 or Pfa1 cells with stable FSP1 overexpression were treated with +/- 4OHT [1 μ M] +/- Ferrostatin-1 (Fer1) [1 μ M] for 36h. qPCR of the indicated transcripts was performed. **E)** PMLFs treated as in (B), qPCR of the indicated transcripts was performed. **F)** PMLFs treated as in (C), qPCR of the indicated transcripts was performed. Data are means +/- SEM of at least three independent experiments were applicable. One- or two-way ANOVA was used to calculate p-values. ns: not significant; *: p<0.05; **: p<0.01; ***: p<0.001; ****: p<0.0001. qPCR (C, D, F) were contributed by Jenny Stroh and Maria Nenchova.

Prostaglandins can be produced via TLR4 and NF- κ B signalling while NFAT, CREB and c/EBP β transcription factors are also involved in their induction³⁷⁰. In order to distinguish the origin of the released prostaglandins in mutually exclusive to ferroptosis, wildtype lung fibroblasts (PMFLs) were also treated with LPS with the combination of ferroptosis inhibitor Fer1. LPS treatment for 3 and 6 hours significantly upregulated *Ptges* and *Ptgs2* but, unlike RSL3

treatment, this upregulation was not reversed by Fer1 (Figure 20A, 20B). Moreover, none of the other enzymes were regulated upon TLR4 signalling activation (Figure 20C, 20D). So, the upregulation of the genes upon ferroptosis induction in the oxylipin synthesis describes a unique role lipidROS in the prostaglandin synthesis enzymatic machinery.

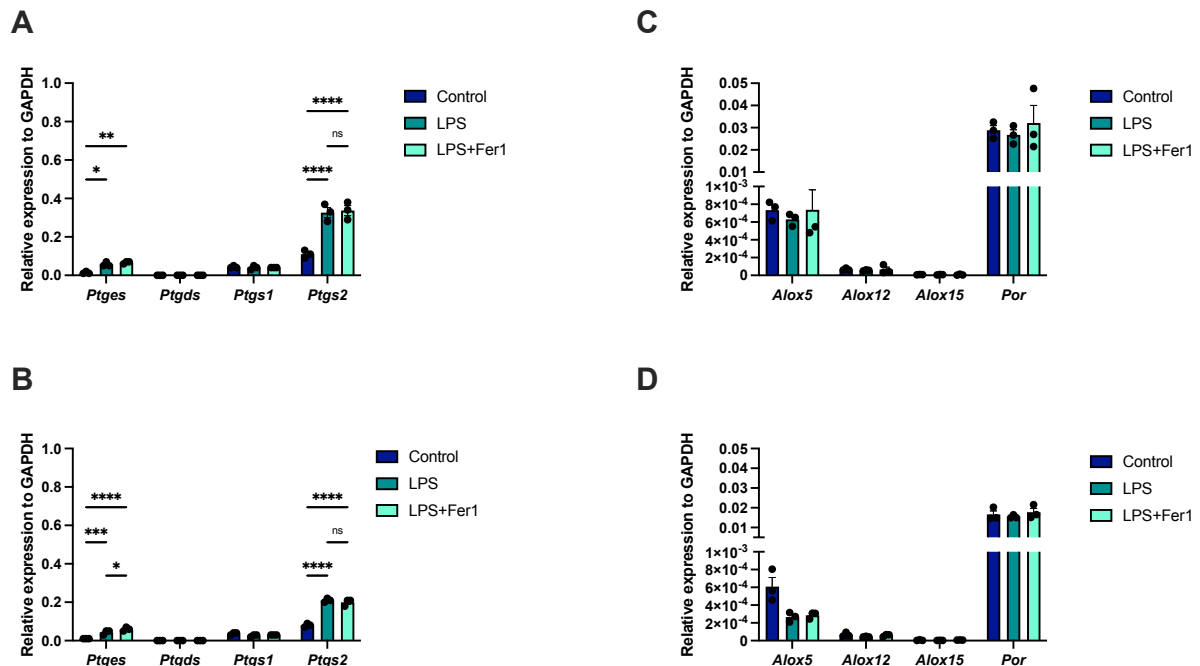


Figure 20. LPS-induced Ptgs2 induction is independent of ferroptosis.

A) Primary mouse lung fibroblasts (PMLFs) were treated with +/- LPS [10ng/ml] +/- Fer1 [1µM] for 3h. qPCR of the indicated transcripts was performed. **B)** PMLFs were treated with +/- LPS [10ng/ml] +/- Fer1 [1µM] for 6h. qPCR of the indicated transcripts was performed. **C)** PMLFs treated as in (A), qPCR of the indicated transcripts was performed. **D)** PMLFs treated as in (B), qPCR of the indicated transcripts was performed. Data are means +/- SEM of at least three independent experiments were applicable. One- or two-way ANOVA was used to calculate p-values. ns: not significant; *: p<0.05; **: p<0.01; ***: p<0.001; ****: p<0.0001. qPCR experiments(A-D) were contributed by Emre Güngör.

To compile a detailed list of oxylipins released by ferroptotic cells, supernatants were collected from several groups of Pfa1 cells: untreated control cells, cells treated with Tamoxifen for 48 hours with and without Fer-1, and cells treated only with Fer-1 (Figure 21A). These supernatants were then analysed using targeted mass spectrometry, comparing the results against empty media (without cells to account for media consumption), utilizing a library of 34 oxylipins³⁶⁸. In total, 19 from 34 oxylipins monitored were identified and quantified in media. The main subgroups include prostaglandins, lipoxin, mono-hydroxides, and di-hydroxides. 4 out of the 19 were significantly increased over live cell and media control (specifically released) and 13 over live cell control but not media (specific changes in consumption) upon induction of ferroptosis.

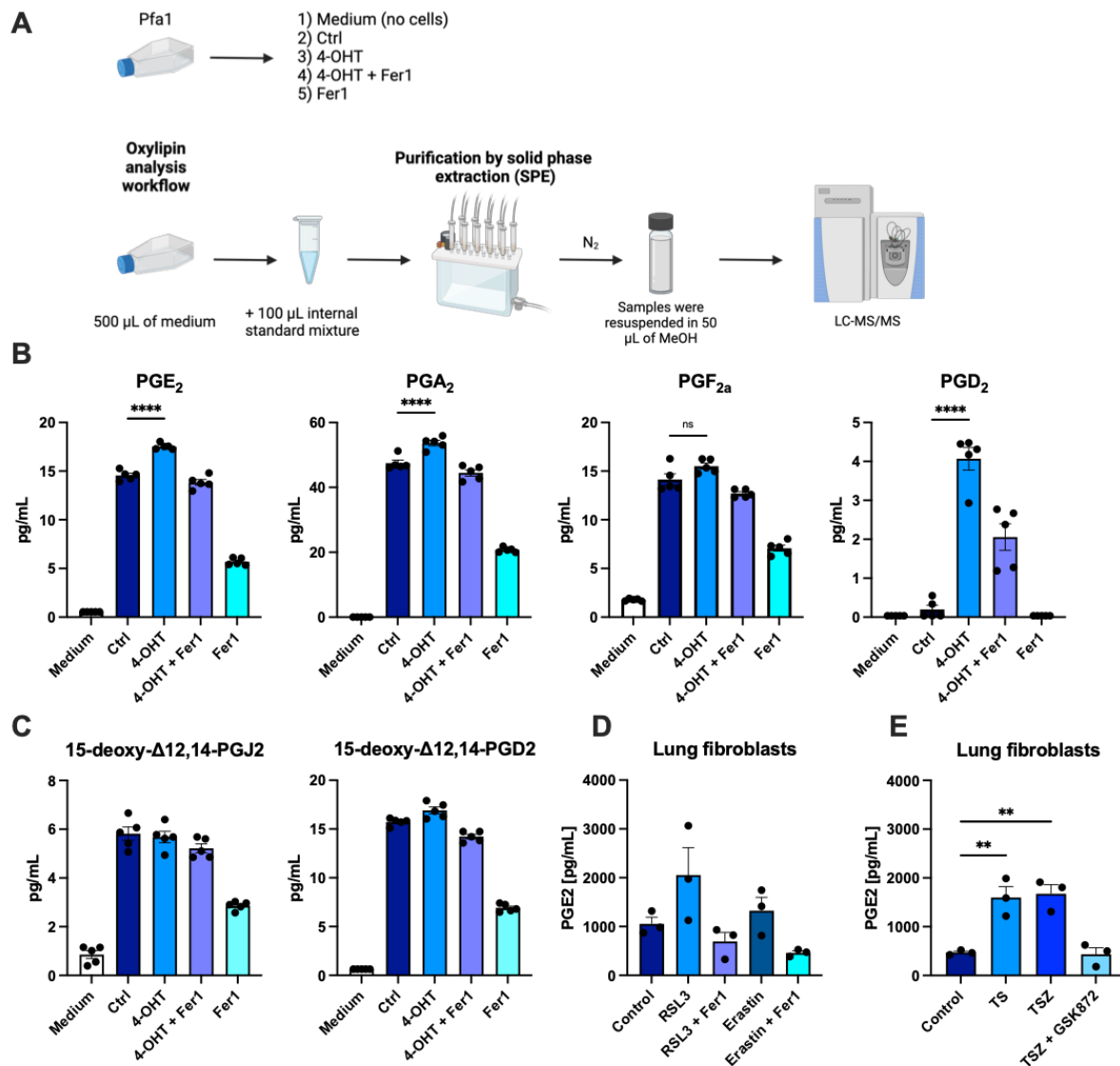


Figure 21. Ferroptotic cells release different types of prostaglandins.

A) Schematic of lipidomics experimental design to obtain ferroptotic oxylipins. **B)** Pfa1 cells were treated +/- 4OHT [1 μ M] +/- Ferrostatin-1 [1 μ M] for 72 h, supernatants (n=5 per condition) were collected, and concentrations of the indicated prostaglandins was quantified by mass spectrometry using standards as compared to media. **C)** Pfa1 cells treated as in (B) and concentrations of the indicated PGD₂-derived oxylipins were quantified by mass spectrometry using standards as compared to media. **D)** Primary mouse lung fibroblasts (PMLFs) treated with +/- RSL3 [1 μ M] +/- Fer1 [1 μ M] +/- Erastin [1 μ M] for 24h. PGE₂ was quantified using ELISA. **E)** PMLFs treated with +/- TNF α [20ng/ml] +/- Birinapant [1 μ M] +/- Emricasan [2,5 μ M] for 24h. PGE₂ was quantified using ELISA. Data are means +/- SEM of at least three independent experiments were applicable. One- or two-way ANOVA was used to calculate p-values. ns: not significant; *: p<0.05; **: p<0.01; ***: p<0.001; ****: p<0.0001. Lipidomics experiment (B, C) was contributed by Adriano de Britto Chaves Filho.

Ferroptotic supernatants contained significantly higher amounts of prostaglandins (PGE₂, PGA₂, PGD₂) (Figure 21B). On the contrary, PGD₂-derived oxylipins (15-deoxy- Δ 12,14-PGD₂ and 15-deoxy- Δ 12,14-PGJ₂) were also detected but they were not significantly increased upon ferroptosis induction (Figure 21C). The release of PGE₂ was also observed in PMLFs

undergoing RSL3-induced ferroptosis (Figure 21D). Importantly, PGE2 release was detected in PMLFs experiencing extrinsic apoptosis or necroptosis as well (Figure 21E), indicating that PGE2 release is a common feature across various types of regulated cell death. Additionally, several other oxylipins were found to be relatively more abundant in the secretomes of ferroptotic cells compared to those of live cells, likely due to reduced consumption from the cell culture media following the induction of cell death (Figure 22). Taken together, ferroptosis induces expression of *Ptgs2* independent of TLR4 signalling and the release of inflammatory oxylipins.

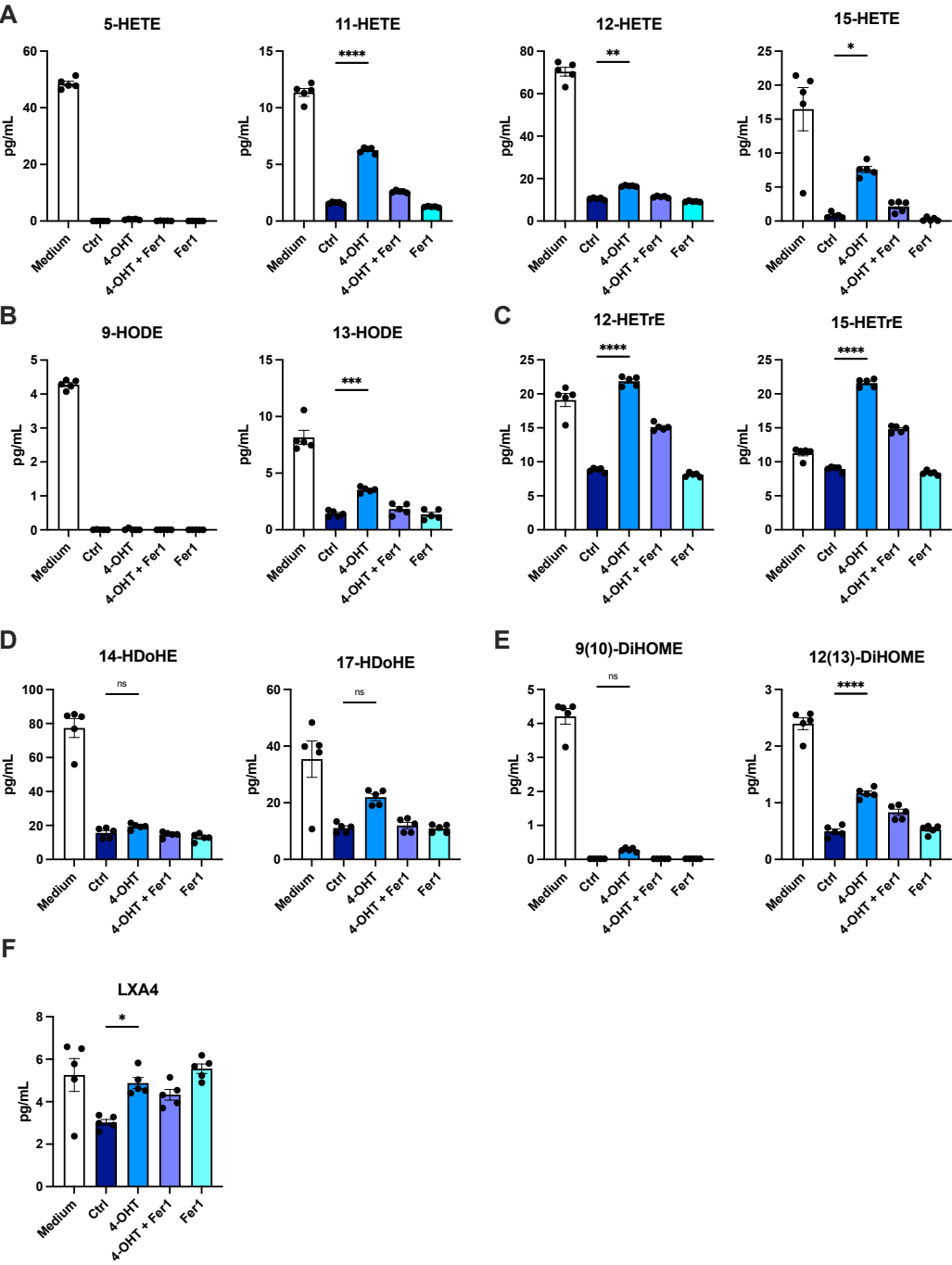


Figure 22. Ferroptosis induces the production and release of inflammatory oxylipins.

A-F) Pfa1 cells were treated +/- 4OHT [1 μ M] +/- Ferrostatin-1 [1 μ M] for 72 h, supernatants (n=5 per condition) were collected, and concentrations of the indicated HETE, HODE, HETre, HDoHE, DiHOME and lipoxin A4 oxylipins was quantified by mass spectrometry using standards as compared to media. One- or two-way ANOVA was used to calculate p-values. ns: not significant; *: p<0.05; **: p<0.01; ***: p<0.001; ****: p<0.0001. Lipidomics experiment (A-F) was contributed by Adriano de Britto Chaves Filho.

2.1.4. Ferroptotic cells release small metabolites

Metabolic reprogramming is a defining feature of macrophages that drives their activation during inflammation^{371,372}. Apoptotic cells can release nucleotides that act as effective DAMPs, facilitating their clearance³⁰⁵. In addition to nucleotides, apoptotic cells have been shown to release various other metabolites that can influence inflammatory responses³⁷³. Most of all, the impact of intracellular metabolism and the types of small metabolites released from ferroptotic cells have not been thoroughly investigated. To screen for the release of small molecules, PMLFs were treated with inducers of ferroptosis (RSL3 or erastin), apoptosis (TNF/Smac mimetic, TS), and necroptosis (TNF/Smac mimetic/Emricasan, TES). Cells undergoing ferroptosis exhibited the highest levels of ATP release (Figure 23A), occurring before cell death and accumulation of lipidROS (Figure 23B, 23G), in comparison to cells undergoing apoptosis and necroptosis (Figure 23C, 23D). Furthermore, overexpression of FSP1 significantly decreased the ATP release and cell death upon ferroptosis induction (Figure 23E, 23F). Consistent with previous reports³²⁶, ferroptotic cells also released oxidized nucleotide 8-Hydroxy-2'-deoxyguanosine (8-OHdG) (Figure 23G).

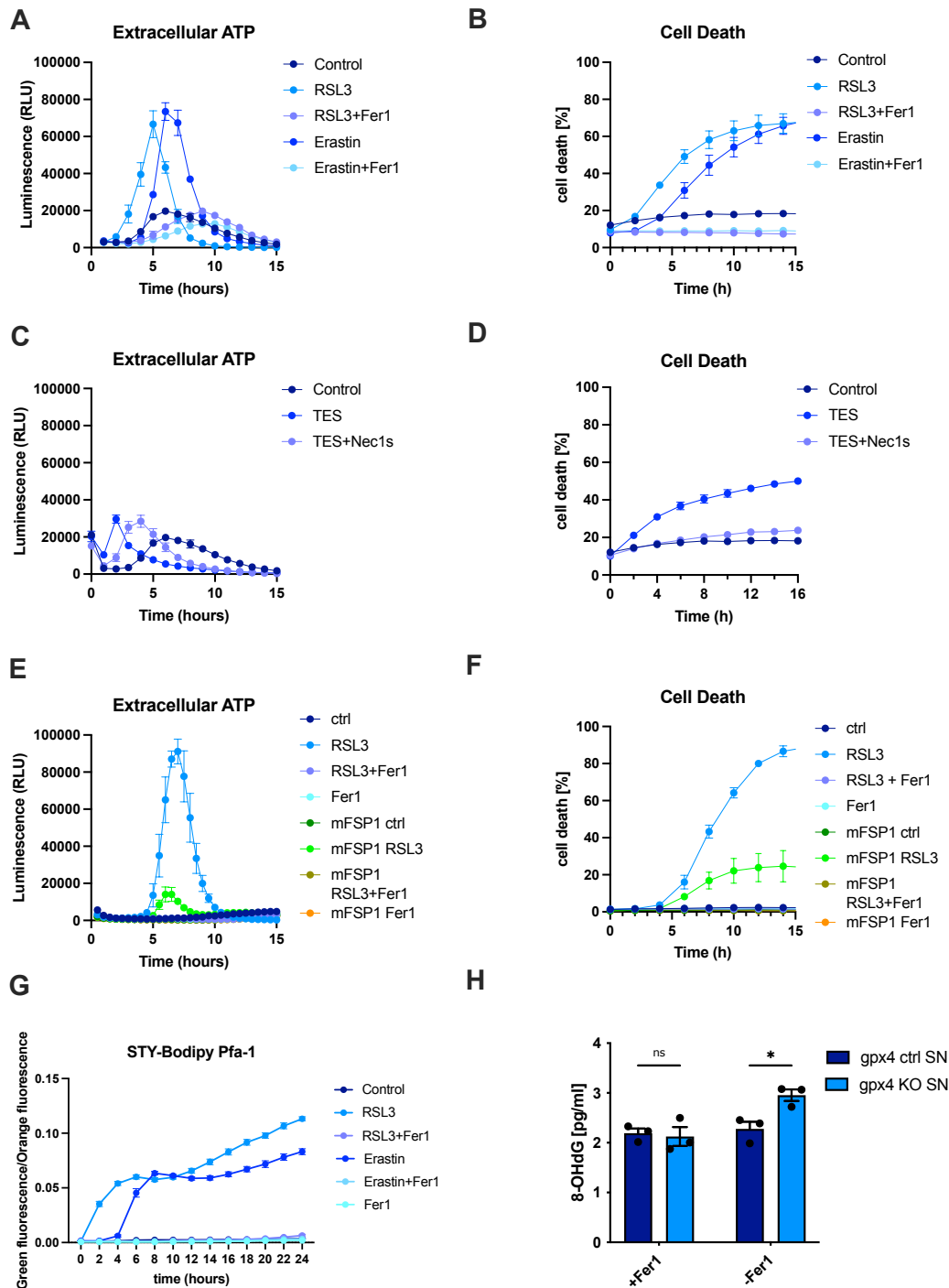


Figure 23. Ferroptotic cells release nucleotides.

A) Primary mouse lung fibroblasts (PMLFs) were treated with RSL3 [1 μ M] or erastin [1 μ M] +/- Ferrostatin-1 [1 μ M] for 15 h. ATP release was measured using the RealTime-Glo™ Extracellular ATP Assay and a luminescence plate reader. Relative Luciferase Units; RLU. **B)** Cells and treatments in (A) were stained with Draq7 [100nM]. Cells were imaged every 2 hours for near-infrared (NIR) count as a measure of dead cells using the IncuCyte live cell imaging system. % Cell death was normalized to confluency. **C)** PMLFs treated with +/- TNF α [20ng/ml] +/- Birinapant [1 μ M] +/- Emericasan [2,5 μ M] (TES) for 15h. ATP release was measured using the RealTime-Glo™ Extracellular ATP Assay and a luminescence plate reader. Relative Luciferase Units; RLU. **D)** Cells and treatments in (A) were stained with Draq7 [100nM]. Cells were imaged every 2 hours for near-infrared (NIR) count as a measure of dead cells using the IncuCyte live cell imaging system. % Cell death was normalized to confluency. **E)** Parental Pfa1 or Pfa1 cells with stable FSP1 overexpression were treated with RSL3 [1 μ M] +/- Ferrostatin-1 [1 μ M] and ATP release was quantified using the RealTime-Glo™ Extracellular ATP Assay

and a luminescence plate reader. Relative Luciferase Units; RLU. **F)** Cells and treatments in (A) were stained with Draq7 [100nM]. Cells were imaged every 2 hours for near-infrared (NIR) count as a measure of dead cells using the IncuCyte live cell imaging system. % Cell death was normalized to confluency. **G)** Pfa1 were treated with RSL3 [1 μ M] or Erastin [1 μ M] +/- Ferrostatin-1 [1 μ M] and stained for lipid ROS accumulation using STY-BODIPY [1 μ M] for 24h. Levels of lipid peroxidation can be monitored by quantifying levels of co-oxidized STY-BODIPY (green, λ_{ex} = 488 nm, λ_{em} = 495–540 nm) emitting green signals over reduced STY-Bodipy (red, λ_{ex} = 561 nm, λ_{em} = 568–630 nm) emitting in the orange spectrum. **H)** GPX4 control or GPX4-deficient SCLC cell lines were kept in the presence of Ferrostatin-1 [1 μ M]. Supernatants were collected 16h after Ferrostatin-1 withdrawal and 8-OHdG was quantified using ELISA. Data are means +/- SEM of at least three independent experiments. One- or two-way ANOVA was used to calculate p-values. ns: not significant; *: p<0.05; **: p<0.01; ***: p<0.001; ****: p<0.0001. Incucyte experiment (G) was contributed by Christina Bebbber.

Therefore, to determine what kind of small metabolites are released from cells undergoing ferroptosis, metabolic profiling was performed on Pfa1 cells. Supernatants and corresponding cell pellets were collected from several groups at 30h (early, no cell death), 48h (late, 50% cell death) and 72h (100% cell death, only supernatant) with the following groups: untreated control cells, cells treated with 4-OHT with and without Fer1, and cells treated only with Fer1 comparing the results against empty media (without cells to account for media consumption) (Figure 24A). A targeted library of over 400 polar metabolites was measured by liquid chromatography mass spectrometry, 174 of which could be detected in cell pellets and 122 in supernatants. Indeed, cells undergoing ferroptosis upon GPX4 deletion (+4OHT) as compared to live cells (-4OHT) showed distinct profiles of intracellular metabolites (Figure 24B). Interestingly, supernatants from cells undergoing ferroptotic cell death were enriched in TCA cycle, methionine cycle, purine and pyrimidine-derivates (Figure 24C).

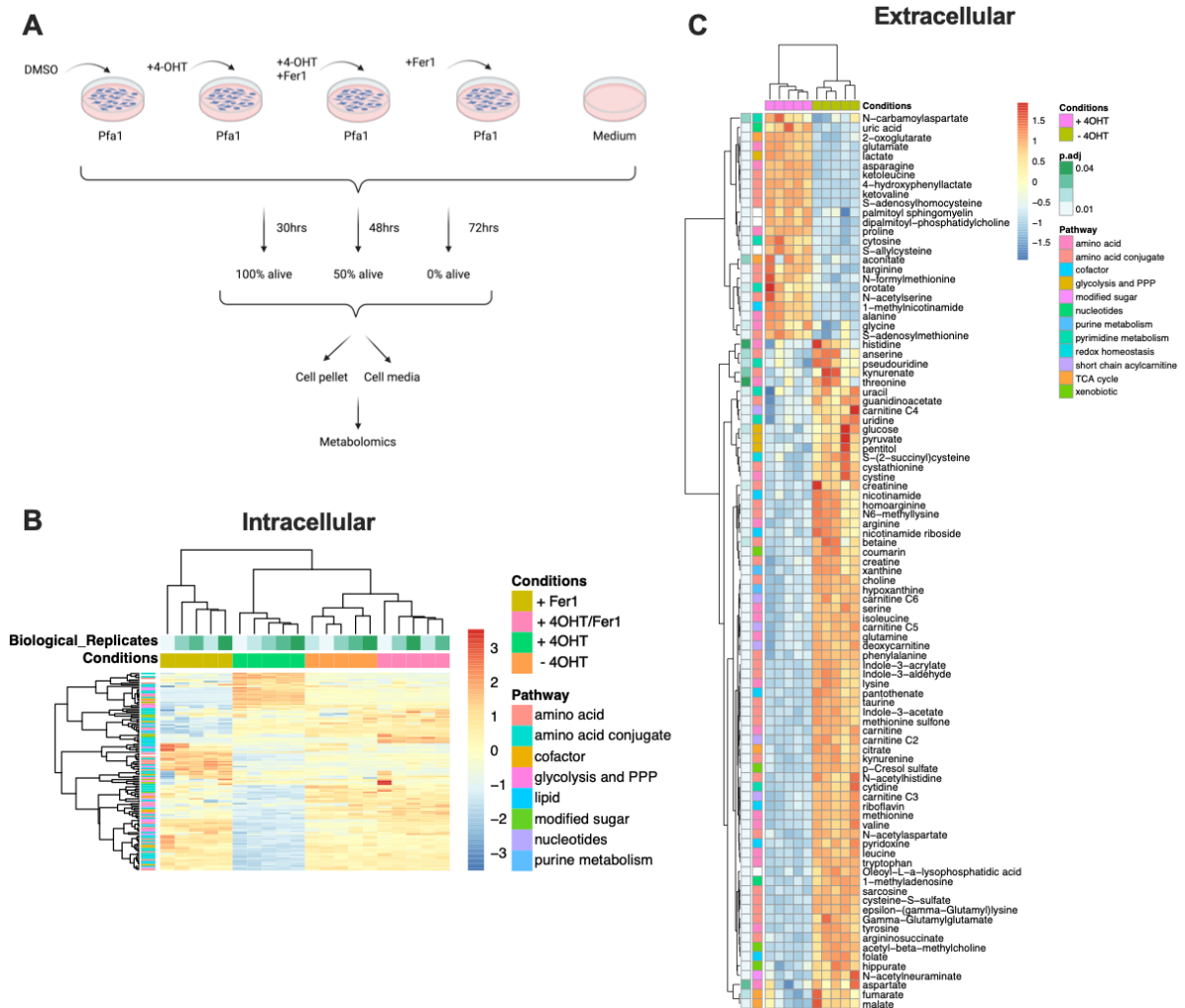


Figure 24. Ferroptotic cells shows different metabolic profiles at different time points.
A) Schematic of metabolomics experimental design to obtain ferroptotic metabolites (n=5 per condition). **B)** Heatmap of significantly different ($p=0.05$) metabolites in media of Pfa1 cells +/- 4OHT [$1\mu\text{M}$] for 48h. Log₂ fold distance is shown. **C)** Heatmap of all metabolites detected within supernatants of all 4 experimental conditions, 48h after 4OHT [$1\mu\text{M}$] stimulation of Pfa1 cells +/- Ferrostatin-1 [$1\mu\text{M}$] stimulation. Log₂ fold change is shown. Data are from 5 biological replicates for metabolomic measurements. One- or two-way ANOVA was used to calculate p-values. ns: not significant; *: $p<0.05$; **: $p<0.01$; ***: $p<0.001$; ****: $p<0.0001$. Metabolomics experiment (A-E) were contributed by Eric Seidel and Christian Frezza

Interestingly, early deletion of GPX4, before any measurable cell death occurred (at 30 hours), led to a significant increase in purine and pyrimidine derivatives. This increase was somewhat, but not completely, mitigated by co-treatment with ferrostatin-1. Metabolites necessary for pyrimidine synthesis, such as orotate, dihydroorotate, and cytosine, were elevated under all conditions involving GPX4 deletion (Figure 25A). The degradation products of purines, including xanthine, inosine, and adenosine were reduced following GPX4 deletion (Figure 25B). Additionally, this early rise in intracellular nucleotides (Figure 25C) was accompanied by an accumulation of metabolites from the pentose phosphate pathway (PPP) (Figure 25D) as

well as an early rise in intracellular TCA cycle metabolites (Figure 25E). Next, significantly enriched metabolites from ferroptotic supernatants were analysed for metabolic pathway enrichment using MetaboAnalyst 6.0³⁷⁴ and the Kyoto Encyclopedia of Genes and Genomes (KEGG). Enrichment in metabolites from the TCA cycle, methionine cycle, purine and pyrimidine synthesis, and other pathways associated with ferroptosis protection, such as the GSH pathway was also confirmed (Figure 25F).

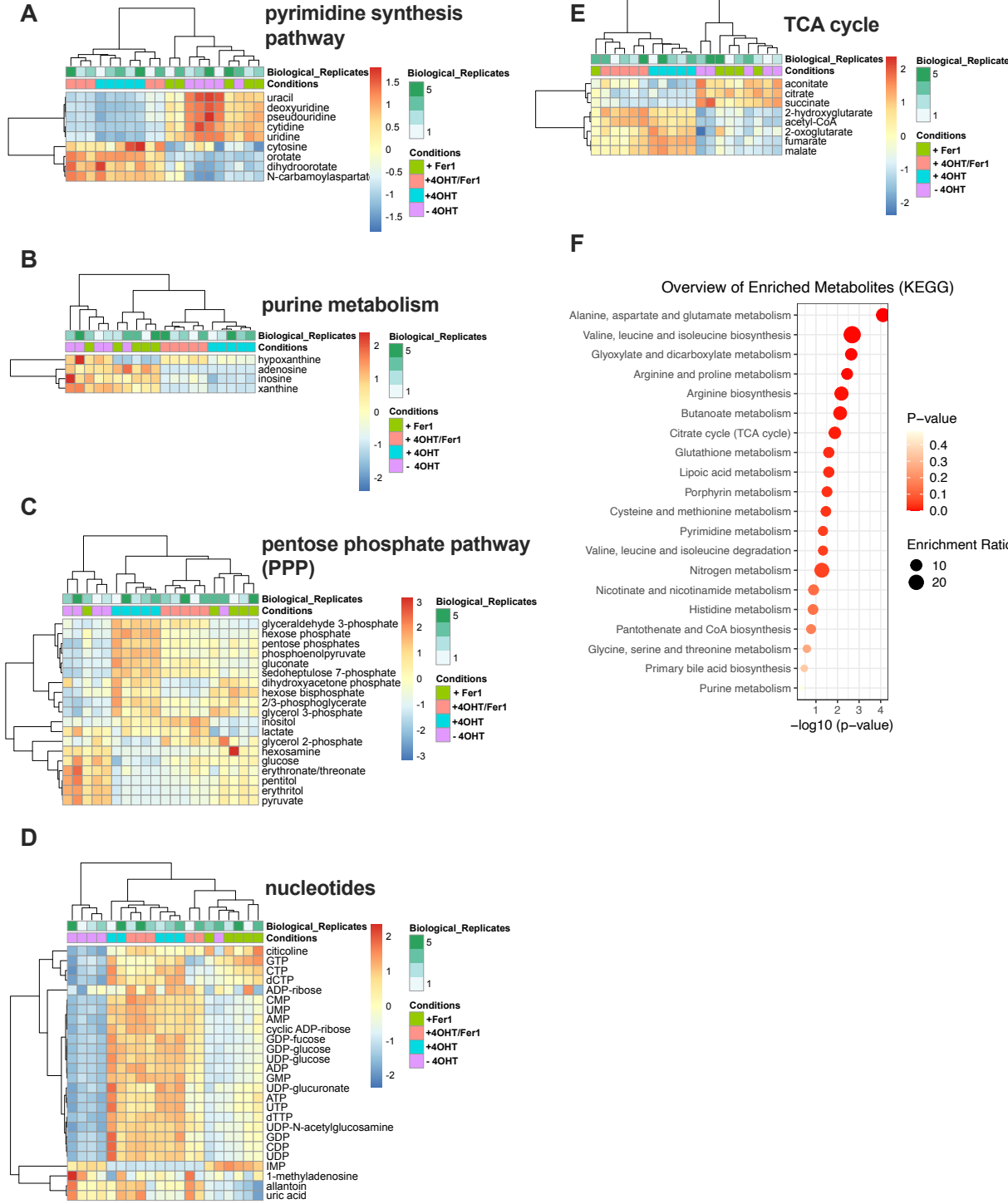


Figure 25. Early ferroptotic cells activate nucleotide synthesis and release metabolites of active anabolism.

A) Heatmap of pyrimidine synthesis metabolites in cell pellets 30 h after 4OHT [1 μ M] stimulation of Pfa1 cells +/- Ferrostatin-1 [1 μ M]. Log₂ fold change is shown. **B)** Heatmap of purine metabolism metabolites in cell pellets 30 h after 4OHT [1 μ M] stimulation of Pfa1 cells +/- Ferrostatin-1 [1 μ M]. Log₂ fold change is shown. **C)** Heatmap of pentose phosphate pathway (PPP) metabolites in cell pellets 30 h after 4OHT [1 μ M] stimulation of Pfa1 cells +/- Ferrostatin-1 [1 μ M]. Log₂ fold change is shown. **D)** Heatmap of nucleotides in cell pellets 30 h after 4OHT [1 μ M] stimulation of Pfa1 cells +/- Ferrostatin-1 [1 μ M]. Log₂ fold change is shown. **E)** Heatmap of TCA cycle metabolites in cell pellets 30 h after 4OHT [1 μ M] stimulation of Pfa1 cells +/- Ferrostatin-1 [1 μ M]. **F)** KEGG pathway enrichment of metabolites ferroptotic supernatants (48 h +4OHT [1 μ M]) is plotted by $-\log_{10}$ p-value using MetaboAnalyst 6.0³⁷⁴. Heatmaps show 5 independent biological replicates for metabolomics measurements. One- or two-way ANOVA was used to calculate p-values. ns: not significant; *: p<0.05; **: p<0.01; ***: p<0.001; ****: p<0.0001. Metabolomics experiment (A-E) were contributed by Eric Seidel and Christian Frezza.

2.2. Ferroptotic supernatants induce macrophage reprogramming

2.2.1. Ferroptotic supernatants induce transcriptional reprogramming of macrophages

Having identified that ferroptotic cells release both protein and non-protein secretomes with putative immune-modulatory activity, we decided to test this on macrophages. Primary mouse bone marrow-derived cells were isolated and differentiated into primary F48/80+/CD11b+ bone marrow-derived macrophages (pBMDMs) as described before³⁷⁵ (Figure 26A, 26B). Exposure to ferroptotic supernatants had no effect on BMDM differentiation and maturation (Figure 26C, 26D). Next, BMDMs were exposed to filtered ferroptotic supernatants +/- Fer-1 for 24 hours followed by RNA-sequencing (Figure 26E). Ferroptotic supernatant exposed pBMDMs showed upregulation of markers consistent with macrophage priming as well as enrichment in gene ontology (GO) terms associated with immune activation (Figure 26G). Amongst the upregulated transcripts were the MIF receptor *CD74* and *Ptger3*, a PGE₂ receptor identified (Figure 26F) and validated (Figure 26H). RNA-seq results further supported the identified ligands such as MIF and class of prostaglandins of the multi-omics approach.

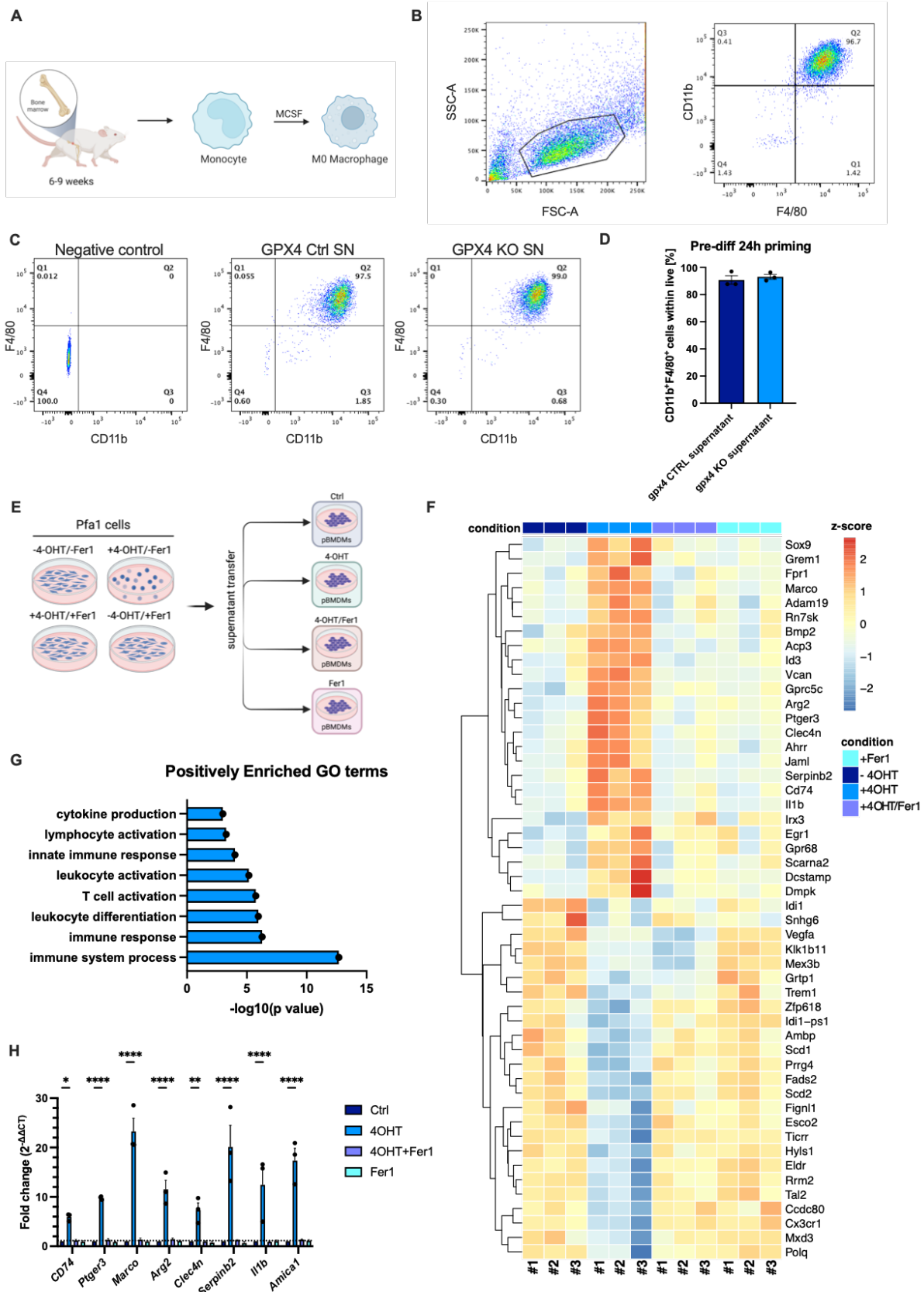


Figure 26. Exposure to supernatants from ferroptotic cells triggers a transcriptional reprogramming in macrophages.

A) Schematic of pBMDMs isolation and differentiation. 6-9-week old C57BL/6N strain mice were sacrificed and bone marrow cells were isolated and differentiated for 7 days with M-CSF [25ng/ml] as described before. **B)** pBMDMs differentiation at day 7 was confirmed with CD11b⁺ F4/80⁺ gating

within live cells. Cells were analysed by flow cytometry. **C)** pBMDMs were incubated with supernatants from GPX4 CTRL or GPX4 KO SCLC cell lines 24 h after Fer1 withdrawal. Representative flow cytometry analysis is shown. **D)** pBMDMs from (C) were quantified for combined CD11b+, F4/80+ within live cells. **E)** Schematic of supernatant transfer strategy from Pfa1 to pBMDMs (n=3 per condition). **F)** Differentiated pBMDMs were incubated for 24 h with the supernatants shown in (E), and then subjected to RNA sequencing. The 25 most significantly upregulated and downregulated genes are displayed, with the genes clustered row-wise according to their expression patterns. **G)** Positively enriched GO terms in pBMDMs exposed to ferroptotic supernatants. **H)** pBMDMs were subjected to the indicated supernatants from Pfa1 cells for 24h. The indicated transcripts were quantified by qPCR. Data are means +/- SEM of at least three independent experiments. All images were created with BioRender.com. One- or two-way ANOVA was used to calculate p-values. ns: not significant; *: p<0.05; **: p<0.01; ***: p<0.001; ****: p<0.0001. RNA sequencing analysis (F, G) was contributed by Ali Abdallah.

As a control to test whether pBMDMs exposed to other regulated necrosis-derived supernatants would respond similarly or not, necroptotic supernatants from cells undergoing necroptosis upon induction of ZBP1 overexpression in the presence of caspase inhibition³⁷⁶ were generated. In this way, necroptosis can be induced without the use of TNF which can act as a direct stimulant to macrophages. Cells harbouring the empty vector (ZBP1 EV cells) exhibited negligible cell death, even following treatment with emricasan whereas the overexpression of ZBP1 (ZBP1 OE cells) resulted in a significant increase in cell death (Figure 27A, 27B). LDH leakage was similarly observed in ZBP1 and emricasan-induced necroptosis (Figure 27C). Interestingly, treating pBMDMs with necroptotic supernatants did not lead to the induction of any genes that are activated in response to exposure to ferroptotic supernatants (Figure 27D).

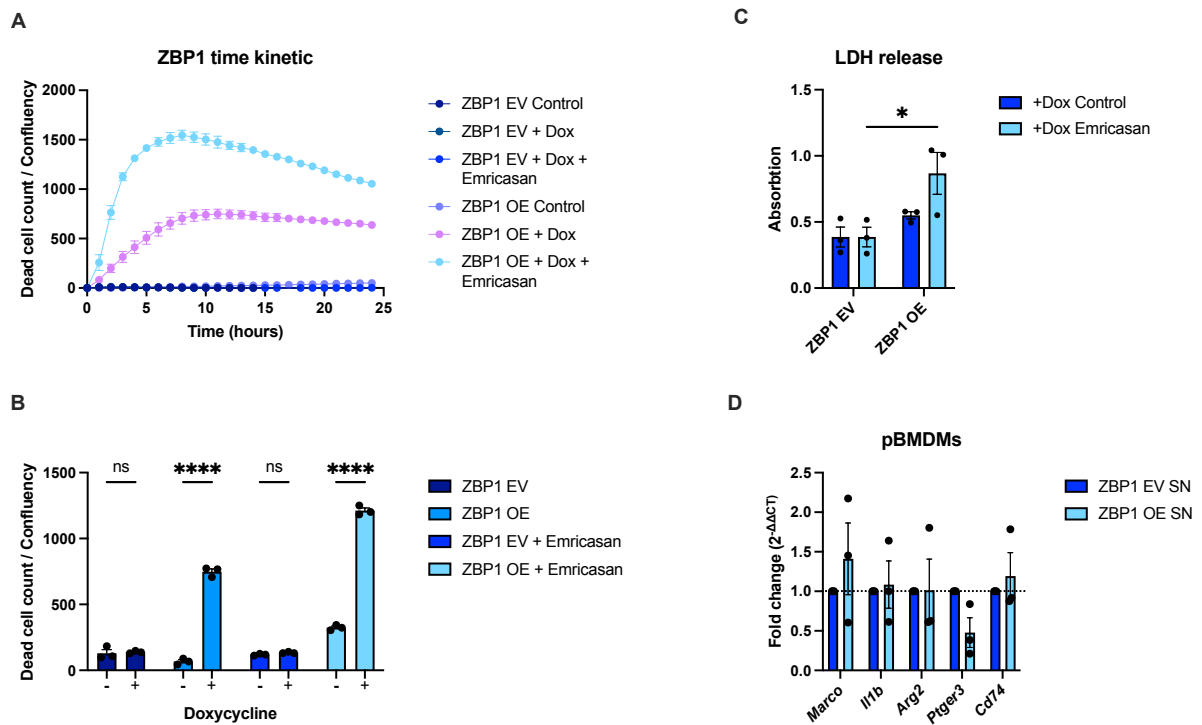


Figure 27. Inducible ZBP1 overexpression leads to necroptotic cell death.

A) Empty vector inducible (ZBP1 EV) ZBP1-inducible (ZBP1 OE) iMEFs³⁷⁶ were pre-treated +/- doxycycline [1 μ g/ml] for 16 hours and +/- Emericasan [2.5 μ M] for 24h. DRAQ7 [100nM] was added to all wells to visualize dead cells. Images were acquired every 2h using the IncuCyte SX5 bioimaging platform. Time kinetic is shown. **B)** Cells and treatments in (A) were stained with DraQ7 [100nM]. Cells were imaged every 2 hours for near-infrared (NIR) count as a measure of dead cells using the IncuCyte live cell imaging system. **C)** ZBP1 EV and ZBP1 OE cells treated as in (B) were subjected to LDH quantification. **D)** pBMDMs were incubated with ZBP1 EV or ZBP1 OE supernatants (SN) + Emericasan [2.5 μ M] for 24 h. The indicated transcripts were quantified by qPCR. Data are means +/- SEM of at least three independent experiments were applicable. One- or two-way ANOVA was used to calculate p-values. ns: not significant; *: p<0.05; **: p<0.01; ***: p<0.001; ****: p<0.0001. Incucyte experiments (A, B) were contributed by Maria Nenchova, qPCR experiment (D) was contributed by Jenny Stroh.

2.2.2. Ferroptotic supernatants prime macrophages

As previous studies identified TLR4/TRIF signalling activation in neutrophils upon ferroptotic cell death³⁵⁰, macrophages were tested for cytokine secretion in response to TLR4 stimulation via LPS in the presence and absence of ferroptotic supernatants. Immortalized BMDMs (iBMDMs) were primed with either control or ferroptotic supernatant with or without interferon-gamma (IFN- γ)/LPS treatment (Figure 28A). As Fer1 treatment alone had an effect regarding TNF α (Figure 28B) and IL6 (Figure 28C) secretion from iBMDMs, further activation experiments were done with supernatants derived from cells with a constitutive GPX4 knockout that can only be cultured in the presence of Fer1 but resulting in ferroptotic cell death upon withdrawal of Fer1 (Figure 28D). Exposure to these ferroptotic secretomes had similar effect on TNF α and IL6 secretion with significantly increased upon IFN- γ /LPS treatment

in iBMDMs (Figure 28E, 28F) as well as pBMDMs (Figure 28G, 28H) but did not change the percentage intracellular TNF α levels of primary mature F4/80+CD11b+ BMDMs (Figure 28I), suggesting enhanced/prolonged activation of individual pBMDMs. Of note, elevated levels of *I1b* mRNA (Figure 26H), did not result in increased IL-1 β secretion from BMDMs incubated with ferroptotic supernatants in the presence and absence of additional IFN- γ /LPS treatment (Figure 28J, 28K).

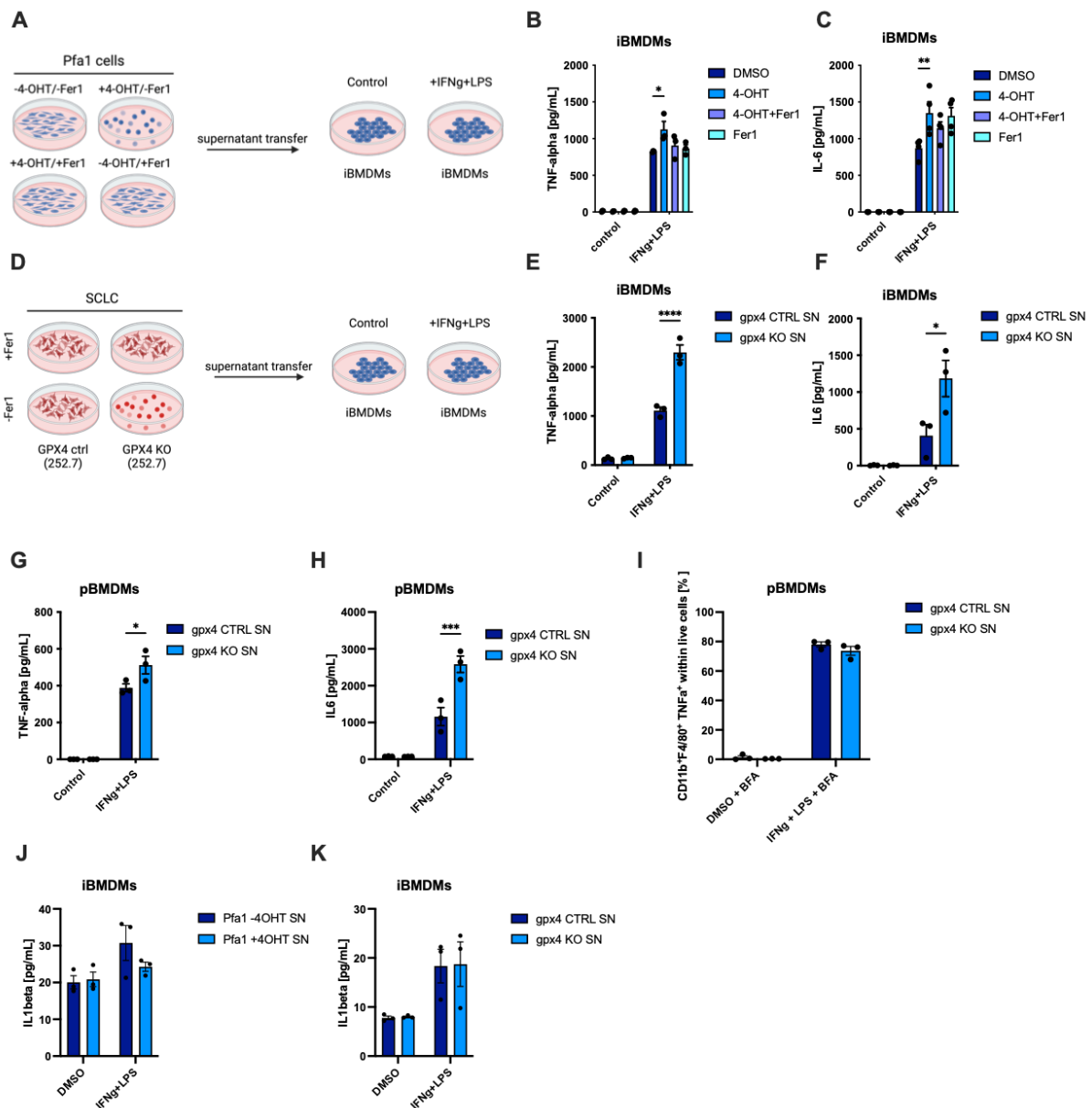


Figure 28. Ferroptotic supernatants prime macrophages.

A) Schematic of supernatant transfer strategy from Pfa1 ctrl. or KO cells 72h after +/- 4OHT [1 μ M] +/- Ferrostatin-1 (Fer1) [1 μ M] treatment iBMDMs. **B)** iBMDMs were incubated with Pfa1 ctrl. or KO supernatants for 6h with IFN gamma [25ng/ml], after which LPS [10ng/ml] was added for a total of 24 h. TNF-alpha was quantified using ELISA. **C)** iBMDMs were incubated with Pfa1 ctrl. or KO supernatants 6h with IFN gamma [25ng/ml], after which LPS [10ng/ml] was added for a total of 24 h. IL-6 was quantified using ELISA. **D)** Schematic of supernatant transfer strategy from GPX4 control and GPX4 KO SCLC cells 24h after Ferrostatin-1 withdrawal to iBMDMs. **E)** iBMDMs were incubated with ctrl. or KO supernatants for 6h with IFN gamma [25ng/ml], after which LPS [10ng/ml] was added for a total of 24

h. TNF-alpha was quantified using ELISA. **F**) iBMDMs were incubated with ctrl. or KO supernatants 6h with IFN gamma [25ng/ml], after which LPS [10ng/ml] was added for a total of 24 h. IL-6 was quantified using ELISA. **G**) pBMDMs were incubated with ctrl. or KO supernatants for 6h with IFN gamma [25ng/ml], after which LPS [10ng/ml] was added for a total of 24 h. TNF-alpha was quantified using ELISA. **H**) pBMDMs were incubated with ctrl. or KO supernatants 6h with IFN gamma [25ng/ml], after which LPS [10ng/ml] was added for a total of 24 h. IL-6 was quantified using ELISA. **I**) Differentiated pBMDMs were treated with ctrl. or KO supernatants for 6h IFN gamma [25ng/ml], LPS [10ng/ml] and Brefeldin A (BFA) [5µg/ml]. Combined CD11b+, F4/80+ within live cells were quantified using flow cytometry. **J**) iBMDMs were incubated with Pfa1 ctrl. or KO supernatants as indicated for 6h with IFN gamma [25ng/ml], after which LPS [10ng/ml] was added for a total of 24 h. IL1b was quantified using ELISA. **K**) iBMDMs were incubated with SCLC ctrl. or KO supernatants as indicated for 6h with IFN gamma [25ng/ml], after which LPS [10ng/ml] was added for a total of 24 h. IL1b was quantified using ELISA. Data are means +/- SEM of at least three independent experiments. All images were created with BioRender.com. One- or two-way ANOVA was used to calculate p-values. ns: not significant; *: p<0.05; **: p<0.01; ***: p<0.001; ****: p<0.0001.

To determine if the "priming substance" in ferroptotic supernatants is part of the protein or non-protein secretome, supernatants were boiled to denature the protein components. Notably, the boiled supernatants from ferroptotic cells maintained their priming activity, strongly suggesting that the non-protein fraction released from these cells is responsible for this effect (Figure 29A, 29B). Notably, overexpression of FSP1 in the cells producing the supernatants was enough to reduce the supernatants' priming activity on macrophages (Figure 29C).

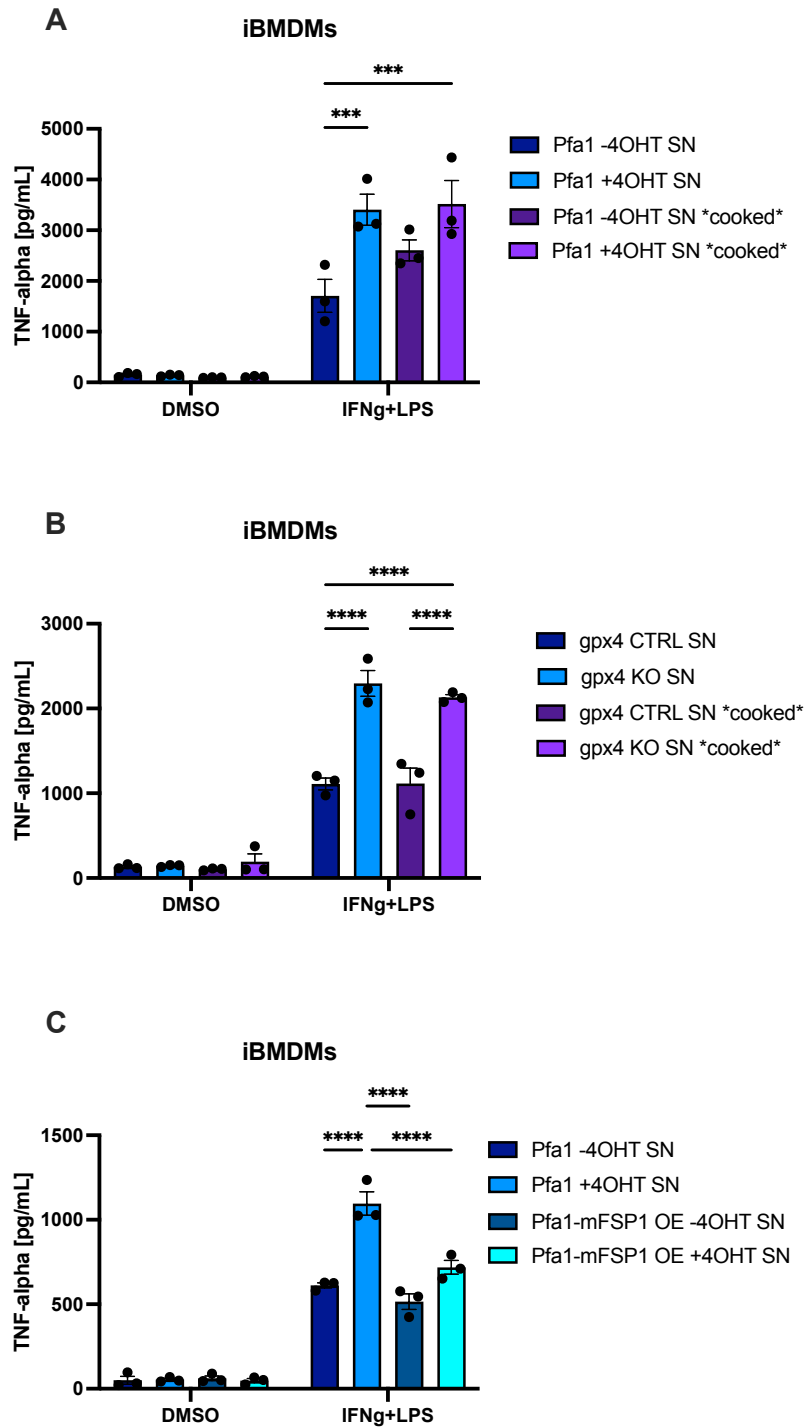


Figure 29. The non-protein fraction of ferroptotic supernatants is responsible for priming.

A) iBMDMs were incubated with Pfa1 ctrl. Or KO supernatants or boiled (*cooked*) supernatants for 6h with IFN gamma [25ng/ml], after which LPS [10ng/ml] was added for a total of 24 h. TNF-alpha was quantified using ELISA. **B)** iBMDMs were incubated with GPX4 ctrl. Or KO supernatants or boiled (*cooked*) supernatants for 6h with IFN gamma [25ng/ml], after which LPS [10ng/ml] was added for a total of 24 h. TNF-alpha was quantified using ELISA. **C)** iBMDMs were incubated with Pfa1 ctrl. Or Pfa1-FSP1 OE supernatants for 6h with IFN gamma [25ng/ml], after which LPS [10ng/ml] was added for a total of 24 h. TNF-alpha was quantified using ELISA. Data are means +/- SEM of at least three independent experiments. One- or two-way ANOVA was used to calculate p-values. ns: not significant; *: p<0.05; **: p<0.01; ***: p<0.001; ****: p<0.0001.

iBMDMs were primed with necroptotic supernatants derived from ZBP1-inducible MEFs (ZBP1 OE) did not show enhanced TNF or IL-6 secretion as compared to vector control (ZBP1 EV) supernatants upon stimulation (Figure 30A, 30B). Together, these findings reveal that ferroptotic secretomes, and specifically the non-protein components, uniquely prime macrophages for activation, a capability not observed with necroptotic supernatants.

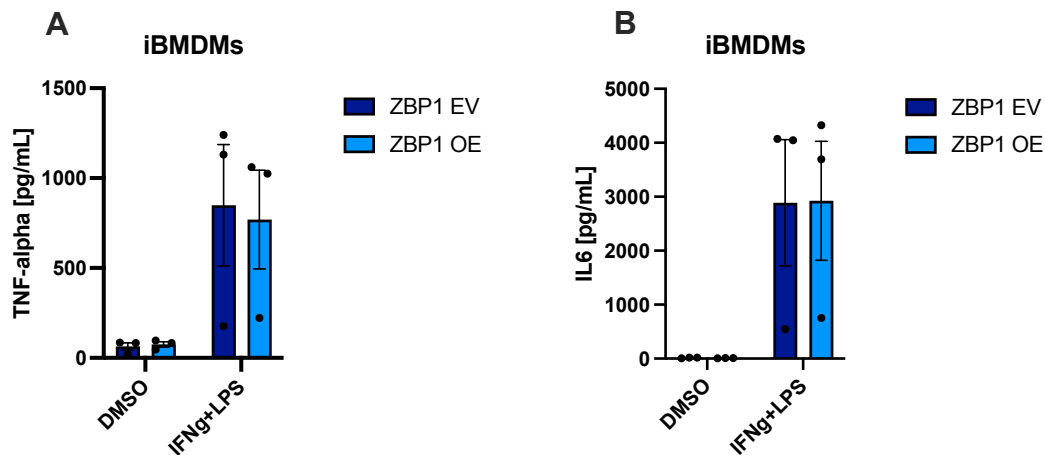


Figure 30. Necroptotic supernatants fail to prime macrophages.

A) iBMDMs were incubated with empty vector (EV) or supernatants from ZBP1 induced (ZBP1 OE) + Emricasan [2.5 μ M] for 6h with IFN gamma [25ng/ml], after which LPS [10ng/ml] was added for a total of 24 h. TNF alpha was quantified using ELISA. **B)** iBMDMs were incubated with empty vector (EV) or supernatants from ZBP1 induced (ZBP1 OE) + Emricasan [2.5 μ M] for 6h with IFN gamma [25ng/ml], after which LPS [10ng/ml] was added for a total of 24 h. IL-6 was quantified using ELISA. Data are means +/- SEM of at least three independent experiments were applicable. One- or two-way ANOVA was used to calculate p-values. ns: not significant; *: p<0.05; **: p<0.01; ***: p<0.001; ****: p<0.0001. ELISA experiments (A, B) were contributed by Jenny Stroh.

2.2.3. Ferroptotic secretome-exposed macrophages also show signs of trained immunity

Given that *Clec4n* (Dectin-2), a C-type lectin receptor and *I1b* were upregulated in pBMDMs treated with ferroptotic secretomes and fumarate release was detected in ferroptotic cells, an experimental setup of “trained immunity” in macrophages was performed (Figure 30A). Cells isolated from mouse bone marrow, undifferentiated BMDMs, were trained with either control or ferroptotic supernatants for 24 hours and left for a resting period for 7 days. The resting period was followed by re-stimulation with LPS- a TL4 ligand or PAM3CSK- a TLR2 ligand. Intriguingly, cells trained with ferroptotic supernatant showed a significantly increased response to both secondary which was measured by TNF α and IL6 secretion from macrophages (Figure 31B, 31C). In addition to the protein levels, mRNA levels of *Tnf* and *I16* were upregulated upon training with ferroptotic supernatants (Figure 31D, 31E). Of note, the variability between the biological repeats is potentially derived from the not-ideal replication

of the 'training' treatment with freshly isolated bone-marrow derived cells, resulting in a trend but not reaching significance between non-ferroptotic and ferroptotic supernatants. Even though the effect of gender or age of the mice have been optimized, results were still showing variability. Besides the variability, the medium control for the secondary stimulus, in this case DMEM, caused high levels of cytokine release. As the ferroptotic supernatants were of RPMI origin, we sought to compare the effect of RPMI and DMEM alone on the 'training' status of macrophages as well as in activation post-secondary stimulus. Replacement of DMEM with RPMI medium sufficiently lowered the activation levels of medium control (Figure 31F, 31G) but again failing to reach significance. Epigenetic markers and metabolic changes were also checked by western blotting and seahorse assays but both failed to show additional evidence for the 'trained' phenotype of macrophages (data not shown). A recent study has reported the induction of distinct trained-immunity programs in human monocytes³⁷⁷. The characterization of gene expression profiles via single-cell RNA sequencing revealed a high heterogeneity of cytokines and chemokine markers across monocyte subpopulations suggesting that the existence of a subpopulation with low trained immunity phenotype can also explain the variability and lack of defined 'trained' phenotype.

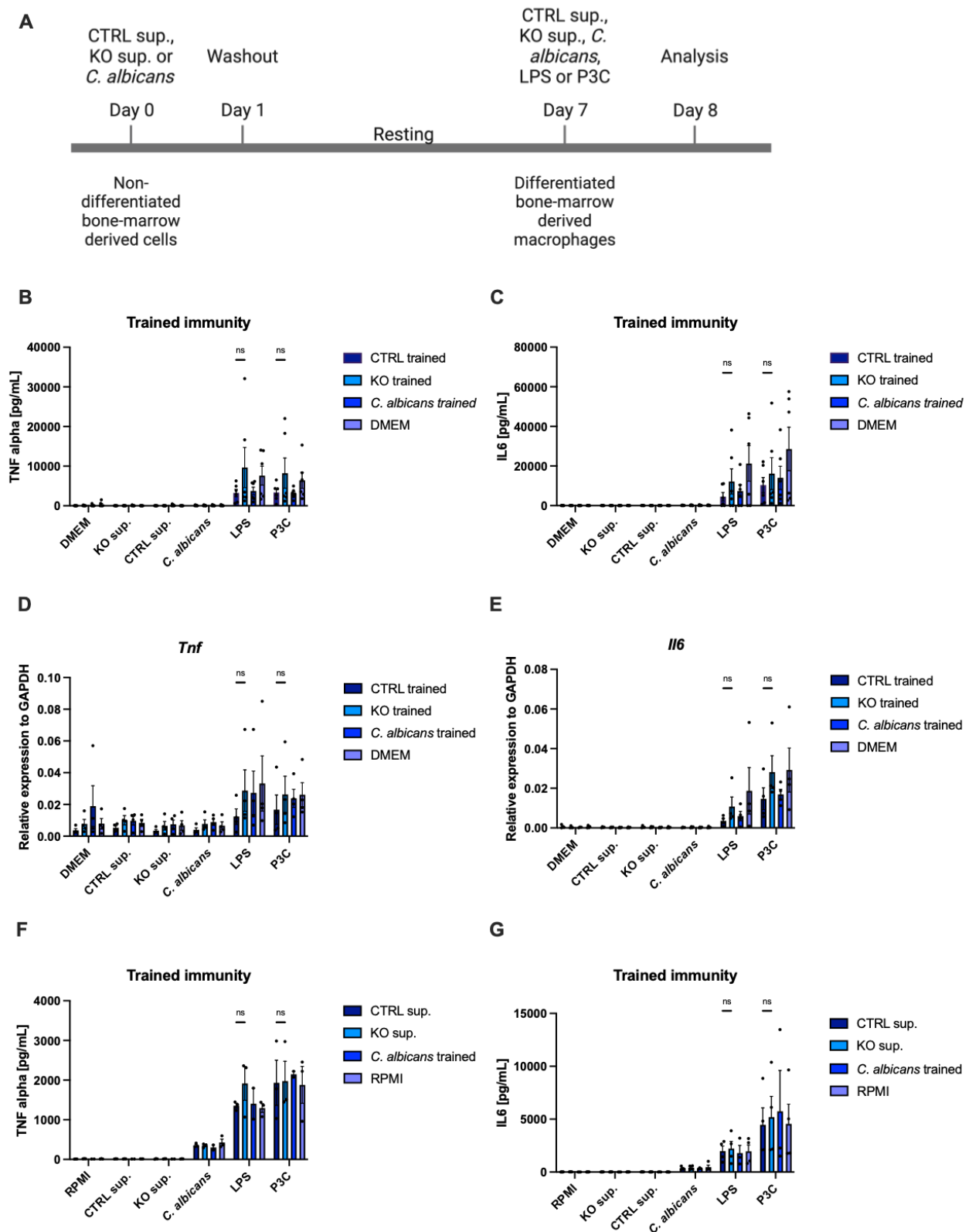


Figure 31. Ferroptotic-exposed macrophages also show signs of trained immunity.

A) Experimental setup for “trained immunity”. **B)** pBMDMs were trained with ctrl. or KO supernatants, *C. albicans* or DMEM for 24h and left for a resting/differentiation period of 6 days. On day 7, macrophages were challenged with ctrl. or KO supernatants, *C. albicans*, TLR4 ligand LPS, TLR2 ligand PAM3CSK (P3C) for 24 h. TNF-alpha was quantified using ELISA. **C)** pBMDMs were trained with ctrl. or KO supernatants, *C. albicans* or DMEM for 24h and left for a resting/differentiation period of 6 days. On day 7, macrophages were challenged with ctrl. or KO supernatants, *C. albicans*, TLR4 ligand LPS,

TLR2 ligand PAM3CSK (P3C) for 24 h. IL-6 was quantified using ELISA. **D-E**) pBMDMs were subjected to the indicated supernatants from (B). The indicated transcripts were quantified by qPCR. Data are means +/- SEM of at least three independent experiments. **F**) pBMDMs were subjected to the indicated supernatants from (B) with a medium change to RPMI. TNF-alpha was quantified using ELISA. **G**) pBMDMs were subjected to the indicated supernatants from (B) with a medium change to RPMI. IL-6 was quantified using ELISA. Data are means +/- SEM of at least three independent experiments were applicable. All images were created with BioRender.com. One- or two-way ANOVA was used to calculate p-values. ns: not significant; *: p<0.05; **: p<0.01; ***: p<0.001; ****: p<0.0001.

2.2.4. Ferroptosis *in vivo*

In order to study the inflammatory consequences of ferroptosis *in vivo*, a GPX4^{fl/fl} mouse line was used. Since GPX4 KO in mice is embryonically lethal, a floxed allele model was previously developed and is commercially available³⁷⁸. Upon adenoviral Cre administration intratracheally, we induced *Gpx4* deletion in the lung. To this end, 9-12-week-old mice were inhaled with adenoviral Cre (Figure 32A) and sacrificed after 3 weeks, followed by immune analysis via flow cytometry. Non-inhaled controls showed no differences between different cell types (data not shown). GPX4 KO lungs showed slightly elevated CD45+ cells, (Figure 32B). There were no significant differences between myeloid (CD11b+) and dendritic (CD11c+) cells (Figure 32C), neutrophils (CD11b+ Gr1+), M1- macrophages (CD11b+ CD80+) or M2 macrophages (CD11b+ CD206+ and CD11b+ Arg1+) (Figure 32D). There was however a significant difference significantly higher percentages of CD4+ T helper cells as well as a trend for elevated CD8+ cytotoxic T cells in GPX4 KO lungs (Figure 32E).

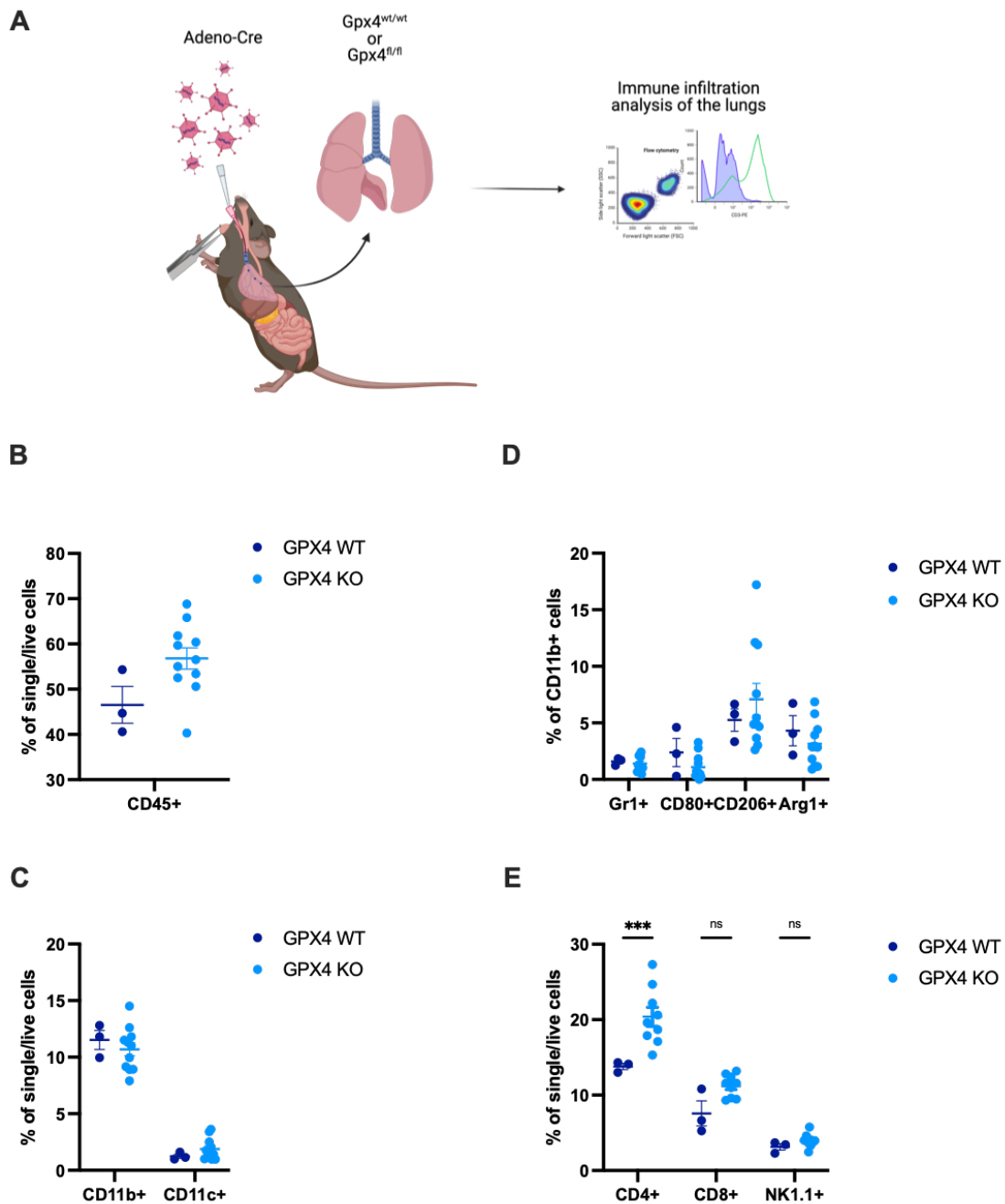


Figure 32. Ferroptosis induction *in vivo* via *Gpx4* deletion induces CD4⁺ T cell recruitment

A) Experimental setup for intratracheally inhalations of the mice. **B-E)** Flow cytometry analysis of the lungs from inhaled GPX4^{wt/wt} and GPX4^{fl/fl} mice. Mice were sacrificed 3 weeks after the inhalation. All images were created with BioRender.com. One- or two-way ANOVA was used to calculate p-values. ns: not significant; *: p<0.05; **: p<0.01; ***: p<0.001; ****: p<0.0001. FACS experiments (B-E) were contributed by Ariadne Androulidaki.

Next, the same samples were subjected to qPCR analysis for the levels of inflammatory markers. Surprisingly, several inflammatory factors were significantly elevated in GPX4 KO lungs including *Tnf*, *Irf3* and *Zbp1* (Figure 33A, 33B). For a deeper analysis on the transcriptional changes upon ferroptosis induction in the lungs upon, samples were sent for RNA sequencing. Results showed different transcriptional profile between GPX4 WT and KO

samples (Figure 33C). Pathway analysis using STRING showed enrichment in autoimmune disease, infection and antigen processing and presentation in GPX4 KO samples (Figure 33D). Hence, our data reveal that although mosaic deletion of GPX4 in the lung alone can lead to transcriptional upregulation in inflammatory genes, it is insufficient to trigger a massive cellular inflammatory response *in vivo*, rather GPX4 deletion seems to ‘prime’ the tissue for an inflammatory response as highlighted by elevated secretion of several inflammatory cytokines.

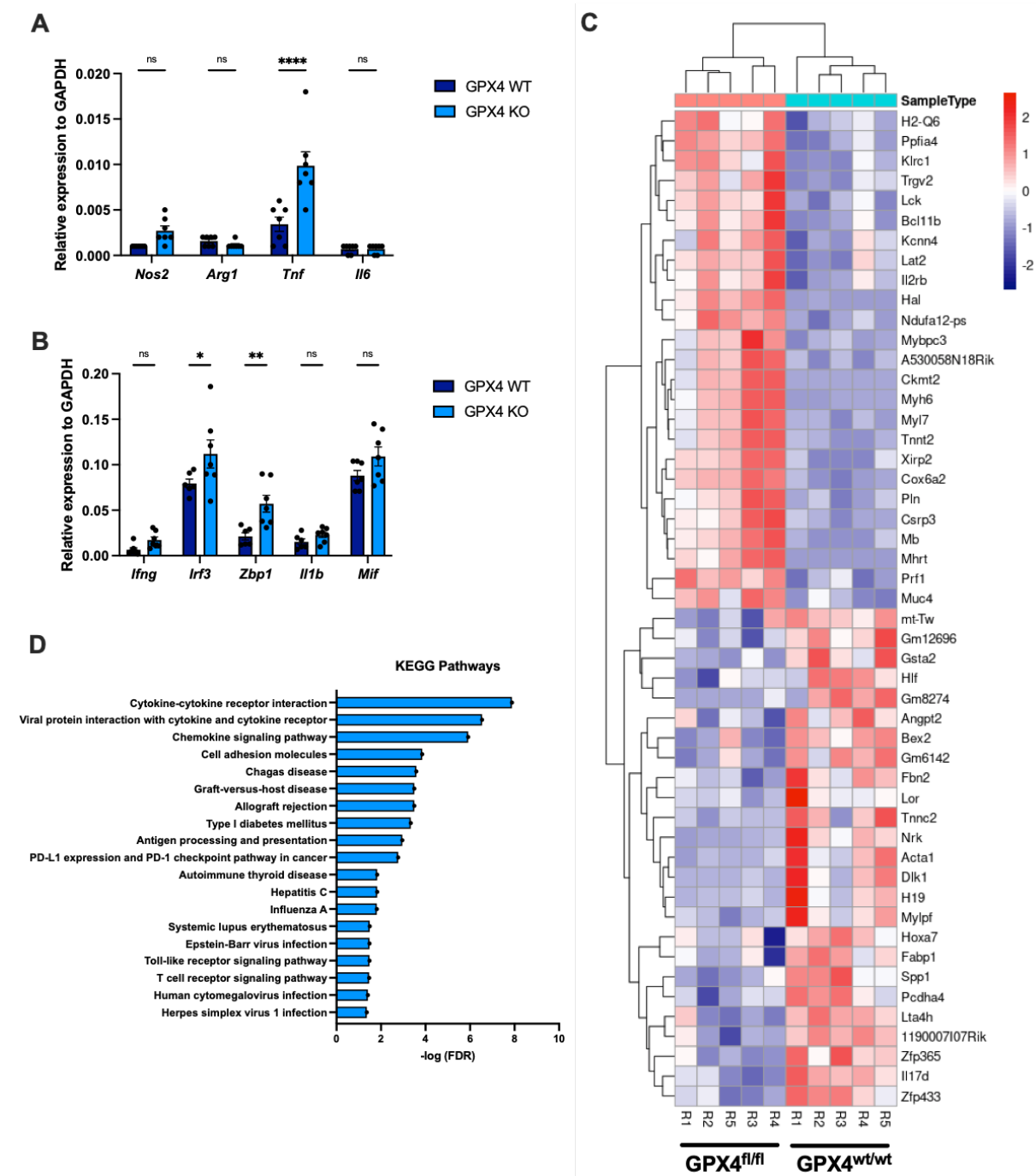


Figure 33. *Gpx4* deletion in the lungs shows signs of inflammation

A-B) qPCR analysis of the lungs from inhaled GPX4^{wt/wt} and GPX4^{fl/fl} mice. The indicated transcripts were quantified by qPCR. **C)** 5 WT and 5 GPX4^{FL/FL} mice of both genders were intratracheally inhaled with 10×10^7 PFU (plaque-forming units) of Adeno-Cre. Three weeks later mice were sacrificed, lungs were excised, RNA isolated and sequenced by RNA-seq. The top 25 differentially expressed genes between both groups are plotted as a heatmap. **D)** KEGG pathways enriched in GPX4^{FL/FL} lungs. One- or two-way ANOVA was used to calculate p-values. ns: not significant; *: p<0.05; **: p<0.01; ***: p<0.001; ****: p<0.0001. RNA sequencing analysis (C, D) was contributed by Ali Abdallah.

3. Discussion

Ferroptosis is a recently described form of regulated cell death that has been implicated in diseases with involvement of inflammation. However, it is not clear if ferroptosis can trigger inflammation as shown by other pathways of regulated cell death such as necroptosis and pyroptosis. The nature of potential DAMPs directly released from ferroptotic cells as well as the mechanisms and type of inflammatory response triggered in immune cells have remained unexplored so far. In this study, it has been identified for the first time, through a multi-omics approach, the first detailed and unbiased analysis of proteins, oxylipins, and metabolites that are released from ferroptotic cells and its subsequent effect on macrophages.

3.1. Investigating the protein fraction of ferroptotic secretome

Over the past decades, the discovery of various types of regulated necrosis has transformed cell death research. With the identification of numerous cell death pathways, the focus to understanding not only the mechanisms and machineries involved but also the immunological consequences of cell death have become relevant. Notably, regulated necrosis pathways involve the rupture of the plasma membrane and cell lysis, leading to the release of cytosolic contents into the extracellular space¹. In this scenario, endogenous non-inflammatory components and organelles from healthy cells can be identified as damage-associated molecular patterns (DAMPs) when they are released, secreted, or exposed during cell death or damage, thereby acquiring immunomodulatory functions²⁵⁰. Mechanistically, DAMPs and alarmins function as ligands that activate immune cells expressing pattern recognition receptors (PRRs), leading to the production of immune factors like cytokines and chemokines. The most well-known DAMPs, play an important role as adjuvants in immunogenic cell death (ICD) but the relationship between ferroptosis and ICD is not yet completely clear. To understand the DAMP-PRR axis in ferroptosis, which links cell death to immunity, it is essential to investigate the specific nature of DAMPs and alarmins released during cell death³⁷⁹. A comprehensive analysis of ferroptotic secretome has been lacking to date.

In this study, different classes of ferroptotic secretome were investigated. Initially the protein fraction of the secretome revealed 353 proteins of which 48 were enriched in ferroptosis supernatants (Figure 17D). The functional network analysis revealed enrichments in innate

immune system and related pathways. Even though the protein fraction was lacking the *bona-fide* chemo-cytokines, the pro-inflammatory cytokine MIF release was identified from ferroptotic cells. Until now only pyroptotic cells were shown to release MIF in addition to other cytokines and alarmins³⁶⁰. Of note, MIF is usually stored within the cytoplasm pre-made and potentially released upon membrane rupture, this can also be seen as induction of ferroptosis did not increase mRNA levels (Figure 18A). The immunomodulatory effects of MIF has been previously characterized as it can enhance M1 polarization of BMDMs *in vitro* in a dose-dependent manner³⁶⁵ and recombinant MIF can also induce the secretion of significant amounts of TNF α in BMDMs³⁶⁶. In addition to its effects on immune cells, MIF was also shown reduce the oxidative stress and lipid peroxidation *in vitro* and *in vivo* by increasing GSH levels playing a role in tubular injury by counteracting cell death³⁶⁷. This study by Stoppe et al. shows a protective role of MIF by potently limiting necroptosis and lipid peroxidation thus ferroptosis by restoring intracellular GSH. As ferroptosis was shown to play a significant role in acute kidney injury (AKI) resulting in the breakdown of renal tubules³⁴⁸, it brings the question whether the release of MIF *in vivo* upon AKI from ferroptotic cells can act as an auto-inhibitory mechanism.

Although several common proteins, including MIF, can be released from both ferroptotic and necroptotic cells, there was a notable absence of any typical NF- κ B-induced proteins in ferroptotic supernatants. Not only in the total released proteome, but also in the newly translated proteome that was previously analysed from the same cell setup in mass spectrometry by a previous study in the lab, lacked chemo- and cytokines production in cells undergoing ferroptosis (data not shown). Absence of necroptosis associated chemo- and cytokines in ferroptosis can also be the result of the lack of RIPK3 activation during ferroptosis as it was shown to be important for CXCL1 production during necroptosis³⁸⁰. It is also worth to mention that due to different abundances of peptides, some might not be detected without enrichment or prefractionation in mass spectrometry. Especially proteins with low molecular weights, including most cytokines, provide less peptides. Indeed, in ELISA assays we could detect basal levels of CXCL1 which were not detected in proteomics. Taken together, even though the protein fraction supernatants from ferroptotic cells contain the pro-inflammatory cytokine MIF in the absence of chemo- and cytokines, experiments performed after the heat-

inactivation of ferroptotic supernatants suggest the non-protein fraction have an effect macrophage polarization.

3.2. Ferroptotic oxylipins and metabolites can influence macrophage phenotype

In addition to the released protein fraction, the non-protein fraction including oxylipins and metabolites were investigated. Several oxylipins with inflammatory potential most importantly prostaglandins were detected in the ferroptotic secretome. Previous studies have shown that ferroptosis is associated to *Ptgs2*¹²⁰, the gene encoding for COX-2 that is involved in the synthesis of PGE₂. PGE₂ is the most abundant eicosanoid lipid in the inflammatory environment although mechanism of which of its suppression of inflammation is not always so clear. Current consensus rests on the activation of protein kinase A (PKA) downstream of the PGE₂ receptors EP2 and EP4 via cAMP. Activated PKA can induce phosphorylation in the transcription factor CREB to elevate the levels of anti-inflammatory cytokines such as interleukin-10 (IL-10)³⁸¹. In the cell death context, it has been described as an inhibitory DAMP released from necroptotic cells and when combined with various PPR ligands it can suppress inflammatory responses by downregulating *Tnf* and *Ifnb1* mRNA³¹⁷. PGE₂ has also been recently described as a vital component of the pyroptotic secretome that plays a role in tissue repair³⁸². Even though it has been described as a marker gene induced upon ferroptosis, release of prostaglandins has not been properly documented from ferroptotic cells. Indeed, knockdown of GPX4 in NIH-3T3 cells resulted in the release of COX2-dependent PGE2 and PGF2 α ³³³. Here we show that a wide range of prostaglandins that are released from ferroptotic cells and the lipidROS dependency of *Ptgs2* and PGE₂ shown to be unique to ferroptosis. Yet, interestingly, *Fer1* significantly lowered basal release of prostaglandins suggesting lipidROS is also involved in their constitutive production. Cyclooxygenases responsible for cellular prostaglandin biosynthesis requires activation via the existing endogenous peroxides^{383,384}. The presence strong radical-trapping agents (RTAs) such as *Fer1* can influence the intracellular redox environment as they act as scavengers for peroxides or free radicals within the cell. Such actions would dampen the production and accumulation of lipid hydroperoxides necessary to activate the COX-2, subsequently lowering the basal prostaglandin levels.

When comparing ATP release between cells undergoing ferroptosis and those undergoing necroptosis, we observed that a robust ATP release is a distinctive trait of cells dying due to

GPX4 inhibition. Interestingly, this ATP release was significantly reduced when FSP1 was overexpressed, suggesting that FSP1's enhancement of radical-trapping ubiquinol production^{125,126} can mitigate this effect. Although ATP release was detected shortly after GPX4 inhibition (30 hours), it was not present in the supernatants of GPX4-depleted cells (48 and 72 hours). Early ferroptotic cell pellets depleted of GPX4 showed a significant accumulation of intracellular nucleotides, accompanied with an increased intermediates of nucleotide synthesis and the pentose phosphate pathway (PPP) prior to cell death. PPP is an alternative metabolic pathway to glycolysis and also plays a role against oxidative stress via NADPH production providing the cells with ribose-5-phosphate that is important for nucleotide synthesis³⁸⁵. As NADPH is vital in neutralizing reactive oxygen intermediates and regenerating reduced GSH from its oxidized form GSSG³⁸⁶, it is plausible to think that upon GPX4 deletion general ROS can lead to PPP activation. Together, these data suggest that early ferroptotic cells might activate the PPP to maintain basal levels of energy homeostasis.

Metabolites enriched in ferroptotic cells show a distinct metabolite profile that can be reversed upon Fer1 addition, confirming their lipidROS dependent enrichment. Interestingly, supernatants from cells undergoing ferroptotic cell death were significantly enriched in methionine cycle, TCA cycle, purine and pyrimidine-derivates. Methionine cycle metabolites S-adenosylmethionine (SAM), S-adenosylhomocysteine (SAH) and 1-methylnicotinamide (MNA) are found to be abundant in ferroptotic supernatants. Intermediates of methionine cycle such as SAM can function as substrates for epigenetic modifications linking cellular metabolism with epigenetic regulation³⁸⁷. This has been shown in the case of T cells where methionine-dependent SAM biosynthesis maintains histone methylation³⁸⁸. Not only the methylation state, but also the activation of BMDMs can be affected upon SAM treatment as it can enhance LPS-induced pro-IL-1 β expression³⁸⁹. While methylation state can rely on SAM availability, as it functions as the universal methyl donor in cells, demethylation requires TCA cycle intermediates such as α -ketoglutarate (also termed 2-oxoglutarate)³⁹⁰. Bystander cells that encounter ferroptotic cells would be exposed to these metabolites and might potentially undergo epigenetic changes. This is significantly important in immune cells as it can affect the "primed" or a "trained" state of innate immune cells. Methionine intermediates are also required by proliferating cells, and in cancer cells where gene promoters are hypo- or hyper-

methyated, reduction in the cellular methylation potential (SAM/SAH) can lead to cell cycle arrest determining the outcome of cancer³⁹¹.

TCA cycle intermediates that were enriched in ferroptotic supernatants, mainly α -ketoglutarate and glutamate in combination with ATP and lactate fall in the line with a previous study¹⁵⁰ describing glutaminolysis as one of the crucial hallmarks of ferroptosis. Ferroptotic cells also released increased amounts of lactate, suggestive of increased rates of glycolysis. High glycolytic rates leading to lactate release was shown to alter metabolism in human monocytes upon *M. tuberculosis* infection leading to increased levels of TNF α and IL-1 β production³⁹². In combination with methionine and TCA cycle intermediates, a well described DAMP uric acid³⁹³ was also detected in ferroptotic supernatants. Of note, TCA cycle intermediates like fumarate and succinate can inhibit certain demethylases and crucially effect trained immunity³⁹⁴. The metabolic rewiring of trained macrophages as a result represents a plausible mechanism behind the integration of immunometabolic and epigenetic programs in trained immunity that might be caused by ferroptotic cells. While macrophages trained with ferroptotic secretomes had a trend of secreting higher levels of pro-inflammatory cytokines, there were no detectable metabolic changes as measured by Seahorse assays (data not shown). Differences in trained immunity ligands might differ in the characteristics of macrophages as some can lack the pre-defined metabolic rewiring but still keep the epigenetic changes to enrich for pro-inflammatory cytokines. For example, the aldosterone-trained macrophage is different from cells trained by prototypical microbial inducers of trained immunity³⁹⁵. A recent study has reported the induction of distinct trained-immunity subpopulations in human monocytes. Characterization of gene expression profiles via single-cell RNA sequencing revealed a high heterogeneity of cytokines and chemokine markers across monocyte subpopulations where the existence of a subpopulation with low trained immunity phenotype was also present³⁷⁷. Due to high heterogeneity within trained immunity populations, further epigenetic and single cell characterization can shed more light into the variability we observed in ferroptotic supernatant-trained macrophages.

3.3. Priming of macrophages is linked to the non-protein fraction of ferroptotic secretomes

Ferroptotic cells release a secretome containing protein and non-protein fractions that can potentially have immunomodulatory effects. The host immune response is largely based on the detection of pathogen- or damage-associated patterns (PAMPs or DAMPs) that lead to the activation of various immune cells. The host response is usually divided into two parts: the innate and adaptive immune response. Initial activation of pattern recognition receptors (PRRs) induces the secretion of pro-inflammatory cytokines which subsequently activate the adaptive immune response. After exposure to a pathogen, lymphocytes can recognize and form the memory B and T cells that can be activated upon reencountering with the same pathogen²¹⁰.

Multiple PRRs have been identified as responsive to ferroptotic DAMPs³²³. Recently, TLR4 has been highlighted for its critical role in recruiting immune cells in response to ferroptosis in an *in vivo* ischemia-reperfusion injury model. This immune response was completely abrogated by inhibiting ferroptosis³⁵⁰. Preliminary studies done with ferroptotic cell supernatants on cytokine arrays with two immortalised macrophage cell lines showed very limited production of secreted chemo- and cytokines (data not shown). The extensive multi-omics done in this study on different fractions of the ferroptotic secretome identified certain DAMPs that can be sensed by immune cells. RNA sequencing that was performed with ferroptotic supernatant exposed primary bone marrow derived macrophages revealed enrichment in GO terms associated with immune activation. Besides *CD74*, a MIF receptor, and *Ptger3*, a PGE₂ receptor, further significantly upregulated transcripts related to inflammatory processes included the transcriptional regulator *Id3* that can control the formation of distinct memory CD8+ T cell subsets³⁹⁶, an endogenous inhibitor of MIF^{397,398}, Gremlin-1 (*Grem1*), that can potentially block the M1 polarization of macrophages³⁹⁹. One of the N-formyl peptide (fMLF or fMet-Leu-Phe) receptors (FPRs), *Fpr1*, was also significantly upregulated in macrophages upon exposure to ferroptotic cells. FPRs are a family of PRRs that can elicit important regulatory effects during inflammation and cancer⁴⁰⁰. While fMLF from bacteria were the initial ligands for FPRs⁴⁰¹, it can also derive endogenously from mitochondria as a result of severe cell dysfunction or cell death^{402,403}. Necrotic cells were shown to release mitochondria derived fMLF and activate human monocytes⁴⁰⁴. As ferroptosis is described with

mitochondrial fragmentation and breakdown it is tempting to speculate that ferroptotic cells cause upregulation of *Fpr1* upon detection of fMLF peptides.

In addition to other PPRs upregulated, the scavenger receptor *Marco* was also enriched in primary BMDMs upon ferroptotic secretomes. Besides its main function as regulator of phagocytosis, *Marco* can participate in cell-cell recognition to start inflammatory responses⁴⁰⁵. Ligands include acetylated low-density lipoprotein (acLDL)⁴⁰⁶, oxidised LDL (oxLDL)⁴⁰⁷ but also apoptotic cells⁴⁰⁸. *Marco* is highly expressed in tumour-associated macrophages (TAMs) and monocytic myeloid-derived suppressor cells (mMDSCs)^{409,410} contributing to tumour progression by suppressing NK- and T-cell antitumor functions. *Marco* is one of the scavenger receptors that can tether DAMPs to other PPRs such as TLR2, could very well be the mechanism behind the phagocytosis of ferroptotic cells as it also happens via TLR2 signalling³³¹. Another upregulated gene in ferroptotic-exposed macrophages, versican (*Vcan*), is an ECM-derived peptidoglycan that can lead to the production of pro-inflammatory cytokines in macrophages by TLR2 activation driving metastasis^{411,412}. Upregulation of *Vcan* in myeloid cells potentially support the cells in their own microenvironment as a part of the inflammatory response. *Vcan* expression by macrophages thought to be critical for promoting metastasis as its highly expressed in tumour-associated macrophages (TAMs) by mediating mesenchymal to epithelial transition (MET) of metastatic tumour cells⁴¹³. More work is needed to elucidate the role that versican plays in monocyte/macrophage involvement upon encountering ferroptotic cells, as it can change the course of cancer progression. We also found *Clec4n* (Dectin-2), a C-type lectin receptor, and *Il1b* to be upregulated in BMDMs treated with ferroptotic secretomes. Given that the related C-type lectin receptor Dectin-1 and IL-1 β have both been shown to promote a state of “trained immunity” in macrophages, our claim that ferroptotic secretomes may elicit trained immunity of macrophages was further supported but as mentioned before needs to be studied in more detail.

In addition to the potentially ferroptotic supernatant-trained macrophages, we thought to test whether ferroptotic cells can also “prime” the macrophages in which the effect of the immune-relevant genes is further enhanced with a secondary challenge. The M1/M2 polarization model offers a straightforward way to differentiate between two types of macrophages based on their metabolic activities⁴¹⁴. M1 macrophages are associated with

tumor regression and the inhibition of tumor growth, while M2 macrophages promote tumor development by producing angiogenesis factors and inhibiting M1 macrophages, thereby suppressing antitumor immunity⁴¹⁵. Based on this, both immortal and primary BMDMs were primed with ferroptotic supernatants and further polarized with IFN γ + LPS (M1) and IL-4 (M2) stimuli. Even though the polarization was confirmed via western blotting by ARG1 expression, there were no significant chemo- or cytokines detected from M2 polarized macrophages (data not shown). Whereas M1 polarization in addition to ferroptotic supernatants significantly increased TNF α and IL-6 secretion from macrophages, it didn't affect their phagocytosis capabilities (data not shown). The additional excitability of macrophages upon encountering ferroptotic cells brings the question of what might be responsible for the LPS-induced enhanced cytokine secretion from ferroptotic-secretome exposed macrophages. Even though the protein fraction of the secretome was heat-inactivated by cooking of the supernatants, the additive effect of ferroptotic secretome were still present on macrophages linking the source of the ligand to the non-protein fraction that is composed of lipid mediators, metabolites and potentially other heat-stable small molecules that are not measured. Notably, necroptotic supernatants were unable to enhance LPS-induced cytokine secretion.

For an efficient ICD during infection or cancer DAMPs (responsible for adjuvanticity) and antigens needs to be presented to T-cells in a well-established manner. It is important to emphasize that although the release of DAMPs is necessary for ICD, it does not necessarily ensure the induction of immunogenicity⁴¹⁶. While macrophages are responsible for the initial phagocytosis, the main cells capable of antigen presentation are dendritic cells (DCs) that mature and get activated in the presence of DAMPs. A recent study showed that even though DCs engulfed and underwent maturation after co-cultured with ferroptotic cancer cells, they failed to perform antigen cross-presentation that would affect T-cell stimulation and proliferation³³⁶. At the same time ferroptotic neurons were shown to secrete factors that promote T-cell activation and cytokine production⁴¹⁷. The limited activation of macrophages observed without LPS might result from a unique combination of pro- and anti-inflammatory modulators in ferroptotic supernatants. Since any of the metabolites, oxylipins, or other non-protein mediators not examined in this study could mediate these priming effects on macrophages, extensive future research will be necessary to identify the specific class of these modulators.

3.4. Ferroptosis and inflammation in tissue pathology

In this study, we've made use of an *in vivo* model for ferroptosis in the lung by targeted mosaic knockout of *Gpx4* upon viral Cre administration. The role of ferroptosis in the pathological progression of various lung diseases such as acute lung injury (ALI)^{354,354,418–421}, radiation-induced lung injury (RILI)^{356,422}, chronic obstructive pulmonary disease (COPD)^{355,423}, asthma^{424–426}, infections^{427–429} and cancer^{126,362,430–433} has been acknowledged. Additionally, numerous interventions—such as ferroptosis inducers and inhibitors, iron chelators, lipid peroxidation inhibitors, and antioxidants—have been explored for ferroptosis-related lung diseases⁴³⁴. Upon analysis of different immune cell groups in the lung upon ferroptosis induction, only CD4+ T cells were significantly upregulated. Meanwhile on the gene level, upregulation in *Tnf*, *Irf3* and *Zbp1* strongly suggests a type I interferon response and potentially NF-κB-driven inflammatory environment in the lung. Further pathway enrichment done with the identified hits from RNA sequencing were also strongly linked to cytokine-cytokine receptor interactions hinting at an acute inflammatory profile post ferroptotic cell death. Resident alveolar macrophages are major regulators of the lung inflammatory microenvironment and the first line of defence against infectious and non-infectious stimuli⁴³⁵. Most of the alveolar macrophages display plasticity, with both M1 and M2 phenotypes simultaneously allowing them to quickly switch in between⁴³⁶. Inhibiting ferroptosis has been demonstrated as an effective approach to alleviate pulmonary inflammation and tissue damage in acute respiratory distress syndrome (ARDS) including LPS-³⁵⁴ and intestinal ischemia/reperfusion (IRI)-⁴¹⁹ induced acute lung injury (ALI), acute radiation-induced lung injury (RILI)⁴²² and chronic obstructive pulmonary disease (COPD)³⁵⁵. Ferroptosis induced by bacterial infection can also exacerbate the tissue injury in bacterial pneumonia⁴²⁸. Therefore, ferroptosis induction in the lung epithelial tissue can affect the polarization state alveolar macrophages and subsequently the outcome of infection or cancer.

DAMPs that are released upon ferroptosis not only harms epithelial and endothelial cells but can also recruit and activate immune cells, further amplifying the damage. Cell death can have a sensitizing effect on the tissue but not lead to a full-blown inflammation. This hypothesis was tested by a study conducted by Dai and colleagues in the pancreas, who observed similar results in *Gpx4* wild-type versus knockout mice using the same conditional knockout *in vivo* model³²⁶. Their findings revealed that knockout (KO) mice experienced increased mortality

and pancreatic injury compared to wild-type (WT) mice when subjected to cerulein- or arginine-induced pancreatitis. Furthermore, DAMPs specifically 4-HNE and 8-hydroxy-2'-deoxyguanosine (8-OHG) was released from ferroptotic pancreas cells leading to the activation of TMEM173/STING pathway. Notably, both the acute pancreatitis and the KRAS-driven PDAC model had increased M1 macrophage infiltration upon ferroptosis. This suggests that GPX4 KO mice are more vulnerable to pancreatic tissue damage than WT mice, supporting our hypothesis that ferroptotic cell death might prime tissues for an amplified immune response.

Although other regulated necrosis pathways like necroptosis and pyroptosis have been shown to exacerbate inflammation in various diseases, a growing body of literature suggests that ferroptosis may initiate inflammation or sensitize tissues to other inflammatory events. Importantly, immunogenic cell death recruits and activates immune cells through alarmins, which are hypothesized to trigger additional necrotic cell death pathways. As such, a sequence wherein one type or regulated necrosis precedes another *in vivo* is possible. However, the specific molecular pathways and mechanisms that would drive primary and secondary necroinflammation, as well as the hierarchical sequence of these events, remain to be fully understood. Overall, there is strong evidence that ferroptosis is closely linked to pronounced inflammatory responses, marked by increased levels of proinflammatory cytokines in damaged tissues. These findings collectively suggest that ferroptosis plays a crucial role in early inflammatory processes *in vivo*, and that preventing necroinflammation could offer a new therapeutic approach for addressing inflammatory tissue damage and disease.

3.5. Concluding remarks and future perspectives

In conclusion, our study presents the first comprehensive catalogue of ferroptotic secretomes and compares these with factors released from necroptotic cells. Our data support the idea, that ferroptotic secretomes contain some factors with innate immune activity but lack other *bona fide* inflammatory chemo- and cytokines. While many features are shared in the release profiles of cells undergoing regulated necrosis, we found that significant metabolite release is a distinctive characteristic of ferroptosis. Further experiments done with pBMDMs exposed to ferroptotic supernatants expressed increased levels of *Il1b* mRNA which is one of the hallmarks of inflammasome priming. Potential target pathways that are involved in the

transcriptional reprogramming of macrophages can be further identified by utilizing different knockout strains of pBMDMs to fully decipher how the ligand/receptor systems are involved in macrophage-priming. Given our *in vitro* data also pointing towards trained immunity, an immune response augmenting anti-pathogen immune activation, implementing a single cell RNA-sequencing experiment in *Gpx4*-knockout lungs *in vivo* can allow us to identify which populations are affected most by GPX4 ablation and which immune cell compartments account for the observed difference in inflammatory signatures. In addition to this finely resolved information on immune cell states, we should be able to see possible stromal reactions such as fibroblast recruitment and activation as a response to tissue injury. Overall, our data provide a foundational basis for exploring the potential cell-type specificity of ferroptosis-induced immune responses in the future.

4. Materials and Methods

4.1. Animals

4.1.1. Tissue harvest

Mice from the C57BL/6N strain were obtained from in-house breeding at the CECAD in vivo research facility at the Cologne University Medical Center, Cologne, Germany, and housed in compliance with animal welfare regulations according to the local animal welfare authority (Landesamt für Natur, Umwelt und Verbraucherschutz Nordrhein-Westfalen, Germany) under specific-pathogen-free conditions with food and water ad libitum and a regular 12-hour light-dark-cycle. For tissue harvest, animals were handled and sacrificed in compliance with Directive 2010/63/EU. Primary murine bone marrow derived macrophages (pBMDMs)³⁷⁵ and primary lung fibroblasts (PMLFs)⁴³⁷ were generated as previously described.

4.1.2. Inhalations

9-12 weeks old mice were anesthetized with Ketavet (100 mg/kg) and Xylazine (20 mg/kg) by intraperitoneal injection followed by intratracheal inhalation of replication-deficient adenovirus expressing Cre (Ad5-CMV-Cre, 1×10^{11} PFU, University of Iowa) mixed with OptiMEM and CaCl₂ (10mM).

4.2. Chemicals and reagents

Murine His-TNF-alpha was kindly provided by Prof. Dr. Henning Walczak.

Table 4-1. Chemicals, peptides, and recombinant proteins

Name	Company	Catalogue Number
2-Propanol	Roth	Cat# 9866.5
37% Formaldehyde	VWR	Cat# 1.039.992.500
3,3',5,5' tetramethylbenzidine (TMB)	Sigma Aldrich	Cat# 87748
30% H ₂ O ₂	Sigma Aldrich	Cat# 95313
Acetic Acid (CH ₃ COOH)	Roth	Cat# 3738.2
Acetone	Sigma Aldrich	Cat# 179124
Acetonitrile hypergrade for LC-MS	Merck Millipore	Cat# 1.00029.2500
Amersham ECL Prime Western Blotting Detection Reagent	Cytiva	Cat# RPN2235
Ammonium carbonate	Merck Millipore	Cat# 207861-500G
Ammonium hydroxide solution	Merck Millipore	Cat# 221228-1L-A

Ammonium persulfate	Sigma Aldrich	Cat# 431532
Arg-10 HCL	Silantes	Cat# 201604102
Benzonase HC	Merck Millipore	Cat# 71206
Birinapant	Selleck Chem	Cat# S7015
Bovine Serum Albumin (BSA)	Sigma Aldrich	Cat# A7030
BODIPY™ 581/591 C11	Invitrogen	Cat# D3861
Brefeldin A	Biolegend	Cat# 420601
Calcium chloride (CaCl ₂)	Roth	Cat# CN92.1
CAA (2-Chloracetamid)	Merck Millipore	Cat# 79-07-2
Collagenase IV	Sigma Aldrich	Cat# C5138
cOmplete™, EDTA-free Protease Inhibitor Cocktail	Sigma Aldrich	Cat# 4693132001
Dimethyl sulfoxide (DMSO)	PAN Biotech	Cat# P60-36720100
Dithiothreitol (DTT)	VWR	Cat# 441496P
DNase IV	Sigma Aldrich	Cat# D5025
Doxycycline	VWR	Cat# J63805.06
DRAQ7	Biolegend	Cat# 424001
Emricasan	Hözel	Cat# HY-10396
Erastin	Biomol	Cat# 5449/10
Ethanol 99%, absolute	Roth	Cat# 9065.3
Ethylenediaminetetraacetic acid (EDTA)	VWR	Cat# 1084520250
Ferrostatin-1	Cayman Chemicals	Cat# 17729
Formic acid	Honeywell/Fluka	Cat# 607-001-00-0
GSK872	Millipore	Cat# 530389
ITS+1	Sigma-Aldrich	Cat# I2521
Hyaluronidase V	Sigma-Aldrich	Cat# H6254
Ketaset	ZOETIS	Cat# 116810
LPS from E. coli, Serotype EH100 (Ra) (TLRGRADE™) (Ready-to-Use)	Enzo	Cat# ALX-581-010-L001
Lys-8 HCL	Silantes	Cat# 211604102
Lysyl Endopeptidase (LysC)	WAKO	Cat# 129-02541
Methanol-LC-MS grade	VWR	Cat# 1.06035.2500
Murine His-TNF-alpha	Walczak lab	Kupka et al. ⁴³⁸
ML210	Tocris	Cat# 6429/10
N, N, N', N'-Tetramethylethylenediamine (TEMED)	Sigma	Cat# T9281
Necrostatin-1s	Abcam	Cat# ab221984
PhosSTOP™	Sigma	Cat# 4906837001
Ponceau S	Sigma	Cat# P3504
Propidium iodide (PI)	Sigma	Cat# P4170
Protease inhibitor	Sigma-Aldrich	Cat# 4693132001

Recombinant Murine M-CSF	Peprotech	Cat# 315-02
RIPA buffer	Thermo Fisher	Cat# 89901
ROTIPHORESE® Gel 30	Roth	Cat# 3029.2
RSL3	Selleck Chem	Cat# S8155
Skim milk powder	VWR	Cat# A0830
Sodium Acetate Trihydrate (CH ₃ COONa.3H ₂ O)	VWR	Cat# 1062671000
Sodium Azide	Sigma	Cat# S2002-100G
Sodium Chloride (NaCl)	VWR	Cat# 1064045000
Sodium dodecyl sulphate (SDS)	Sigma Aldrich	Cat# L3771-100G
STY-BODIPY	Cayman Chemical	Cat# Cay27089-500
Sulfuric acid 10% (H ₂ SO ₄)	VWR	Cat# 95441000
SuperSignal™ West Femto Maximum Sensitivity Substrate	Thermo Fisher	Cat# 34095
Tamoxifen (4-OHT)	Sigma Aldrich	Cat# H7904-5MG
TEAB	Sigma Aldrich	Cat# T7408
Tris	VWR	Cat# 1083872500
Tris-HCl	VWR	Cat# 648313-250
Triton x100	VWR	Cat# 1086031000
Trypsin-EDTA (%0.25)	Gibco	Cat# 25200056
Tween 20	VWR	Cat# 0777-1L
Urea	Sigma Aldrich	Cat# U1250
Valine-d8	CK-Isotopes	Cat# DLM-488
Xylazine	Serumberg	-

Table 4-2. Critical commercial assays

Name	Company	Catalogue Number
Bicinchoninic acid (BCA) protein assay	Biorad	Cat# 774985
Click Chemistry Capture Kit	Jena Bioscience	Cat# CLK-1065
CytoTox 96® Non-Radioactive Cytotoxicity Assay	Promega	Cat# G1780
LunaScript RT SuperMix Kit	NEB	Cat# E3010L
Luna Universal qPCR Master Mix	NEB	Cat# M3003E
NucleoSpin RNA Kit	Macherey-Nagel	Cat# 740955250
RealTime-Glo™ Extracellular ATP Assay	Promega	Cat# GA5010

4.3. Nucleic acid techniques

4.3.1. RNA isolation and cDNA synthesis

Total RNA from tissues was isolated using the NucleoSpin RNA kit (Macherey-Nagel, 740955.250) according to the manufacturer's protocol. cDNA synthesis from the isolated RNA

was reverse transcribed using the LunaScript RT SuperMix Kit (NEB, E3010L) following the protocol provided by the manufacturer (Table 4-3, 4-4).

Table 4-3. cDNA reaction components

Name	Amount in 20 μ l Reaction	Concentration	Final concentration in 10 μ l
LunaScript RT SuperMix	4 μ l	5X	1X
cDNA	Variable*	*Up to 1 μ g	Variable
H ₂ O	To 20 ml	-	

Table 4-4. cDNA synthesis thermocycler protocol

Cycle Step	Temperature	Time	Cycles
Primer Annealing	25°C	2 minutes	1
cDNA Synthesis	55°C	10 minutes	
Heat Inactivation	95°C	1 minute	
Hold	4°C	∞	

4.3.2. Determination of DNA concentration

The Nanodrop 8000 spectrophotometer (Thermo Fisher Scientific) was used to determine the concentration of nucleic acids. The purity of DNA and RNA is reported by the ratio of absorbance at 260 nm to 280 nm. A ratio of OD₂₆₀/OD₂₈₀ about 1.8 was considered as sufficiently purified DNA samples. A ratio of OD₂₆₀/OD₂₈₀ of 2.0 was considered as sufficiently purified RNA samples.

4.3.3. Quantitative realtime PCR analysis

For quantitative real-time PCR (qRT-PCR) analysis, Luna[®] Universal qPCR Master Mix (NEB, M3003S) was mixed with nuclease-free water (NEB, B1500L), forward and reverse primers (Thermo Fisher) reconstituted in nuclease free water (NEB, B1500L) and cDNA (Table 4-5). Real-time qPCR was performed in quadruplets on the Quant Studio 5 qRT-PCR machine. Relative expression of gene transcripts was analysed via the 2- Δ CT or the 2- $\Delta\Delta$ CT method to the reference gene Glycerinaldehyde-3-phosphate-Dehydrogenase (GAPDH).

Table 4-5. qPCR reaction components

Name	Amount in 10 μ l Reaction	Concentration	Final concentration in 10 μ l
Primer Mix (Forward & Reverse)	1 μ l	10 μ M	100 nM

Luna® Universal qPCR Master Mix	2µl	2x	1x
cDNA	2µl	5 ng/µl	10 ng
H ₂ O	1µl	-	

Table 4-6. qPCR primer sequences

Primer	Sequence (5' > 3')	Species	Source
Alox5 forward	ACTACATCTACCTCAGCCTCATT	<i>M. Musculus</i>	Harvard Primer Bank
Alox5 reverse	GGTGACATCGTAGGAGTCCAC	<i>M. Musculus</i>	Harvard Primer Bank
Alox12 forward	TCCCTCAACCTAGTGCGTTTG	<i>M. Musculus</i>	Harvard Primer Bank
Alox12 reverse	GTTGCAGCTCCAGTTTCGC	<i>M. Musculus</i>	Harvard Primer Bank
Alox15 forward	GGCTCCAACAACGAGGTCTAC	<i>M. Musculus</i>	Harvard Primer Bank
Alox15 reverse	AGGTATTCTGACACATCCACCTT	<i>M. Musculus</i>	Harvard Primer Bank
Amica1 forward	ATGCTTTGCCTCCTGAAACTG	<i>M. Musculus</i>	Harvard Primer Bank
Amica1 reverse	TGATTCACCCACATGCACTCT	<i>M. Musculus</i>	Harvard Primer Bank
Arg2 forward	TCCTCCACGGGCAAATTCC	<i>M. Musculus</i>	Harvard Primer Bank
Arg2 reverse	GCTGGACCATATTCCACTCCTA	<i>M. Musculus</i>	Harvard Primer Bank
Cd74 t2 forward	CCGCCTAGACAAGCTGACC	<i>M. Musculus</i>	Harvard Primer Bank
Cd74 t2 reverse	ACAGGTTTGGCAGATTTCCGGA	<i>M. Musculus</i>	Harvard Primer Bank
Clec4n t1 forward	AAGCGGAGCAGAATTTTCATCA	<i>M. Musculus</i>	Harvard Primer Bank
Clec4n t1 reverse	CCATTTGCCATTACCTTGTGGA	<i>M. Musculus</i>	Harvard Primer Bank
Gapdh forward	CTCCCACTCTTCCACCTTCG	<i>M. Musculus</i>	Harvard Primer Bank
Gapdh reverse	GCCTCTCTTGCTCAGTGTCC	<i>M. Musculus</i>	Harvard Primer Bank
Il1beta forward	GAAATGCCACCTTTTGACAGTG	<i>M. Musculus</i>	Harvard Primer Bank

Il1beta reverse	TGGATGCTCTCATCAGGACAG	<i>M. Musculus</i>	Harvard Primer Bank
Il6 forward	CTGCAAGAGACTTCCATCCAG	<i>M. Musculus</i>	Harvard Primer Bank
Il6 reverse	AGTGGTATAGACAGGTCTGTTGG	<i>M. Musculus</i>	Harvard Primer Bank
Marco forward	ACAGAGCCGATTTTGACCAAG	<i>M. Musculus</i>	Harvard Primer Bank
Marco reverse	CAGCAGTGCAGTACCTGCC	<i>M. Musculus</i>	Harvard Primer Bank
Mif forward	CAGAGGGGTTTCTGTCCGAG	<i>M. Musculus</i>	NCBI
Mif reverse	GTGCACTGCGATGTACTGTG	<i>M. Musculus</i>	NCBI
Por forward	ATGGGGGACTCTCACGAAGAC	<i>M. Musculus</i>	Harvard Primer Bank
Por reverse	TCTTGCTGAACTCCGGTATCTC	<i>M. Musculus</i>	Harvard Primer Bank
Ptgds forward	TGCAGCCCAACTTTCAACAAG	<i>M. Musculus</i>	Harvard Primer Bank
Ptgds reverse	TGGTCTCACACTGGTTTTTCT	<i>M. Musculus</i>	Harvard Primer Bank
Ptger3 forward	CCGGAGCACTCTGCTGAAG	<i>M. Musculus</i>	Harvard Primer Bank
Ptger3 reverse	CCCCACTAAGTCGGTGAGC	<i>M. Musculus</i>	Harvard Primer Bank
Ptges forward	GGATGCGCTGAAACGTGGA	<i>M. Musculus</i>	Harvard Primer Bank
Ptges reverse	CAGGAATGAGTACACGAAGCC	<i>M. Musculus</i>	Harvard Primer Bank
Ptgs1 forward	ATGAGTCGAAGGAGTCTCTCG	<i>M. Musculus</i>	Harvard Primer Bank
Ptgs1 reverse	GCACGGATAGTAACAACAGGGA	<i>M. Musculus</i>	Harvard Primer Bank
Ptgs2 forward	TGAGCAACTATTCCAAACCAGC	<i>M. Musculus</i>	Harvard Primer Bank
Ptgs2 reverse	GCACGTAGTCTTCGATCACTATC	<i>M. Musculus</i>	Harvard Primer Bank
Serpib2 t1 forward	GTGCTGGGGGTAACACTGAAC	<i>M. Musculus</i>	Harvard Primer Bank
Serpib2 t1 reverse	GCGAAATCACAGCCACTGAAG	<i>M. Musculus</i>	Harvard Primer Bank

Serpinb2 t2 reverse	GGTGTGTTGATTGTTGAGCTGA	<i>M. Musculus</i>	Harvard Primer Bank
Tnf forward	CAGGCGGTGCCTATGTCTC	<i>M. Musculus</i>	Harvard Primer Bank
Tnf reverse	CGATCACCCCGAAGTTCAGTAG	<i>M. Musculus</i>	Harvard Primer Bank

4.4. Cell culture techniques

Table 4-7. Cell culture reagents

Name	Company	Catalogue Number
ACK lysis buffer	Thermo Fisher	Cat# A1049201
DMEM, high glucose, pyruvate	Thermo Fisher	Cat# 41966052
DMEM, high glucose, no glutamine, no phenol red	Thermo Fisher	Cat# 31053028
DMEM, high glucose, GlutaMAX™ supplement	Thermo Fisher	Cat# 61965059
EDTA (Versene), 1%, in PBS, without Ca ²⁺ and Mg ²⁺	Genexon Bioscience	Cat# C4263.0100
Fetal Bovine Serum (FBS)	Sigma	Cat# 10500064
HBSS without Ca ²⁺ and Mg ²⁺	Lonza	Cat# 10-547F
ITS+1 Liquid Media Supplement (100×)	Sigma	Cat# I2521
OptiMEM	Thermo Fisher	Cat# 31985062
PBS, pH 7.4	Thermo Fisher	Cat# 10010056
Penicillium/Streptomycin (P/S)	Sigma	Cat# P4333-100ML
Reagent Reservoirs	VWR	Cat# 613-1174
RPMI 1640 medium	Thermo Fisher	Cat# 21875091
SILAC DMEM FBS Kit	Silantes	Cat# 282006500
75 cm ² Cell Culture Flask	Greiner	Cat# 658175
175 cm ² Cell Culture Flask	Greiner	Cat# 660175
6 Well Cell Culture Plate	Greiner	Cat# 657160
24 Well Cell Culture Plate	Greiner	Cat# 662160
96 Well Cell Culture Plate	Greiner	Cat# 655180
5 mL Serological pipettes	Greiner	Cat# 606180
10 mL Serological pipettes	Greiner	Cat# 607180

Table 4-8. Cell lines

Cell line	Organism	Tissue	Source
GPX4 Control	<i>M. Musculus</i>	GPX4 Control mouse small cell lung cancer tumor line RP252.7	Bebber et al. ³⁶²

GPX4 KO	<i>M. Musculus</i>	GPX4 KO mouse small cell lung cancer tumor line RP252.7	Bebber et al. ³⁶²
Pfa1	<i>M. Musculus</i>	Tamoxifen-inducible GPX4KO mouse embryonic fibroblast	Seiler et al. ³⁶¹
Pfa1-mFSP1 OE	<i>M. Musculus</i>	mFSP1 overexpressing, tamoxifen-inducible GPX4KO mouse embryonic fibroblast	Doll et al. ¹²⁵
CL13	<i>M. Musculus</i>	Immortalized murine bone marrow-derived macrophages	De Nardo et al. ⁴³⁹
ZBP1-EV	<i>M. Musculus</i>	ZBP1-empty vector-inducible mouse embryonic fibroblast	Jiao et al. ³⁷⁶
ZBP1-OE	<i>M. Musculus</i>	ZBP1-overexpression-inducible mouse embryonic fibroblast	Jiao et al. ³⁷⁶
pBMDMs	<i>M. Musculus</i>	Primary bone marrow derived macrophages	von Karstedt lab
PMLFs	<i>M. Musculus</i>	Primary lung fibroblasts	von Karstedt lab

4.4.1. Cell lines and culture conditions

Murine SCLC cell lines were cultured in RPMI; Pfa1 and Pfa1-mFSP1OE cells were cultured in DMEM GlutaMAX™; CL13 BMDMs were cultured in DMEM medium. All cells were kept at 37°C with 5% CO₂ and all media were supplemented with 10% FCS and 1% P/S. All cell lines were tested for mycoplasma at regular intervals (mycoplasma barcodes, Eurofins Genomics).

4.5. Protein analysis techniques

4.5.1. Cell lysis and protein isolation from cells

To analyse the protein expression of a specific protein in different cell lines and under different conditions, cells were washed once with PBS and lysed RIPA buffer (Thermo Fischer, 89901) containing protease and phosphatase inhibitors (Sigma, 4693132001 and 4906837001) on ice or overnight at -20°C. Lysates were centrifuged for 20 minutes at 13000 rpm at 4°C. Supernatant containing the whole protein fraction was then transferred into a new reaction tube to determine the protein concentration using bicinchoninic acid (BCA) protein assay

(Biorad, 774985) according to the manufacturer's instructions. The absorbance of each sample was measured at 750 nm with plate reader (Thermo scientific, Multiskan SkyHigh).

4.5.2. SDS - Polyacrylamide Gel Electrophoresis (PAGE)

To resolve the proteins, sodium dodecyl sulphate polyacrylamide gel electrophoresis (SDS-PAGE) consisting of a stacking gel with a polyacrylamide percentage of 4% followed by separation gel with differing percentages (Table 4-9) were used. Equal amounts of protein were mixed with a final concentration of 1x reducing sample buffer and 200 mM DTT. Cell lysates were heated for 10 minutes at 80°C in order to speed up the process of denaturation. Gel electrophoresis of proteins was performed using the Mini-PROTEAN® Tetra Cell System (1658004) by Biorad. Proteins were separated via gel electrophoresis at 80V for 30 minutes followed by 180V for 1 hour in 1x Tris-Glycine SDS Running buffer (Biorad, 1610772).

Table 4-9. SDS-PAGE composition

Components	12,5% Separating gel	15% Separating gel	4% Stacking gel
	Volume for 2 gels		Volume for 2 gels
30% Acrylamide	6.3ml	7.5ml	700µl
1.5 M Tris, pH 8.8	3.8ml	3.8ml	-
0.5 M Tris, pH 6.8	-	-	1.3ml
10% (w/v) Ammonium persulfate	75µl	75µl	33µl
TEMED	7.5µl	7.5µl	5µl
MilliQ	4.9ml	3.6ml	3ml

4.5.3. Western blot analysis

Trans-Blot® Turbo Transfer System (Biorad, 1704270) was used for the transfer of the proteins from the SDS gel to the nitrocellulose membrane. After protein transfer, ponceau solution was used to confirm transfer and membranes were blocked in PBS with 0.1% Tween 20 (PBS-T) with 5% (w/v) skim milk powder (VWR, A0830) for 1 hour. Next, membranes were incubated with the primary antibodies (Table 4-10) overnight at 4°C. The following day membranes were washed three times with PBST for a total amount of 30 minutes. Incubation with secondary antibody conjugated with horse radish peroxidase (HRP) was done at room temperature for 1 hour. After secondary antibody incubation the membrane was washed again three times with PBST for a total amount of 30 minutes. The membranes were developed using Amersham ECL Prime Western Blotting Detection Reagent (RPN2235, Cytiva) or SuperSignal™ West Femto

Maximum Sensitivity Substrate (34095, Thermo Fisher). The FUSION Solo S system and software (Vilber) were used to image the membranes.

Table 4-10. Western blot antibodies

Name	Company	Catalogue Number
HRP Goat Anti-Mouse IgG H+L	Biotium	Cat# 20400-1mg RRID: AB_3083795
HRP Goat Anti-Rabbit IgG (H+L)	Biotium	Cat# 20402-1mg, RRID: AB_3083796
Mouse monoclonal anti β -ACTIN	Sigma Aldrich	Cat# A1978 RRID: AB_476692
Rabbit monoclonal anti MIF	Cell Signaling Technology	Cat# 87501S RRID: AB_2943242
Rabbit polyclonal anti GPX4	Abcam	Cat# ab41787 RRID: AB_941790

4.5.4. Enzyme-linked immunosorbent assay (ELISA)

Corresponding ELISA kits (Table 4-11) were used according to the manufacturer's instructions to detect and quantify the cyto- and chemokines in the supernatants from the cell lines. Supernatants were collected and stored at -20°C until analysis.

Table 4-11. ELISAs

Name	Company	Catalogue Number
8-OHdG ELISA	BioVision	Cat# K4160-100
Mouse CXCL1/KC DuoSet ELISA	R&D Systems	Cat# DY453
Mouse CXCL2/MIP-2 DuoSet ELISA	R&D Systems	Cat# DY452
Mouse IL-1beta/IL-1F2 DuoSet ELISA	R&D Systems	Cat# DY401
Mouse IL-6 DuoSet ELISA	R&D Systems	Cat# DY406
Mouse MIF DuoSet ELISA	R&D Systems	Cat# DY1978
Mouse TNF-alpha DuoSet ELISA	R&D Systems	Cat# DY410
Prostaglandin E2 Parameter Assay Kit	R&D Systems	Cat# KGE004B

4.6. Fluorescence activated cell sorting (FACS)

Table 4-12. FACS antibodies

Name	Company	Catalogue Number
APC anti-mouse/human CD11b Antibody	Biolegend	Cat# 101212
APC anti-mouse CD11c Antibody	Biolegend	Cat# 117309
APC anti-mouse CD45 Antibody	Biolegend	Cat# 103112
BD Horizon™ V450 Rat anti-Mouse CD4	BD Biosciences	Cat# 560470

Brilliant Violet 421™ anti-mouse CD206 (MMR) Antibody	Biolegend	Cat# 141717
Brilliant Violet 421™ anti-mouse TNF- α Antibody	Biolegend	Cat# 506327
CD11b Monoclonal Antibody (M1/70), PE, eBioscience™	Invitrogen	Cat# 12-0112-82
eBioscience™ Fixable Viability Dye eFluor™ 660	Thermo Fisher	Cat# 65-0864-14
eBioscience™ Fixable Viability Dye eFluor™ 780	Thermo Fisher	Cat# 65-0865-14
F4/80 Monoclonal Antibody (BM8), FITC	Invitrogen	Cat# 11-4801-82
FITC anti-mouse CD14 Antibody	Biolegend	Cat# 123307
FITC anti-mouse CD80 Antibody	Biolegend	Cat# 104705
FITC anti-mouse NK-1.1 Antibody	Biolegend	Cat# 108705
Ly-6G/Ly-6C Monoclonal Antibody (RB6-8C5), FITC	Thermo Fisher	Cat# 11-5931-82
PE anti-mouse CD8a Antibody	Biolegend	Cat# 100708

4.6.1. BODIPY C11 staining

For lipid ROS quantification, 5000 Pfa1 cells were seeded in 500 μ l of the respective medium in 24-well plates (Greiner, 662160) with and without 4-OHT and Fer-1. 30 minutes before lysing at different time points BODIPY C11 was added at 5 μ M to each well. Cells were washed, detached and a minimum of 5000 events were measured using BD LSRFortessa with at least three replicates per condition.

4.6.2. Propidium iodide (PI) staining

Cells were washed, detached and harvested by centrifugation for 5 min at 1200 rpm. To quantify cell death by damaged cell membrane, the cell pellet was then resuspended in 200 μ l of PBS with 2% FCS and 1 μ g/ml propidium iodide (PI).

4.6.3. pBMDM staining

Fresh or frozen bone marrow cells were used to generate pBMDMs as previously described³⁷⁵ using 25ng/ml M-CSF in the medium. At day 6 post differentiation, 300 000 pBMDMs were seeded in 6-well plates and incubated with non-ferroptotic or ferroptotic supernatants for 24hours to confirm the differentiation. Macrophages were removed from the plates with ice-cold PBS and stained with the following antibodies/dyes: fixable viability dye eFluor™ 780, APC anti-mouse/human CD11b, FITC F4/80 Monoclonal Antibody (BM8). For intracellular TNF α staining, at day 6 300 000 pBMDMs were seeded in 6-well plates and incubated with non-ferroptotic or ferroptotic supernatants containing 25ng/ml IFN gamma, 10ng/ml LPS and

5µg/ml Brefeldin A for 6 hours. Macrophages were removed from the plates with ice-cold PBS and stained with the following antibodies/dyes: fixable viability dye eFluor™ 780, APC anti-mouse/human CD11b, FITC F4/80 Monoclonal Antibody (BM8), Brilliant Violet 421™ anti-mouse TNF-α.

4.6.4. Immune cell analysis from murine lungs

In order to isolate immune cells from lungs, whole tissue was dissected and minced with scalpels into fragments small enough to be aspirated into a 5 ml pipette at RT. 45 ml of tissue suspension was incubated with 5ml of a 10x Triple Enzyme Mix (1 g Collagenase IV, 100 mg Hyaluronidase and 20,000 Units DNase IV into 80 ml HBSS) at RT for 90 min on a shaker at 80 rpm. Cell suspension was repeatedly pipetted to further dissociate cells, centrifuged at 50 x *g* at RT for 10 min and the supernatant was collected by passing it through a 70 µm nylon strainer. The bigger pellets in the bottom of the tube were then discarded and the filtered supernatant was centrifuged at 200 x *g* for 5 min. Cell pellets were washed with 10 ml Wash Buffer (1g BSA and 2ml 0.5 M EDTA in 800 ml HBSS) at 200 x *g* for 5 min once and were resuspended with 2 ml ACK lysing buffer (Gibco) for 1 min to deplete red blood cells. Cells were washed with PBS and immediately stained for live/dead cells using the Fixable Viability Dye eFluor 660 or eFluor 450 (eBioscience) (1:1000) in PBS for 30 min, at 4 °C. Cells were then washed twice with FACS buffer (PBS, 2% FCS) and stained with the respective FACS antibodies (1:1000) for another 30min, at 4°C. Fc block (CD16/32, Biolegend, 1:50) was used 15min before adding the antibodies for blocking Fc receptors. For subsequent intracellular stainings, cell pellets were resuspended in 200µl Fixation/Permeabilization buffer (eBioscience) and incubated overnight at 4 °C. The next day, cells were washed with 1x Permeabilization buffer (eBioscience) and incubated for 15 min with 2% goat serum before adding the respective intracellular antibodies 1:50, for 30 min at 4 °C in 1x Permeabilization buffer. After washing twice with 1x Permeabilization buffer cells were resuspended in FACS buffer. Measurements were acquired using a BD LSR Fortessa flow cytometer and data were analysed with the FlowJo (10.6.1) software.

4.7. Cell death assays

Cell viability was determined by different types of cell death assays monitoring cell membrane integrity by incorporation of intercalating agents into dsDNA or the release of lactate dehydrogenase (LDH).

4.7.1. Live cell imaging (IncuCyte)

1000 Pfa1, Pfa1-mFSP1-OE cells were plated in 96-well plates and treated with or without 4-OHT (5 μ M), and Ferrostatin-1 (Fer1, 1 μ M). 5000 lung fibroblasts were plated in 96-well plates and treated with or without RSL3 (1 μ M), erastin (10 μ M), ferrostatin-1 (Fer1, 1 μ M), TNF α (20ng/ml), birinapant (1 μ M), emricasan (2,5 μ M), nec1s (10 μ M). 5000 ZBP1-overexpression-inducible and empty ZBP1-empty vector-inducible MEFs were plated in 96-well plates and pre-treated with or without doxycycline (1 μ /ml) and treated with or without emricasan (2,5 μ M). For dead cell quantification DRAQ7 (100nM) was used. For lipid ROS quantification STY-BODIPY (1 μ M) was used. Cells were imaged every 2h using the 10x objective within the IncuCyte SX5 live cell imaging system (Sartorius). Analysis for confluence, DRAQ7- positive (dead), reduced- and oxidized-BODIPY positive cells was performed using the Software IncuCyte 2021B (Sartorius).

4.7.2. LDH release assay

Pfa1 and mFSP1-overexpressing Pfa1 cells were seeded on a 24-well plate at 5000 cell per well and treated with or without 4-OHT and Fer 1 as described as above for 72 hours. ZBP1-overexpression-inducible and empty ZBP1-empty vector-inducible mouse embryonic fibroblast (MEFs) were seeded on a 24-well plate at 35 000 cells per well and pre-treated with or without doxycycline 16 hours and treated with or without emricasan as described above for 24 hours. Supernatants were collected at the respective indicated times post treatment with different drug concentrations and the presence of LDH was quantified by using CytoTox 96[®] Non-Radioactive Cytotoxicity Assay according to the manufacturer's instructions.

4.8. Quantification of proteins in ferroptotic supernatants

Pfa1 cells were labelled with heavy Arg10 and Lys8 using SILAC DMEM with 1% glutamine, 10% FBS and 1% PS for 6 passages, and isotope integration was confirmed via mass spectrometry as described below. For ferroptotic supernatant harvest, 2.3 million cells were seeded on 15 cm dishes in labelled medium in presence of 1 μ M tamoxifen or in unlabelled

medium in presence of DMSO (triplicates for each condition). After 40h, medium was replaced with heavy or unlabelled SILAC medium containing 0%FCS and 1% ITS+1. 72 hours later, supernatants were collected, cleared by centrifugation (3 min;300g: 4°C) and concentrated using Amicon Ultra centrifugal filters (Sigma Aldrich) at a 10 kDa cutoff for 25 min at 3200 g and 4°C followed by another 10 min at 3200g upon adding 10 mL ice cold PBS. Proteins were precipitated from filtrates using the 4-fold volume of ice-cold acetone for 15 min at -80°C followed by overnight incubation at -20°C and centrifugation for 15 min at 16000 g and 4°C. Air-dried pellets were then lysed in 100 µL lysis buffer (8M Urea in 50 mM TEAB containing protease inhibitor cocktail), and nucleic acids were removed using 50 U Benzonase HC (Merck Millipore) at 37°C for 30 min followed by centrifugation at 20000 g for 15 min. 50 µg of pooled protein (25 µg unlabelled and labelled, respectively) was then digested by subsequent treatment with 5 mM DTT (25 min, 1h), 40 mM chloracetamide (30 min at rt), LysC endopeptidase (enzyme : substrate ratio of 1:75; 4 h at 25°C) and trypsin (enzyme : substrate ratio of 1:75; overnight at 25°C). At the next day, samples were acidified by adding formic acid to a final concentration of 1%. Samples were cleared by centrifugation (full speed for 5 min) and loaded onto a stage tip column (5 min at 2600 rpm) followed by washing with 0.1% formic acid and 0.1%formic acid in 80% acetonitrile and air-drying.

All samples were analysed by the CECAD Proteomics Facility on a Q Exactive Plus Orbitrap (Thermo Scientific) mass spectrometer that was coupled to an EASY nLC (Thermo Scientific). Peptides were loaded with solvent A (0.1% formic acid in water) onto an in-house packed analytical column (50 cm, 75 µm inner diameter, filled with 2.7 µm Poroshell EC120 C18, Agilent). Peptides were chromatographically separated at a constant flow rate of 250 nL/min using the following gradient: 3-5% solvent B (0.1% formic acid in 80 % acetonitrile) within 1.0 min, 5-30% solvent B within 121.0 min, 30-40% solvent B within 19.0 min, 40-95% solvent B within 1.0 min, followed by washing and column equilibration. The mass spectrometer was operated in data-dependent acquisition mode. The MS1 survey scan was acquired from 300-1750 m/z at a resolution of 70,000. The top 10 most abundant peptides were isolated within a 1.8 Th window and subjected to HCD fragmentation at a normalized collision energy of 27%. The AGC target was set to 5e5 charges, allowing a maximum injection time of 55 ms. Product ions were detected in the Orbitrap at a resolution of 17,500. Precursors were dynamically excluded for 25.0 s. All mass spectrometric raw data were processed with MaxQuant 2.0.3⁴⁴⁰

using default parameters. Briefly, MS2 spectra were searched against the canonical murine Uniprot reference proteome (UP000000589, downloaded at: 26.08.2020) including a list of common contaminants. False discovery rates on protein and PSM level were estimated by the target-decoy approach to 1% (Protein FDR) and 1% (PSM FDR) respectively. The minimal peptide length was set to 7 amino acids and carbamidomethylation at cysteine residues was considered as a fixed modification. Oxidation (M) and Acetyl (Protein N-term) were included as variable modifications. Multiplicity was set to 2 and Arg10 as well as Lys8 were defined as labels for the heavy channel and the re-quantify option was enabled. The match-between runs option was enabled between replicates in each sample group. LFQ quantification was enabled using default settings. Final data analysis was performed in Perseus 1.6.15⁴⁴¹ based on normalized ratios between heavy and light channel.

4.9. Quantification of oxidized phospholipids in ferroptotic supernatants

200.000 Pfa1 cells were seeded on 10 cm dishes in presence of DMSO, 1 μ M tamoxifen and 1 μ M Fer1 in 8 ml phenol-red free medium. Supernatants were collected upon centrifugation for 5 min at 3000 rpm and 4°C and 1 mL was subsequently snap frozen in liquid nitrogen. Sample preparation for oxylipin analysis was performed as previously described with modifications³⁶⁸. Medium samples were previously centrifuged to remove cellular debris. Briefly, 500 μ L of supernatant was added by 100 μ L of internal standard mixture. Samples were vortexed and applied into solid-phase extraction (SPE) Strata C18-E columns (50 mg; 8B-S001-DAM, Phenomenex). The SPE columns were washed with 1 mL of 5% methanol and the oxylipins were eluted using 100% methanol. Samples were dried under N₂ gas and dissolved in 50 μ L of methanol for analysis. The oxylipin analysis was carried out by Q-Exactive Plus (Thermo) interfaced with an ultra-high-performance liquid chromatography (Vanquish, Thermo). The chromatographic and mass spectrometry conditions for analysis of oxylipins was carried out as described, with modifications. Samples were loaded into a UPLC BEH shield Reversed Phase C18 column (2.1 x 100 mm; 1.7 μ m; Waters) with a flow rate of 0.4 mL/min and oven temperature maintained at 40 °C. The mobile phase A consisted of formic acid/water/acetonitrile (0.02:70:30), while mobile phase B composed of acetonitrile/isopropanol (70:30). Oxidized lipids were separated by a gradient as follows: from 0.1 to 40% B over the first 3.5 min, from 40 to 75% B from 3.5-6.0 min, from 75 to 99% B from 6.0-6.5 min, hold at 99% B from 6.5-10.5 min, decreased from 99 to 0.1% B during 10.5–

11 min, and hold at 0.1% B from 11–15 min. The mass spectrometry was operated in negative ionization mode. The ESI parameters used in this analysis were: sheath gas (30 au), auxiliary gas (10 au), spray voltage (2.5 kV), ion transfer temperature: 320°C, S-lens RF level: 55% and aux gas heater temperature: 120 °C. Data for lipid molecular species identification and quantification was obtained by parallel reaction monitoring (PRM) experiment. PRM data was acquired with a resolution setting of 17,500 at 200 m/z, AGC target 5e4 counts, Maximum IT 50 ms, isolation window 1.5 m/z. Collision energy (CE) was individually optimized for each ion. Specific fragment ions monitored for each oxidized lipid specie were manually identified using SeeMS and ChemDraw softwares. Quantification was performed by monitoring the peak area of specific fragments for each analyte using Skyline software. The area ratio obtained for each oxidized lipid was calculated by dividing the peak area of the lipid by the corresponding internal standard. The concentration of lipid species was calculated by applying the area ratio in a calibrate curve constructed for each analyte. The concentration of oxylipins was expressed in pg/mL of medium.

4.10. Quantification of intracellular and supernatant metabolites

Metabolite Extraction

For metabolomics analysis of ferroptotic supernatants, Pfa1 cells were seeded on 6 well plates in presence of DMSO, 1 μ M tamoxifen, 1 μ M Fer1 or 1 μ M Tamoxifen and 1 μ M Fer1(25.000 cells per well; pentaplicates per condition), and samples were harvested at 24 h (cells + supernatant), 48 h (cells + supernatant) and 72 h supernatant only). For sample harvest, supernatants were centrifuged at full speed and 4°C for 5 min, and 50 μ L of the cleared supernatants were added to 350 μ L ice-cold extraction solution (50% methanol, 30% acetonitrile (both from Fisher Scientific), 20% ultrapure water, 5 μ M valine-d8 (CK isotopes) on dry ice. Cells were washed twice with ice-cold PBS and subsequently incubated with 100 μ L extraction solution for 20 min in a dry ice/methanol bath, followed by scraping. Supernatants and cell samples were then stirred vigorously in a thermomixer at full speed and 4 °C followed by 20 min centrifugation at 4°C and full speed. Cleared samples were stored at -80°C and submitted for further metabolomic analysis. Chromatographic separation of metabolites was achieved using a Millipore Sequant ZIC-pHILIC analytical column (5 μ m, 2.1 \times 150 mm) equipped with a 2.1 \times 20 mm guard column (both 5 mm particle size) with a binary solvent system. Solvent A was 20 mM ammonium carbonate, 0.05% ammonium hydroxide;

Solvent B was acetonitrile. The column oven and autosampler tray were held at 40 °C and 4 °C, respectively. The chromatographic gradient was run at a flow rate of 0.200 mL/min as follows: 0–2 min: 80% B; 2-17 min: linear gradient from 80% B to 20% B; 17-17.1 min: linear gradient from 20% B to 80% B; 17.1-23 min: hold at 80% B. Samples were randomized and the injection volume was 5 µl. A pooled quality control (QC) sample was generated from an equal mixture of all individual samples and analysed interspersed at regular intervals.

Metabolite measurement by LC-MS

Metabolites were measured with Vanquish Horizon UHPLC coupled to an Orbitrap Exploris 240 mass spectrometer (both Thermo Fisher Scientific) via a heated electrospray ionization source. The spray voltages were set to +3.5kV/-2.8 kV, RF lens value at 70, the heated capillary held at 320 °C, and the auxiliary gas heater held at 280 °C. The flow rate for sheath gas, aux gas and sweep gas were set to 40, 15 and 0, respectively. For MS1 scans, mass range was set to $m/z=70-900$, AGC target set to standard and maximum injection time (IT) set to auto. Data acquisition for experimental samples used full scan mode with polarity switching at an Orbitrap resolution of 120000. Data acquisition for untargeted metabolite identification was performed using the AcquireX Deep Scan workflow, an iterative data-dependent acquisition (DDA) strategy using multiple injections of the pooled sample. DDA full scan-ddMS2 method for AcquireX workflow used the following parameters: full scan resolution was set to 60000, fragmentation resolution to 30000, fragmentation intensity threshold to $5.0e3$. Dynamic exclusion was enabled after 1 time and exclusion duration was 10s. Mass tolerance was set to 5ppm. Isolation window was set to 1.2 m/z . Normalized HCD collision energies were set to stepped mode with values at 30, 50, 150. Fragmentation scan range was set to auto, AGC target at standard and max IT at auto. Mild trapping was enabled. Metabolite identification was performed in the Compound Discoverer software (v 3.2, Thermo Fisher Scientific). Metabolite identities were confirmed using the following parameters: (1) precursor ion m/z was matched within 5 ppm of theoretical mass predicted by the chemical formula; (2) fragment ions were matched within 5 pm to an in-house spectral library of authentic compound standards analysed with the same ddMS2 method with a best match score of over 70; (3) the retention time of metabolites was within 5% of the retention time of a purified standard run with the same chromatographic method.

Data analysis

Chromatogram review and peak area integration were performed using the Tracefinder software (v 5.0, Thermo Fisher Scientific) resulting in raw peak data. Next, we used the R package MetaProViz (v.2.0.1) for all subsequent data analysis. First, using the MetaProViz Preprocessing() function, the raw peak area for each detected metabolite was subjected to the “Modified Filtering Rule”⁴⁴², half minimum missing value imputation, and normalized against the total ion count (TIC) of that sample to correct any variations introduced from sample handling through instrument analysis. In case of media supernatant samples MetaProViz Preprocessing() function parameter “CoRe” was set to “TRUE” and the pre-processed mean value of each metabolite detected in the fresh culture medium (incubated in the absence of cells) were subtracted from the metabolites detected in the supernatant samples. Testing for outliers based on the Hotelling’s T2 test⁴⁴³, with 0.99 confidence interval. Afterwards, differential metabolomics analysis was performed (MetaProViz DMA() function) to calculate the Log2FC in case of intracellular samples or the Log2(Distance) in case of supernatant media samples (parameter CoRe=TRUE). The p-value and t.test was calculated using t.test and adjusted using fdr. The results were visualized using MetaProViz VizVolcano and VizHeatmap relying on the dependencies EnhancedVolcano (v. 1.20.0)⁴⁴⁴ and pheatmap (v. 1.0.12).

4.11. RNA Sequencing

For RNA sequencing, 500 000 primary bone marrow derived macrophages (pBMDMs) were plated in 6-well plates with 25ng/ml M-CSF after 7-day differentiation. Fresh, filtered supernatants with or without 4-OHT (5 μ M), Ferrostatin-1 (Fer1, 1 μ M) incubated with pBMDMs for 24 hours. The next day, cells were washed with PBS and RNA was isolated using the NucleoSpin RNA kit (740955.5, Macherey-Nagel) according to the manufacturer’s instructions. cDNA libraries amplified from the 3’ UTR were generated from total RNA using the Lexogen QuantSeq kit (Lexogen, Austria) according to the standard protocol and sequenced with a 50-bp single-end protocol on Illumina HiSeq4000 sequencer (Illumina, USA). Primary data analysis was conducted using the RNA-seq pipeline from the nf-core suite (v3.7)⁴⁴⁵; sequencing reads were aligned to the GRCh38 (v103) human reference genome using STAR (v2.7.10a)⁴⁴⁶. Gene quantification was conducted using Salmon (v1.5.2)⁴⁴⁷. The

pipeline was executed with default parameters. Downstream differential expression analysis was performed using DESeq2 (v1.36.0)⁴⁴⁸, with default parameters. To enhance the accuracy of fold-change estimation, we included mouse ID as a batch effect in the design matrix. For some comparisons (Fer1 vs. Ctrl and 4-OH vs. Ctrl), the original p-values inferred by DESeq2 revealed significant deviation from the expected uniform null distribution, suggesting low sensitivity. To correct for this, we recomputed the raw p-values using fdrtool (v1.2.17)⁴⁴⁹ to increase the power of the differential expression procedure while maintaining efficient control for false discovery. Subsequently, the Benjamini-Hochberg procedure was applied to correct the p-values for multiple tests.

GO enrichment analysis was conducted using gprofiler2 (v0.2.2)⁴⁵⁰. The selection criteria focused on differentially expressed genes, as defined above. Using ordered gene query and gProfiler's "g_SCS" method for p-value adjustment, which accounts for the hierarchical structure of GO terms, enriched GO terms were identified among the differentially expressed genes. We defined genes as differentially expressed if they exhibited an absolute log₂FoldChange greater than 1 and an adjusted p-value lower than 0.05. For the heatmap generation, we focused exclusively on genes identified as differentially expressed (DEGs) in the 4-OH versus Ctrl comparison. These DEGs were ranked by the absolute log₂ of fold change, and algorithmically predicted genes were excluded, leaving only those validated through experimental methods. Given that we have only three replicates per condition, to minimize the risk of false positives, we retained only genes that demonstrated non-zero counts per million (CPM) in all three replicates of at least one experimental condition. Subsequently, we selected the top 25 upregulated and the top 25 downregulated genes for the heatmap visualization. Additionally, we applied the variance stabilization transformation procedure from DESeq2 for normalization of the counts, setting the 'blind' parameter to FALSE, to account for design peculiarities as recommended by the DESeq2 authors. To mitigate the mouse batch effect, we utilized the function removeBatchEffect from R package limma⁴⁵¹.

5. References

1. Galluzzi, L. *et al.* Molecular mechanisms of cell death: recommendations of the Nomenclature Committee on Cell Death 2018. *Cell Death Differ* **25**, 486–541 (2018).
2. Kerr, J. F. R., Wyllie, A. H. & Currie, A. R. Apoptosis: A Basic Biological Phenomenon with Wideranging Implications in Tissue Kinetics. *Br J Cancer* **26**, 239–257 (1972).
3. Häcker, G. The morphology of apoptosis. *Cell Tissue Res* **301**, 5–17 (2000).
4. Thornberry, N. A. & Lazebnik, Y. Caspases: Enemies Within. *Science* **281**, 1312–1316 (1998).
5. Shi, L., Kam, C. M., Powers, J. C., Aebersold, R. & Greenberg, A. H. Purification of three cytotoxic lymphocyte granule serine proteases that induce apoptosis through distinct substrate and target cell interactions. *The Journal of experimental medicine* **176**, 1521–1529 (1992).
6. Elmore, S. Apoptosis: A Review of Programmed Cell Death. *Toxicol Pathol* **35**, 495–516 (2007).
7. Brumatti, G., Salmanidis, M. & Ekert, P. G. Crossing paths: interactions between the cell death machinery and growth factor survival signals. *Cell. Mol. Life Sci.* **67**, 1619–1630 (2010).
8. Kelekar, A. & Thompson, C. B. Bcl-2-family proteins: the role of the BH3 domain in apoptosis. *Trends in Cell Biology* **8**, 324–330 (1998).
9. Vaux, D. L., Cory, S. & Adams, J. M. Bcl-2 gene promotes haemopoietic cell survival and cooperates with c-myc to immortalize pre-B cells. *Nature* **335**, 440–442 (1988).
10. Boise, H. *et al.* bcl-x, a bcl-2-Related Gene That Functions as a Dominant Regulator of Apoptotic Cell Death. *Cell* **74**, 597–608 (1993).
11. Zhou, P., Qian, L., Kozopas, K. M. & Craig, R. W. Mcl-1, a Bcl-2 Family Member, Delays the Death of Hematopoietic Cells Under a Variety of Apoptosis-Inducing Conditions. *Blood* **89**, 630–643 (1997).
12. Oltval, Z. N., Milliman, C. L. & Korsmeyer, S. J. Bcl-2 heterodimerizes in vivo with a conserved homolog, Bax, that accelerates programmed cell death. *Cell* **74**, 609–619 (1993).
13. Chittenden, T. *et al.* Induction of apoptosis by the Bcl-2 homologue Bak. *Nature* **374**, 733–736 (1995).
14. Hsu, S. Y., Kaipia, A., McGee, E., Lomeli, M. & Hsueh, A. J. W. Bok is a pro-apoptotic Bcl-2 protein with restricted expression in reproductive tissues and heterodimerizes with selective anti-apoptotic Bcl-2 family members. *Proc. Natl. Acad. Sci. U.S.A.* **94**, 12401–12406 (1997).
15. Inohara, N. *et al.* Mtd, a Novel Bcl-2 Family Member Activates Apoptosis in the Absence of Heterodimerization with Bcl-2 and Bcl-XL. *Journal of Biological Chemistry* **273**, 8705–8710 (1998).
16. Yang, E., Zha, J., Jockel, J., Boise, L. H. & Korsmeyer, S. J. Bad, a Heterodimeric Partner for Bcl-x, and Bcl-2, Displaces Bax and Promotes Cell Death. *Cell* **80**, 285–291 (1995).

17. Wang, K., Yin, X. M., Chao, D. T., Milliman, C. L. & Korsmeyer, S. J. BID: a novel BH3 domain-only death agonist. *Genes Dev.* **10**, 2859–2869 (1996).
18. O'Connor, L. Bim: a novel member of the Bcl-2 family that promotes apoptosis. *The EMBO Journal* **17**, 384–395 (1998).
19. Nakano, K. & Vousden, K. H. PUMA, a Novel Proapoptotic Gene, Is Induced by p53. *Molecular Cell* **7**, 683–694 (2001).
20. Oda, E. *et al.* Noxa, a BH3-Only Member of the Bcl-2 Family and Candidate Mediator of p53-Induced Apoptosis. *Science* **288**, 1053–1058 (2000).
21. Du, C., Fang, M., Li, Y., Li, L. & Wang, X. Smac, a Mitochondrial Protein that Promotes Cytochrome c-Dependent Caspase Activation by Eliminating IAP Inhibition. *Cell* **102**, 33–42 (2000).
22. Liu, X., Kim, C. N., Yang, J., Jemmerson, R. & Wang, X. Induction of Apoptotic Program in Cell-Free Extracts: Requirement for dATP and Cytochrome c. *Cell* **86**, 147–157 (1996).
23. Dewson, G. *et al.* To Trigger Apoptosis, Bak Exposes Its BH3 Domain and Homodimerizes via BH3:Groove Interactions. *Molecular Cell* **30**, 369–380 (2008).
24. O'Neill, K. L., Huang, K., Zhang, J., Chen, Y. & Luo, X. Inactivation of prosurvival Bcl-2 proteins activates Bax/Bak through the outer mitochondrial membrane. *Genes Dev.* **30**, 973–988 (2016).
25. Chinnaiyan, A. M. The Apoptosome: Heart and Soul of the Cell Death Machine. *Neoplasia* **1**, 5–15 (1999).
26. Hill, M. M., Adrain, C., Duriez, P. J., Creagh, E. M. & Martin, S. J. Analysis of the composition, assembly kinetics and activity of native Apaf-1 apoptosomes. *EMBO J* **23**, 2134–2145 (2004).
27. Rothe, M., Pan, M.-G., Henzel, W. J., Ayres, T. M. & V. Goeddel, D. The TNFR2-TRAF signaling complex contains two novel proteins related to baculoviral inhibitor of apoptosis proteins. *Cell* **83**, 1243–1252 (1995).
28. Deveraux, Q. L. Cleavage of human inhibitor of apoptosis protein XIAP results in fragments with distinct specificities for caspases. *The EMBO Journal* **18**, 5242–5251 (1999).
29. Deveraux, Q. L. IAPs block apoptotic events induced by caspase-8 and cytochrome c by direct inhibition of distinct caspases. *The EMBO Journal* **17**, 2215–2223 (1998).
30. Srinivasula, S. M. *et al.* A conserved XIAP-interaction motif in caspase-9 and Smac/DIABLO regulates caspase activity and apoptosis. *Nature* **410**, 112–116 (2001).
31. Ashkenazi, A. & Dixit, V. M. Death Receptors: Signaling and Modulation. *Science* **281**, 1305–1308 (1998).
32. Brakebusch, C., Nophar, Y., Kemper, O., Engelmann, H. & Wallach, D. Cytoplasmic truncation of the p55 tumour necrosis factor (TNF) receptor abolishes signalling, but not induced shedding of the receptor. *The EMBO Journal* **11**, 943–950 (1992).
33. Itoh, N. & Nagata, S. A novel protein domain required for apoptosis. Mutational analysis of human Fas antigen. *Journal of Biological Chemistry* **268**, 10932–10937 (1993).
34. Tartaglia, L. A., Ayres, T. M., Wong, G. H. W. & Goeddel, D. V. A novel domain within the 55 kd TNF receptor signals cell death. *Cell* **74**, 845–853 (1993).

35. Chinnaiyan, A. M. *et al.* FADD/MORT1 Is a Common Mediator of CD95 (Fas/APO-1) and Tumor Necrosis Factor Receptor-induced Apoptosis. *Journal of Biological Chemistry* **271**, 4961–4965 (1996).
36. Pan, G. *et al.* The Receptor for the Cytotoxic Ligand TRAIL. *Science* **276**, 111–113 (1997).
37. Pan, G. *et al.* An Antagonist Decoy Receptor and a Death Domain-Containing Receptor for TRAIL. *Science* **277**, 815–818 (1997).
38. Chinnaiyan, A. M., O'Rourke, K., Tewari, M. & Dixit, V. M. FADD, a novel death domain-containing protein, interacts with the death domain of fas and initiates apoptosis. *Cell* **81**, 505–512 (1995).
39. Kischkel, F. C. *et al.* Apo2L/TRAIL-Dependent Recruitment of Endogenous FADD and Caspase-8 to Death Receptors 4 and 5. *Immunity* **12**, 611–620 (2000).
40. Medema, J. P. *et al.* FLICE is activated by association with the CD95 death-inducing signaling complex (DISC). *The EMBO Journal* **16**, 2794–2804 (1997).
41. Martin, D. A., Siegel, R. M., Zheng, L. & Lenardo, M. J. Membrane Oligomerization and Cleavage Activates the Caspase-8 (FLICE/MACH α 1) Death Signal. *Journal of Biological Chemistry* **273**, 4345–4349 (1998).
42. Scaffidi, C., Schmitz, I., Krammer, P. H. & Peter, M. E. The Role of c-FLIP in Modulation of CD95-induced Apoptosis*. *Journal of Biological Chemistry* **274**, 1541–1548 (1999).
43. Irmeler, M. *et al.* Inhibition of death receptor signals by cellular FLIP. *Nature* **388**, 190–195 (1997).
44. Krueger, A., Schmitz, I., Baumann, S., Krammer, P. H. & Kirchhoff, S. Cellular FLICE-inhibitory Protein Splice Variants Inhibit Different Steps of Caspase-8 Activation at the CD95 Death-inducing Signaling Complex*. *Journal of Biological Chemistry* **276**, 20633–20640 (2001).
45. Kavuri, S. M. *et al.* Cellular FLICE-inhibitory Protein (cFLIP) Isoforms Block CD95- and TRAIL Death Receptor-induced Gene Induction Irrespective of Processing of Caspase-8 or cFLIP in the Death-inducing Signaling Complex*. *Journal of Biological Chemistry* **286**, 16631–16646 (2011).
46. Micheau, O. *et al.* The Long Form of FLIP Is an Activator of Caspase-8 at the Fas Death-inducing Signaling Complex*. *Journal of Biological Chemistry* **277**, 45162–45171 (2002).
47. Hughes, M. A. *et al.* Co-operative and Hierarchical Binding of c-FLIP and Caspase-8: A Unified Model Defines How c-FLIP Isoforms Differentially Control Cell Fate. *Molecular Cell* **61**, 834–849 (2016).
48. Koenig, A. *et al.* The c-FLIPL Cleavage Product p43FLIP Promotes Activation of Extracellular Signal-regulated Kinase (ERK), Nuclear Factor κ B (NF- κ B), and Caspase-8 and T Cell Survival*. *Journal of Biological Chemistry* **289**, 1183–1191 (2014).
49. Micheau, O. & Tschopp, J. Induction of TNF Receptor I-Mediated Apoptosis via Two Sequential Signaling Complexes. *Cell* **114**, 181–190 (2003).
50. Stanger, B. Z., Leder, P., Lee, T.-H., Kim, E. & Seed, B. RIP: A novel protein containing a death domain that interacts with Fas/APO-1 (CD95) in yeast and causes cell death. *Cell* **81**, 513–523 (1995).

51. Yeh, W.-C. *et al.* Early Lethality, Functional NF- κ B Activation, and Increased Sensitivity to TNF-Induced Cell Death in TRAF2-Deficient Mice. *Immunity* **7**, 715–725 (1997).
52. Tada, K. *et al.* Critical Roles of TRAF2 and TRAF5 in Tumor Necrosis Factor-induced NF- κ B Activation and Protection from Cell Death. *Journal of Biological Chemistry* **276**, 36530–36534 (2001).
53. Zheng, C., Kabaleeswaran, V., Wang, Y., Cheng, G. & Wu, H. Crystal Structures of the TRAF2: cIAP2 and the TRAF1: TRAF2: cIAP2 Complexes: Affinity, Specificity, and Regulation. *Molecular Cell* **38**, 101–113 (2010).
54. Mace, P. D., Smits, C., Vaux, D. L., Silke, J. & Day, C. L. Asymmetric Recruitment of cIAPs by TRAF2. *Journal of Molecular Biology* **400**, 8–15 (2010).
55. Samuel, T. *et al.* Distinct BIR Domains of cIAP1 Mediate Binding to and Ubiquitination of Tumor Necrosis Factor Receptor-associated Factor 2 and Second Mitochondrial Activator of Caspases*. *Journal of Biological Chemistry* **281**, 1080–1090 (2006).
56. Lafont, E. *et al.* The linear ubiquitin chain assembly complex regulates TRAIL-induced gene activation and cell death. *The EMBO Journal* **36**, 1147–1166 (2017).
57. O’Donnell, M. A., Legarda-Addison, D., Skountzos, P., Yeh, W. C. & Ting, A. T. Ubiquitination of RIP1 Regulates an NF- κ B-Independent Cell-Death Switch in TNF Signaling. *Current Biology* **17**, 418–424 (2007).
58. Li, H., Kobayashi, M., Blonska, M., You, Y. & Lin, X. Ubiquitination of RIP Is Required for Tumor Necrosis Factor α -induced NF- κ B Activation*. *Journal of Biological Chemistry* **281**, 13636–13643 (2006).
59. Bertrand, M. J. M. *et al.* cIAP1 and cIAP2 Facilitate Cancer Cell Survival by Functioning as E3 Ligases that Promote RIP1 Ubiquitination. *Molecular Cell* **30**, 689–700 (2008).
60. Kelliher, M. A. *et al.* The Death Domain Kinase RIP Mediates the TNF-Induced NF- κ B Signal. *Immunity* **8**, 297–303 (1998).
61. Ea, C.-K., Deng, L., Xia, Z.-P., Pineda, G. & Chen, Z. J. Activation of IKK by TNF α Requires Site-Specific Ubiquitination of RIP1 and Polyubiquitin Binding by NEMO. *Molecular Cell* **22**, 245–257 (2006).
62. Kaczmarek, A., Vandenabeele, P. & Krysko, D. V. Necroptosis: The Release of Damage-Associated Molecular Patterns and Its Physiological Relevance. *Immunity* **38**, 209–223 (2013).
63. Murphy, J. M. *et al.* The Pseudokinase MLKL Mediates Necroptosis via a Molecular Switch Mechanism. *Immunity* **39**, 443–453 (2013).
64. Wang, L., Du, F. & Wang, X. TNF- α Induces Two Distinct Caspase-8 Activation Pathways. *Cell* **133**, 693–703 (2008).
65. O’Donnell, M. A. *et al.* Caspase 8 inhibits programmed necrosis by processing CYLD. *Nat Cell Biol* **13**, 1437–1442 (2011).
66. Cai, Z. *et al.* Plasma membrane translocation of trimerized MLKL protein is required for TNF-induced necroptosis. *Nat Cell Biol* **16**, 55–65 (2014).
67. Chen, X. *et al.* Translocation of mixed lineage kinase domain-like protein to plasma membrane leads to necrotic cell death. *Cell Res* **24**, 105–121 (2014).

68. Dondelinger, Y. *et al.* MLKL Compromises Plasma Membrane Integrity by Binding to Phosphatidylinositol Phosphates. *Cell Reports* **7**, 971–981 (2014).
69. Li, J. *et al.* The RIP1/RIP3 Necrosome Forms a Functional Amyloid Signaling Complex Required for Programmed Necrosis. *Cell* **150**, 339–350 (2012).
70. Cho, Y. *et al.* Phosphorylation-Driven Assembly of the RIP1-RIP3 Complex Regulates Programmed Necrosis and Virus-Induced Inflammation. *Cell* **137**, 1112–1123 (2009).
71. Kaiser, W. J. *et al.* Toll-like Receptor 3-mediated Necrosis via TRIF, RIP3, and MLKL*. *Journal of Biological Chemistry* **288**, 31268–31279 (2013).
72. Maelfait, J. *et al.* Sensing of viral and endogenous RNA by ZBP1/DAI induces necroptosis. *The EMBO Journal* **36**, 2529–2543 (2017).
73. Lin, J. *et al.* RIPK1 counteracts ZBP1-mediated necroptosis to inhibit inflammation. *Nature* **540**, 124–128 (2016).
74. Newton, K. *et al.* RIPK1 inhibits ZBP1-driven necroptosis during development. *Nature* **540**, 129–133 (2016).
75. Seo, J., Nam, Y. W., Kim, S., Oh, D.-B. & Song, J. Necroptosis molecular mechanisms: Recent findings regarding novel necroptosis regulators. *Exp Mol Med* **53**, 1007–1017 (2021).
76. Zychlinsky, A., Prevost, M. C. & Sansonetti, P. J. *Shigella flexneri* induces apoptosis in infected macrophages. *Nature* **358**, 167–169 (1992).
77. Brennan, M. A. & Cookson, B. T. *Salmonella* induces macrophage death by caspase-1-dependent necrosis. *Molecular Microbiology* **38**, 31–40 (2000).
78. Fink, S. L. & Cookson, B. T. Caspase-1-dependent pore formation during pyroptosis leads to osmotic lysis of infected host macrophages. *Cellular Microbiology* **8**, 1812–1825 (2006).
79. von Moltke, J., Ayres, J. S., Kofoed, E. M., Chavarría-Smith, J. & Vance, R. E. Recognition of bacteria by inflammasomes. *Annu Rev Immunol* **31**, 73–106 (2013).
80. Miao, E. A. *et al.* Cytoplasmic flagellin activates caspase-1 and secretion of interleukin 1 β via Ipaf. *Nat Immunol* **7**, 569–575 (2006).
81. Miao, E. A. *et al.* Innate immune detection of the type III secretion apparatus through the NLRC4 inflammasome. *Proceedings of the National Academy of Sciences* **107**, 3076–3080 (2010).
82. Zhao, Y. *et al.* The NLRC4 inflammasome receptors for bacterial flagellin and type III secretion apparatus. *Nature* **477**, 596–600 (2011).
83. Fernandes-Alnemri, T., Yu, J.-W., Datta, P., Wu, J. & Alnemri, E. S. AIM2 activates the inflammasome and cell death in response to cytoplasmic DNA. *Nature* **458**, 509–513 (2009).
84. Hornung, V. *et al.* AIM2 recognizes cytosolic dsDNA and forms a caspase-1-activating inflammasome with ASC. *Nature* **458**, 514–518 (2009).
85. Mariathasan, S. *et al.* Differential activation of the inflammasome by caspase-1 adaptors ASC and Ipaf. *Nature* **430**, 213–218 (2004).
86. He, W. *et al.* Gasdermin D is an executor of pyroptosis and required for interleukin-1 β secretion. *Cell Res* **25**, 1285–1298 (2015).

87. Shi, J. *et al.* Cleavage of GSDMD by inflammatory caspases determines pyroptotic cell death. *Nature* **526**, 660–665 (2015).
88. Ding, J. *et al.* Pore-forming activity and structural autoinhibition of the gasdermin family. *Nature* **535**, 111–116 (2016).
89. Kayagaki, N. *et al.* Non-canonical inflammasome activation targets caspase-11. *Nature* **479**, 117–121 (2011).
90. Kayagaki, N. *et al.* Noncanonical Inflammasome Activation by Intracellular LPS Independent of TLR4. *Science* **341**, 1246–1249 (2013).
91. Shi, J. *et al.* Inflammatory caspases are innate immune receptors for intracellular LPS. *Nature* **514**, 187–192 (2014).
92. Rathinam, V. A. K. *et al.* TRIF Licenses Caspase-11-Dependent NLRP3 Inflammasome Activation by Gram-Negative Bacteria. *Cell* **150**, 606–619 (2012).
93. Broz, P. *et al.* Caspase-11 increases susceptibility to Salmonella infection in the absence of caspase-1. *Nature* **490**, 288–291 (2012).
94. Schauvliege, R., Vanrobaeys, J., Schotte, P. & Beyaert, R. Caspase-11 Gene Expression in Response to Lipopolysaccharide and Interferon- γ Requires Nuclear Factor- κ B and Signal Transducer and Activator of Transcription (STAT) 1*. *Journal of Biological Chemistry* **277**, 41624–41630 (2002).
95. Aachoui, Y. *et al.* Caspase-11 Protects Against Bacteria That Escape the Vacuole. *Science* **339**, 975–978 (2013).
96. Hur, J. *et al.* Induction of caspase-11 by inflammatory stimuli in rat astrocytes: lipopolysaccharide induction through p38 mitogen-activated protein kinase pathway1. *FEBS Letters* **507**, 157–162 (2001).
97. Wang, K. *et al.* Structural Mechanism for GSDMD Targeting by Autoprocessed Caspases in Pyroptosis. *Cell* **180**, 941-955.e20 (2020).
98. Kayagaki, N. *et al.* Caspase-11 cleaves gasdermin D for non-canonical inflammasome signalling. *Nature* **526**, 666–671 (2015).
99. Wang, Y. *et al.* Chemotherapy drugs induce pyroptosis through caspase-3 cleavage of a gasdermin. *Nature* **547**, 99–103 (2017).
100. Rogers, C. *et al.* Cleavage of DFNA5 by caspase-3 during apoptosis mediates progression to secondary necrotic/pyroptotic cell death. *Nat Commun* **8**, 14128 (2017).
101. Yu, P. *et al.* Pyroptosis: mechanisms and diseases. *Sig Transduct Target Ther* **6**, 1–21 (2021).
102. Dolma, S., Lessnick, S. L., Hahn, W. C. & Stockwell, B. R. Identification of genotype-selective antitumor agents using synthetic lethal chemical screening in engineered human tumor cells. *Cancer Cell* **3**, 285–296 (2003).
103. Yagoda, N. *et al.* RAS–RAF–MEK-dependent oxidative cell death involving voltage-dependent anion channels. *Nature* **447**, 865–869 (2007).
104. Dixon, S. J. *et al.* Ferroptosis: An Iron-Dependent Form of Nonapoptotic Cell Death. *Cell* **149**, 1060–1072 (2012).
105. Friedmann Angeli, J. P. *et al.* Inactivation of the ferroptosis regulator Gpx4 triggers acute renal failure in mice. *Nat Cell Biol* **16**, 1180–1191 (2014).

106. Riegman, M. *et al.* Ferroptosis occurs through an osmotic mechanism and propagates independently of cell rupture. *Nat Cell Biol* **22**, 1042–1048 (2020).
107. Yang, W. S. & Stockwell, B. R. Synthetic Lethal Screening Identifies Compounds Activating Iron-Dependent, Nonapoptotic Cell Death in Oncogenic-RAS-Harboring Cancer Cells. *Chemistry & Biology* **15**, 234–245 (2008).
108. Ayala, A., Muñoz, M. F. & Argüelles, S. Lipid Peroxidation: Production, Metabolism, and Signaling Mechanisms of Malondialdehyde and 4-Hydroxy-2-Nonenal. *Oxidative Medicine and Cellular Longevity* **2014**, e360438 (2014).
109. Agmon, E., Solon, J., Bassereau, P. & Stockwell, B. R. Modeling the effects of lipid peroxidation during ferroptosis on membrane properties. *Sci Rep* **8**, 5155 (2018).
110. Stockwell, B. R. Ferroptosis turns 10: Emerging mechanisms, physiological functions, and therapeutic applications. *Cell* **185**, 2401–2421 (2022).
111. Pedrera, L. *et al.* Ferroptotic pores induce Ca²⁺ fluxes and ESCRT-III activation to modulate cell death kinetics. *Cell Death Differ* **28**, 1644–1657 (2021).
112. Yapici, F. I. & Bebbler, C. M. A guide to ferroptosis in cancer. *Molecular Oncology* (2024).
113. Yang, W. S. *et al.* Peroxidation of polyunsaturated fatty acids by lipoxygenases drives ferroptosis. *Proc. Natl. Acad. Sci. U.S.A.* **113**, (2016).
114. Kagan, V. E. *et al.* Oxidized arachidonic and adrenic PEs navigate cells to ferroptosis. *Nat Chem Biol* **13**, 81–90 (2017).
115. Zou, Y. *et al.* Plasticity of ether lipids promotes ferroptosis susceptibility and evasion. *Nature* **585**, 603–608 (2020).
116. Maiorino, M., Conrad, M. & Ursini, F. GPx4, Lipid Peroxidation, and Cell Death: Discoveries, Rediscoveries, and Open Issues. *Antioxidants & Redox Signaling* **29**, 61–74 (2018).
117. Feng, H. & Stockwell, B. R. Unsolved mysteries: How does lipid peroxidation cause ferroptosis? *PLOS Biology* **16**, e2006203 (2018).
118. Pader, I. *et al.* Thioredoxin-related protein of 14 kDa is an efficient L-cystine reductase and S-denitrosylase. *Proc. Natl. Acad. Sci. U.S.A.* **111**, 6964–6969 (2014).
119. Mandal, P. K. *et al.* System xc⁻ and Thioredoxin Reductase 1 Cooperatively Rescue Glutathione Deficiency. *Journal of Biological Chemistry* **285**, 22244–22253 (2010).
120. Yang, W. S. *et al.* Regulation of Ferroptotic Cancer Cell Death by GPX4. *Cell* **156**, 317–331 (2014).
121. Zhu, J. *et al.* Transsulfuration Activity Can Support Cell Growth upon Extracellular Cysteine Limitation. *Cell Metabolism* **30**, 865-876.e5 (2019).
122. Liu, N., Lin, X. & Huang, C. Activation of the reverse transsulfuration pathway through NRF2/CBS confers erastin-induced ferroptosis resistance. *Br J Cancer* **122**, 279–292 (2020).
123. Cao, J. Y. *et al.* A Genome-wide Haploid Genetic Screen Identifies Regulators of Glutathione Abundance and Ferroptosis Sensitivity. *Cell Reports* **26**, 1544-1556.e8 (2019).
124. Hao, S. *et al.* Cysteine Dioxygenase 1 Mediates Erastin-Induced Ferroptosis in Human Gastric Cancer Cells. *Neoplasia* **19**, 1022–1032 (2017).

125. Doll, S. *et al.* FSP1 is a glutathione-independent ferroptosis suppressor. *Nature* **575**, 693–698 (2019).
126. Bersuker, K. *et al.* The CoQ oxidoreductase FSP1 acts parallel to GPX4 to inhibit ferroptosis. *Nature* **575**, 688–692 (2019).
127. Deshwal, S. *et al.* Mitochondria regulate intracellular coenzyme Q transport and ferroptotic resistance via STARD7. *Nat Cell Biol* (2023) doi:10.1038/s41556-022-01071-y.
128. Shimada, K. *et al.* Global survey of cell death mechanisms reveals metabolic regulation of ferroptosis. *Nat Chem Biol* **12**, 497–503 (2016).
129. Zhang, S. *et al.* FSP1 oxidizes NADPH to suppress ferroptosis. *Cell Res* **33**, 967–970 (2023).
130. Shimada, K., Hayano, M., Pagano, N. C. & Stockwell, B. R. Cell-Line Selectivity Improves the Predictive Power of Pharmacogenomic Analyses and Helps Identify NADPH as Biomarker for Ferroptosis Sensitivity. *Cell Chemical Biology* **23**, 225–235 (2016).
131. Mao, C. *et al.* DHODH-mediated ferroptosis defence is a targetable vulnerability in cancer. *Nature* **593**, 586–590 (2021).
132. Mishima, E. *et al.* DHODH inhibitors sensitize to ferroptosis by FSP1 inhibition. *Nature* **619**, E9–E18 (2023).
133. Mishima, E. *et al.* A non-canonical vitamin K cycle is a potent ferroptosis suppressor. *Nature* **608**, 778–783 (2022).
134. Kraft, V. A. N. *et al.* GTP Cyclohydrolase 1/Tetrahydrobiopterin Counteract Ferroptosis through Lipid Remodeling. *ACS Cent. Sci.* **6**, 41–53 (2020).
135. Soula, M. *et al.* Metabolic determinants of cancer cell sensitivity to canonical ferroptosis inducers. *Nat Chem Biol* **16**, 1351–1360 (2020).
136. Barayeu, U. *et al.* Hydropersulfides inhibit lipid peroxidation and ferroptosis by scavenging radicals. *Nat Chem Biol* **19**, 28–37 (2023).
137. Magtanong, L. *et al.* Exogenous Monounsaturated Fatty Acids Promote a Ferroptosis-Resistant Cell State. *Cell Chemical Biology* **26**, 420–432.e9 (2019).
138. Stockwell, B. R. *et al.* Ferroptosis: A Regulated Cell Death Nexus Linking Metabolism, Redox Biology, and Disease. *Cell* **171**, 273–285 (2017).
139. Conrad, M. & Pratt, D. A. The chemical basis of ferroptosis. *Nat Chem Biol* **15**, 1137–1147 (2019).
140. Jiang, X., Stockwell, B. R. & Conrad, M. Ferroptosis: mechanisms, biology and role in disease. *Nat Rev Mol Cell Biol* **22**, 266–282 (2021).
141. Soe-Lin, S. *et al.* Nramp1 promotes efficient macrophage recycling of iron following erythrophagocytosis in vivo. *Proc. Natl. Acad. Sci. U.S.A.* **106**, 5960–5965 (2009).
142. Soe-Lin, S. *et al.* Both Nramp1 and DMT1 are necessary for efficient macrophage iron recycling. *Experimental Hematology* **38**, 609–617 (2010).
143. Muñoz, M., García-Erce, J. A. & Remacha, Á. F. Disorders of iron metabolism. Part 1: molecular basis of iron homeostasis. *J Clin Pathol* **64**, 281–286 (2011).

144. Müllner, E. W. & Kühn, L. C. A stem-loop in the 3' untranslated region mediates iron-dependent regulation of transferrin receptor mRNA stability in the cytoplasm. *Cell* **53**, 815–825 (1988).
145. Mancias, J. D., Wang, X., Gygi, S. P., Harper, J. W. & Kimmelman, A. C. Quantitative proteomics identifies NCOA4 as the cargo receptor mediating ferritinophagy. *Nature* **509**, 105–109 (2014).
146. Hou, W. *et al.* Autophagy promotes ferroptosis by degradation of ferritin. *Autophagy* **12**, 1425–1428 (2016).
147. Ma, S., Henson, E. S., Chen, Y. & Gibson, S. B. Ferroptosis is induced following siramesine and lapatinib treatment of breast cancer cells. *Cell Death Dis* **7**, e2307–e2307 (2016).
148. Brown, C. W. *et al.* Prominin2 Drives Ferroptosis Resistance by Stimulating Iron Export. *Developmental Cell* **51**, 575–586.e4 (2019).
149. Lesbordes-Brion, J.-C. *et al.* Targeted disruption of the hepcidin 1 gene results in severe hemochromatosis. *Blood* **108**, 1402–1405 (2006).
150. Gao, M., Monian, P., Quadri, N., Ramasamy, R. & Jiang, X. Glutaminolysis and Transferrin Regulate Ferroptosis. *Molecular Cell* **59**, 298–308 (2015).
151. Cheng, Z. & Li, Y. What Is Responsible for the Initiating Chemistry of Iron-Mediated Lipid Peroxidation: An Update. *Chem. Rev.* **107**, 748–766 (2007).
152. Wiernicki, B. *et al.* Excessive phospholipid peroxidation distinguishes ferroptosis from other cell death modes including pyroptosis. *Cell Death Dis* **11**, 922 (2020).
153. Doll, S. *et al.* ACSL4 dictates ferroptosis sensitivity by shaping cellular lipid composition. *Nat Chem Biol* **13**, 91–98 (2017).
154. Yuan, H., Li, X., Zhang, X., Kang, R. & Tang, D. Identification of ACSL4 as a biomarker and contributor of ferroptosis. *Biochemical and Biophysical Research Communications* **478**, 1338–1343 (2016).
155. Hashidate-Yoshida, T. *et al.* Fatty acid remodeling by LPCAT3 enriches arachidonate in phospholipid membranes and regulates triglyceride transport. *eLife* **4**, e06328 (2015).
156. Dixon, S. J. *et al.* Human Haploid Cell Genetics Reveals Roles for Lipid Metabolism Genes in Nonapoptotic Cell Death. *ACS Chem. Biol.* **10**, 1604–1609 (2015).
157. Yan, B. *et al.* Membrane Damage during Ferroptosis Is Caused by Oxidation of Phospholipids Catalyzed by the Oxidoreductases POR and CYB5R1. *Molecular Cell* **81**, 355–369.e10 (2021).
158. Zou, Y. *et al.* Cytochrome P450 oxidoreductase contributes to phospholipid peroxidation in ferroptosis. *Nat Chem Biol* **16**, 302–309 (2020).
159. Shintoku, R. *et al.* Lipoxygenase-mediated generation of lipid peroxides enhances ferroptosis induced by erastin and RSL3. *Cancer Science* **108**, 2187–2194 (2017).
160. Wenzel, S. E. *et al.* PEBP1 Wardens Ferroptosis by Enabling Lipoxygenase Generation of Lipid Death Signals. *Cell* **171**, 628–641.e26 (2017).
161. Chu, B. *et al.* ALOX12 is required for p53-mediated tumour suppression through a distinct ferroptosis pathway. *Nat Cell Biol* **21**, 579–591 (2019).

162. Jiang, L. *et al.* Ferroptosis as a p53-mediated activity during tumour suppression. *Nature* **520**, 57–62 (2015).
163. Liang, D. *et al.* Ferroptosis surveillance independent of GPX4 and differentially regulated by sex hormones. *Cell* **186**, 2748-2764.e22 (2023).
164. Li, Y. *et al.* 7-Dehydrocholesterol dictates ferroptosis sensitivity. *Nature* **626**, 411–418 (2024).
165. Freitas, F. P. *et al.* 7-Dehydrocholesterol is an endogenous suppressor of ferroptosis. *Nature* **626**, 401–410 (2024).
166. Zorov, D. B., Juhaszova, M. & Sollott, S. J. Mitochondrial Reactive Oxygen Species (ROS) and ROS-Induced ROS Release. *Physiological Reviews* **94**, 909–950 (2014).
167. Anandhan, A., Dodson, M., Schmidlin, C. J., Liu, P. & Zhang, D. D. Breakdown of an Ironclad Defense System: The Critical Role of NRF2 in Mediating Ferroptosis. *Cell Chemical Biology* **27**, 436–447 (2020).
168. Bellezza, I., Giambanco, I., Minelli, A. & Donato, R. Nrf2-Keap1 signaling in oxidative and reductive stress. *Biochimica et Biophysica Acta (BBA) - Molecular Cell Research* **1865**, 721–733 (2018).
169. Cooper, G. M. The Mechanism of Oxidative Phosphorylation. in *The Cell: A Molecular Approach. 2nd edition* (Sinauer Associates, 2000).
170. Suzuki, S. *et al.* GLS2 Is a Tumor Suppressor and a Regulator of Ferroptosis in Hepatocellular Carcinoma. *Cancer Research* **82**, 3209–3222 (2022).
171. Gao, M. *et al.* Role of Mitochondria in Ferroptosis. *Molecular Cell* **73**, 354-363.e3 (2019).
172. Schmitt, A. *et al.* Dimethyl fumarate induces ferroptosis and impairs NF- κ B/STAT3 signaling in DLBCL. *Blood* **138**, 871–884 (2021).
173. Hassannia, B., Vandenabeele, P. & Vanden Berghe, T. Targeting Ferroptosis to Iron Out Cancer. *Cancer Cell* **35**, 830–849 (2019).
174. Vučković, A.-M. *et al.* Inactivation of the glutathione peroxidase GPx4 by the ferroptosis-inducing molecule RSL3 requires the adaptor protein 14-3-3 ϵ . *FEBS Letters* **594**, 611–624 (2020).
175. Eaton, J. K. *et al.* Selective covalent targeting of GPX4 using masked nitrile-oxide electrophiles. *Nat Chem Biol* **16**, 497–506 (2020).
176. Cheff, D. M. *et al.* The ferroptosis inducing compounds RSL3 and ML162 are not direct inhibitors of GPX4 but of TXNRD1. *Redox Biology* **62**, 102703 (2023).
177. Müller, F. *et al.* Elevated FSP1 protects KRAS-mutated cells from ferroptosis during tumor initiation. *Cell Death Differ* **30**, 442–456 (2023).
178. Nakamura, T. *et al.* Integrated chemical and genetic screens unveil FSP1 mechanisms of ferroptosis regulation. *Nat Struct Mol Biol* **30**, 1806–1815 (2023).
179. Nakamura, T. *et al.* Phase separation of FSP1 promotes ferroptosis. *Nature* **619**, 371–377 (2023).
180. Koppula, P., Zhuang, L. & Gan, B. Cystine transporter SLC7A11/xCT in cancer: ferroptosis, nutrient dependency, and cancer therapy. *Protein & Cell* **12**, 599–620 (2021).

181. Zhang, Y. *et al.* Imidazole Ketone Erastin Induces Ferroptosis and Slows Tumor Growth in a Mouse Lymphoma Model. *Cell Chemical Biology* **26**, 623-633.e9 (2019).
182. Gout, P. W., Buckley, A. R., Simms, C. R. & Bruchovsky, N. Sulfasalazine, a potent suppressor of lymphoma growth by inhibition of the xc – cystine transporter: a new action for an old drug. *Leukemia* **15**, 1633–1640 (2001).
183. Yu, H. *et al.* Sulfasalazine-induced ferroptosis in breast cancer cells is reduced by the inhibitory effect of estrogen receptor on the transferrin receptor. *Oncology Reports* **42**, 826–838 (2019).
184. Nielsen, O. H., Bukhave, K., Elmgreen, J. & Ahnfelt-Rønne, I. Inhibition of 5-lipoxygenase pathway of arachidonic acid metabolism in human neutrophils by sulfasalazine and 5-aminosalicylic acid. *Dig Dis Sci* **32**, 577–582 (1987).
185. Louandre, C. *et al.* The retinoblastoma (Rb) protein regulates ferroptosis induced by sorafenib in human hepatocellular carcinoma cells. *Cancer Letters* **356**, 971–977 (2015).
186. Dixon, S. J. *et al.* Pharmacological inhibition of cystine–glutamate exchange induces endoplasmic reticulum stress and ferroptosis. *eLife* **3**, e02523 (2014).
187. Louandre, C. *et al.* Iron-dependent cell death of hepatocellular carcinoma cells exposed to sorafenib. *International Journal of Cancer* **133**, 1732–1742 (2013).
188. Cramer, S. L. *et al.* Systemic depletion of L-cyst(e)ine with cyst(e)inase increases reactive oxygen species and suppresses tumor growth. *Nat Med* **23**, 120–127 (2017).
189. Harris, I. S. *et al.* Glutathione and Thioredoxin Antioxidant Pathways Synergize to Drive Cancer Initiation and Progression. *Cancer Cell* **27**, 211–222 (2015).
190. Arensman, M. D. *et al.* Cystine–glutamate antiporter xCT deficiency suppresses tumor growth while preserving antitumor immunity. *Proc. Natl. Acad. Sci. U.S.A.* **116**, 9533–9542 (2019).
191. Eling, N., Reuter, L., Hazin, J., Hamacher-Brady, A. & Brady, N. R. Identification of artesunate as a specific activator of ferroptosis in pancreatic cancer cells. *Oncoscience* **2**, 517–532 (2015).
192. Weïwer, M. *et al.* Development of small-molecule probes that selectively kill cells induced to express mutant *RAS*. *Bioorganic & Medicinal Chemistry Letters* **22**, 1822–1826 (2012).
193. Zhang, Y. *et al.* Implications of Withaferin A for the metastatic potential and drug resistance in hepatocellular carcinoma cells via Nrf2-mediated EMT and ferroptosis. *Toxicology Mechanisms and Methods* **33**, 47–55 (2023).
194. Hassannia, B. *et al.* Nano-targeted induction of dual ferroptotic mechanisms eradicates high-risk neuroblastoma. *J Clin Invest* **128**, 3341–3355.
195. Woo, J. H. *et al.* Elucidating Compound Mechanism of Action by Network Perturbation Analysis. *Cell* **162**, 441–451 (2015).
196. Gaschler, M. M. *et al.* Determination of the Subcellular Localization and Mechanism of Action of Ferrostatins in Suppressing Ferroptosis. *ACS Chem. Biol.* **13**, 1013–1020 (2018).
197. Mao, W. *et al.* Statin shapes inflamed tumor microenvironment and enhances immune checkpoint blockade in non–small cell lung cancer. *JCI Insight* **7**, e161940.

198. Viswanathan, V. S. *et al.* Dependency of a therapy-resistant state of cancer cells on a lipid peroxidase pathway. *Nature* **547**, 453–457 (2017).
199. Yao, X. *et al.* Simvastatin induced ferroptosis for triple-negative breast cancer therapy. *Journal of Nanobiotechnology* **19**, 311 (2021).
200. Chen, G.-Q. *et al.* Artemisinin compounds sensitize cancer cells to ferroptosis by regulating iron homeostasis. *Cell Death Differ* **27**, 242–254 (2020).
201. Sato, H. *et al.* Redox Imbalance in Cystine/Glutamate Transporter-deficient Mice *. *Journal of Biological Chemistry* **280**, 37423–37429 (2005).
202. Yant, L. J. *et al.* The selenoprotein GPX4 is essential for mouse development and protects from radiation and oxidative damage insults. *Free Radical Biology and Medicine* **34**, 496–502 (2003).
203. Imai, H. *et al.* Early embryonic lethality caused by targeted disruption of the mouse PHGPx gene. *Biochemical and Biophysical Research Communications* **305**, 278–286 (2003).
204. Chen, L., Hambright, W. S., Na, R. & Ran, Q. Ablation of the Ferroptosis Inhibitor Glutathione Peroxidase 4 in Neurons Results in Rapid Motor Neuron Degeneration and Paralysis *. *Journal of Biological Chemistry* **290**, 28097–28106 (2015).
205. Matsushita, M. *et al.* T cell lipid peroxidation induces ferroptosis and prevents immunity to infection. *Journal of Experimental Medicine* **212**, 555–568 (2015).
206. Medzhitov, R. Inflammation 2010: New Adventures of an Old Flame. *Cell* **140**, 771–776 (2010).
207. Turvey, S. E. & Broide, D. H. Innate immunity. *Journal of Allergy and Clinical Immunology* **125**, S24–S32 (2010).
208. Ochando, J., Mulder, W. J. M., Madsen, J. C., Netea, M. G. & Duivenvoorden, R. Trained immunity — basic concepts and contributions to immunopathology. *Nat Rev Nephrol* **19**, 23–37 (2023).
209. Bonilla, F. A. & Oettgen, H. C. Adaptive immunity. *Journal of Allergy and Clinical Immunology* **125**, S33–S40 (2010).
210. Charles A Janeway, J., Travers, P., Walport, M. & Shlomchik, M. J. Principles of innate and adaptive immunity. in *Immunobiology: The Immune System in Health and Disease. 5th edition* (Garland Science, 2001).
211. Ferrero-Miliani, L., Nielsen, O. H., Andersen, P. S. & Girardin, S. E. Chronic inflammation: importance of NOD2 and NALP3 in interleukin-1 β generation. *Clin Exp Immunol* **147**, 227–235 (2007).
212. Takeuchi, O. & Akira, S. Pattern Recognition Receptors and Inflammation. *Cell* **140**, 805–820 (2010).
213. Marshall, J. S., Warrington, R., Watson, W. & Kim, H. L. An introduction to immunology and immunopathology. *Allergy Asthma Clin Immunol* **14**, 1–10 (2018).
214. Chertov, O., Yang, D., Howard, O. M. Z. & Oppenheim, J. J. Leukocyte granule proteins mobilize innate host defenses and adaptive immune responses. *Immunological Reviews* **177**, 68–78 (2000).

215. Libby, P. Inflammatory Mechanisms: the Molecular Basis of Inflammation and Disease. *Nutrition Reviews* **65**, S140–S146 (2007).
216. Seong, S.-Y. & Matzinger, P. Hydrophobicity: an ancient damage-associated molecular pattern that initiates innate immune responses. *Nat Rev Immunol* **4**, 469–478 (2004).
217. Honda, K. & Taniguchi, T. IRFs: master regulators of signalling by Toll-like receptors and cytosolic pattern-recognition receptors. *Nat Rev Immunol* **6**, 644–658 (2006).
218. Henríquez-Olguín, C. *et al.* Altered ROS production, NF- κ B activation and interleukin-6 gene expression induced by electrical stimulation in dystrophic *mdx* skeletal muscle cells. *Biochimica et Biophysica Acta (BBA) - Molecular Basis of Disease* **1852**, 1410–1419 (2015).
219. Hendrayani, S.-F., Al-Harbi, B., Al-Ansari, M. M., Silva, G. & Aboussekhra, A. The inflammatory/cancer-related IL-6/STAT3/NF- κ B positive feedback loop includes AUF1 and maintains the active state of breast myofibroblasts. *Oncotarget* **7**, 41974–41985 (2016).
220. Kyriakis, J. M. & Avruch, J. Mammalian Mitogen-Activated Protein Kinase Signal Transduction Pathways Activated by Stress and Inflammation. *Physiological Reviews* (2001) doi:10.1152/physrev.2001.81.2.807.
221. Oeckinghaus, A., Hayden, M. S. & Ghosh, S. Crosstalk in NF- κ B signaling pathways. *Nat Immunol* **12**, 695–708 (2011).
222. Pace, J. L., Russell, S. W., Schreiber, R. D., Altman, A. & Katz, D. H. Macrophage activation: priming activity from a T-cell hybridoma is attributable to interferon-gamma. *Proceedings of the National Academy of Sciences* **80**, 3782–3786 (1983).
223. Celada, A., Gray, P. W., Rinderknecht, E. & Schreiber, R. D. Evidence for a gamma-interferon receptor that regulates macrophage tumoricidal activity. *Journal of Experimental Medicine* **160**, 55–74 (1984).
224. Doyle, A. G. *et al.* Interleukin-13 alters the activation state of murine macrophages in vitro: Comparison with interleukin-4 and interferon- γ . *European Journal of Immunology* **24**, 1441–1445 (1994).
225. Stein, M., Keshav, S., Harris, N. & Gordon, S. Interleukin 4 potently enhances murine macrophage mannose receptor activity: a marker of alternative immunologic macrophage activation. *Journal of Experimental Medicine* **176**, 287–292 (1992).
226. Murray, P. J. Macrophage Polarization. *Annual Review of Physiology* **79**, 541–566 (2017).
227. Chen, Y., Zander, R., Khatun, A., Schauder, D. M. & Cui, W. Transcriptional and Epigenetic Regulation of Effector and Memory CD8 T Cell Differentiation. *Front. Immunol.* **9**, 422590 (2018).
228. Luckheeram, R. V., Zhou, R., Verma, A. D. & Xia, B. CD4+T Cells: Differentiation and Functions. *Clinical and Developmental Immunology* **2012**, (2012).
229. Alberts, B. *et al.* B Cells and Antibodies. in *Molecular Biology of the Cell. 4th edition* (Garland Science, 2002).
230. Bistoni, F. *et al.* Evidence for macrophage-mediated protection against lethal *Candida albicans* infection. *Infection and Immunity* **51**, 668–674 (1986).

231. Vecchiarelli, A. *et al.* Protective immunity induced by low-virulence *Candida albicans*: Cytokine production in the development of the anti-infectious state. *Cellular Immunology* **124**, 334–344 (1989).
232. Netea, M. G., Quintin, J. & van der Meer, J. W. M. Trained Immunity: A Memory for Innate Host Defense. *Cell Host & Microbe* **9**, 355–361 (2011).
233. Divangahi, M. *et al.* Trained immunity, tolerance, priming and differentiation: distinct immunological processes. *Nat Immunol* **22**, 2–6 (2021).
234. Kaufmann, E. *et al.* BCG Educates Hematopoietic Stem Cells to Generate Protective Innate Immunity against Tuberculosis. *Cell* **172**, 176-190.e19 (2018).
235. Kleinnijenhuis, J. *et al.* Bacille Calmette-Guérin induces NOD2-dependent nonspecific protection from reinfection via epigenetic reprogramming of monocytes. *Proc. Natl. Acad. Sci. U.S.A.* **109**, 17537–17542 (2012).
236. Quintin, J. *et al.* *Candida albicans* Infection Affords Protection against Reinfection via Functional Reprogramming of Monocytes. *Cell Host & Microbe* **12**, 223–232 (2012).
237. Netea, M. G. *et al.* Trained Immunity: a Tool for Reducing Susceptibility to and the Severity of SARS-CoV-2 Infection. *Cell* **181**, 969–977 (2020).
238. Turner, M. D., Nedjai, B., Hurst, T. & Pennington, D. J. Cytokines and chemokines: At the crossroads of cell signalling and inflammatory disease. *Biochimica et Biophysica Acta (BBA) - Molecular Cell Research* **1843**, 2563–2582 (2014).
239. Lazennec, G. & Richmond, A. Chemokines and chemokine receptors: new insights into cancer-related inflammation. *Trends in Molecular Medicine* **16**, 133–144 (2010).
240. Dennis, E. A. & Norris, P. C. Eicosanoid storm in infection and inflammation. *Nat Rev Immunol* **15**, 511–523 (2015).
241. Qi, H.-Y. & Shelhamer, J. H. Toll-like Receptor 4 Signaling Regulates Cytosolic Phospholipase A2 Activation and Lipid Generation in Lipopolysaccharide-stimulated Macrophages*. *Journal of Biological Chemistry* **280**, 38969–38975 (2005).
242. Ambs, P., Baccarini, M., Fitzke, E. & Dieter, P. Role of cytosolic phospholipase A2 in arachidonic acid release of rat-liver macrophages: regulation by Ca²⁺ and phosphorylation. *Biochem J* **311**, 189–195 (1995).
243. Harizi, H., Corcuff, J.-B. & Gualde, N. Arachidonic-acid-derived eicosanoids: roles in biology and immunopathology. *Trends in Molecular Medicine* **14**, 461–469 (2008).
244. Funk, C. D. Prostaglandins and Leukotrienes: Advances in Eicosanoid Biology. *Science* **294**, 1871–1875 (2001).
245. Serhan, C. N. Lipoxins and aspirin-triggered 15-epi-lipoxins are the first lipid mediators of endogenous anti-inflammation and resolution. *Prostaglandins, Leukotrienes and Essential Fatty Acids* **73**, 141–162 (2005).
246. Serhan, C. N., Chiang, N., Dalli, J. & Levy, B. D. Lipid Mediators in the Resolution of Inflammation. *Cold Spring Harb Perspect Biol* **7**, a016311 (2015).
247. Chen, G. Y. & Nuñez, G. Sterile inflammation: sensing and reacting to damage. *Nat Rev Immunol* **10**, 826–837 (2010).
248. Land, W. G. Use of DAMPs and SAMPs as Therapeutic Targets or Therapeutics: A Note of Caution. *Mol Diagn Ther* **24**, 251–262 (2020).

249. Land, W. Allograft injury mediated by reactive oxygen species: from conserved proteins of *Drosophila* to acute and chronic rejection of human transplants. Part III: interaction of (oxidative) stress-induced heat shock proteins with toll-like receptor-bearing cells of innate immunity and its consequences for the development of acute and chronic allograft rejection. *Transplantation Reviews* **17**, 67–86 (2003).
250. Schaefer, L. Complexity of Danger: The Diverse Nature of Damage-associated Molecular Patterns *. *Journal of Biological Chemistry* **289**, 35237–35245 (2014).
251. Raghavan, B., Martin, S. F., Esser, P. R., Goebeler, M. & Schmidt, M. Metal allergens nickel and cobalt facilitate TLR4 homodimerization independently of MD2. *EMBO reports* **13**, 1109–1115 (2012).
252. Tsai, S.-Y. *et al.* DAMP Molecule S100A9 Acts as a Molecular Pattern to Enhance Inflammation during Influenza A Virus Infection: Role of DDX21-TRIF-TLR4-MyD88 Pathway. *PLOS Pathogens* **10**, e1003848 (2014).
253. Mariathasan, S. *et al.* Cryopyrin activates the inflammasome in response to toxins and ATP. *Nature* **440**, 228–232 (2006).
254. Ghiringhelli, F. *et al.* Activation of the NLRP3 inflammasome in dendritic cells induces IL-1 β -dependent adaptive immunity against tumors. *Nat Med* **15**, 1170–1178 (2009).
255. Zhang, Q. *et al.* Circulating mitochondrial DAMPs cause inflammatory responses to injury. *Nature* **464**, 104–107 (2010).
256. Julian, M. W. *et al.* Mitochondrial Transcription Factor A Serves as a Danger Signal by Augmenting Plasmacytoid Dendritic Cell Responses to DNA. *The Journal of Immunology* **189**, 433–443 (2012).
257. Herb, M. *et al.* Mitochondrial reactive oxygen species enable proinflammatory signaling through disulfide linkage of NEMO. *Science Signaling* **12**, eaar5926 (2019).
258. Dear, J. W. *et al.* Cyclophilin A Is a Damage-Associated Molecular Pattern Molecule That Mediates Acetaminophen-Induced Liver Injury. *The Journal of Immunology* **187**, 3347–3352 (2011).
259. Ishii, K. J. *et al.* Genomic DNA Released by Dying Cells Induces the Maturation of APCs. *The Journal of Immunology* **167**, 2602–2607 (2001).
260. Wu, J. *et al.* Cyclic GMP-AMP Is an Endogenous Second Messenger in Innate Immune Signaling by Cytosolic DNA. *Science* **339**, 826–830 (2013).
261. Komada, T. *et al.* Macrophage Uptake of Necrotic Cell DNA Activates the AIM2 Inflammasome to Regulate a Proinflammatory Phenotype in CKD. *Journal of the American Society of Nephrology* **29**, 1165 (2018).
262. Bernard, J. J. *et al.* Ultraviolet radiation damages self noncoding RNA and is detected by TLR3. *Nat Med* **18**, 1286–1290 (2012).
263. Xu, J., Zhang, X., Monestier, M., Esmon, N. L. & Esmon, C. T. Extracellular Histones Are Mediators of Death through TLR2 and TLR4 in Mouse Fatal Liver Injury. *The Journal of Immunology* **187**, 2626–2631 (2011).
264. Huang, H. *et al.* Histones Activate the NLRP3 Inflammasome in Kupffer Cells during Sterile Inflammatory Liver Injury. *The Journal of Immunology* **191**, 2665–2679 (2013).

265. Lee, E. J. & Park, J. H. Receptor for Advanced Glycation Endproducts (RAGE), Its Ligands, and Soluble RAGE: Potential Biomarkers for Diagnosis and Therapeutic Targets for Human Renal Diseases. *Genomics Inform* **11**, 224–229 (2013).
266. Scaffidi, P., Misteli, T. & Bianchi, M. E. Release of chromatin protein HMGB1 by necrotic cells triggers inflammation. *Nature* **418**, 191–195 (2002).
267. Rovere-Querini, P. *et al.* HMGB1 is an endogenous immune adjuvant released by necrotic cells. *EMBO reports* **5**, 825–830 (2004).
268. Wheeler, D. S. *et al.* Extracellular Hsp72, an endogenous DAMP, is released by virally infected airway epithelial cells and activates neutrophils via Toll-like receptor (TLR)-4. *Respiratory Research* **10**, 31 (2009).
269. Basu, S., Binder, R. J., Ramalingam, T. & Srivastava, P. K. CD91 Is a Common Receptor for Heat Shock Proteins gp96, hsp90, hsp70, and Calreticulin. *Immunity* **14**, 303–313 (2001).
270. Lehnardt, S. *et al.* A Vicious Cycle Involving Release of Heat Shock Protein 60 from Injured Cells and Activation of Toll-Like Receptor 4 Mediates Neurodegeneration in the CNS. *J. Neurosci.* **28**, 2320–2331 (2008).
271. Foell, D. & Roth, J. Proinflammatory S100 proteins in arthritis and autoimmune disease. *Arthritis Rheum* **50**, 3762–3771 (2004).
272. Lee, T.-H. *et al.* Elevation of S100 calcium binding protein A9 in sputum of neutrophilic inflammation in severe uncontrolled asthma. *Annals of Allergy, Asthma & Immunology* **111**, 268-275.e1 (2013).
273. Lipps, C. *et al.* N-terminal fragment of cardiac myosin binding protein-C triggers pro-inflammatory responses in vitro. *Journal of Molecular and Cellular Cardiology* **99**, 47–56 (2016).
274. Srinivasan, N. *et al.* Actin is an evolutionarily-conserved damage-associated molecular pattern that signals tissue injury in *Drosophila melanogaster*. *eLife* **5**, e19662 (2016).
275. Martinon, F., Pétrilli, V., Mayor, A., Tardivel, A. & Tschopp, J. Gout-associated uric acid crystals activate the NALP3 inflammasome. *Nature* **440**, 237–241 (2006).
276. Obeid, M. *et al.* Calreticulin exposure dictates the immunogenicity of cancer cell death. *Nat Med* **13**, 54–61 (2007).
277. Lees, S. *et al.* Bioactivity in an Aggrecan 32-mer Fragment Is Mediated via Toll-like Receptor 2. *Arthritis & Rheumatology* **67**, 1240–1249 (2015).
278. Babelova, A. *et al.* Biglycan, a Danger Signal That Activates the NLRP3 Inflammasome via Toll-like and P2X Receptors. *Journal of Biological Chemistry* **284**, 24035–24048 (2009).
279. Schaefer, L. *et al.* The matrix component biglycan is proinflammatory and signals through Toll-like receptors 4 and 2 in macrophages. *J Clin Invest* **115**, 2223–2233 (2005).
280. Merline, R. *et al.* Signaling by the Matrix Proteoglycan Decorin Controls Inflammation and Cancer Through PDCD4 and MicroRNA-21. *Science Signaling* **4**, ra75–ra75 (2011).
281. Wang, W. *et al.* Ligation of TLR2 by Versican: A Link Between Inflammation and Metastasis. *Archives of Medical Research* **40**, 321–323 (2009).

282. Goodall, K. J., Poon, I. K. H., Phipps, S. & Hulett, M. D. Soluble Heparan Sulfate Fragments Generated by Heparanase Trigger the Release of Pro-Inflammatory Cytokines through TLR-4. *PLOS ONE* **9**, e109596 (2014).
283. Xu, D. *et al.* Stable RAGE-Heparan Sulfate Complexes Are Essential for Signal Transduction. *ACS Chem. Biol.* **8**, 1611–1620 (2013).
284. Lesley, J., Hascall, V. C., Tammi, M. & Hyman, R. Hyaluronan Binding by Cell Surface CD44 *. *Journal of Biological Chemistry* **275**, 26967–26975 (2000).
285. Scheibner, K. A. *et al.* Hyaluronan Fragments Act as an Endogenous Danger Signal by Engaging TLR2. *J Immunol* **177**, 1272–1281 (2006).
286. Taylor, K. R. *et al.* Recognition of Hyaluronan Released in Sterile Injury Involves a Unique Receptor Complex Dependent on Toll-like Receptor 4, CD44, and MD-2 *. *Journal of Biological Chemistry* **282**, 18265–18275 (2007).
287. Yamasaki, K. *et al.* NLRP3/Cryopyrin Is Necessary for Interleukin-1 β (IL-1 β) Release in Response to Hyaluronan, an Endogenous Trigger of Inflammation in Response to Injury *. *Journal of Biological Chemistry* **284**, 12762–12771 (2009).
288. Piccinini, A. M. & Midwood, K. S. Endogenous Control of Immunity against Infection: Tenascin-C Regulates TLR4-Mediated Inflammation via MicroRNA-155. *Cell Reports* **2**, 914–926 (2012).
289. Smiley, S. T., King, J. A. & Hancock, W. W. Fibrinogen Stimulates Macrophage Chemokine Secretion Through Toll-Like Receptor 4. *The Journal of Immunology* **167**, 2887–2894 (2001).
290. You, R., Zheng, M. & McKeown-Longo, P. J. The First Type III Repeat in Fibronectin Activates an Inflammatory Pathway in Dermal Fibroblasts. *The Journal of Biological Chemistry* **285**, 36255 (2010).
291. Zheng, M., Jones, D. M., Horzempa, C., Prasad, A. & McKeown-Longo, P. J. The First Type III Domain of Fibronectin is Associated with the Expression of Cytokines within the Lung Tumor Microenvironment. *Journal of Cancer* **2**, 478–483 (2011).
292. Gondokaryono, S. P. *et al.* The extra domain A of fibronectin stimulates murine mast cells via Toll-like receptor 4. *Journal of Leukocyte Biology* **82**, 657–665 (2007).
293. Shi, Y. & Rock, K. L. Cell death releases endogenous adjuvants that selectively enhance immune surveillance of particulate antigens. *European Journal of Immunology* **32**, 155–162 (2002).
294. Shi, Y., Zheng, W. & Rock, K. L. Cell injury releases endogenous adjuvants that stimulate cytotoxic T cell responses. *Proceedings of the National Academy of Sciences* **97**, 14590–14595 (2000).
295. Zappasodi, R. *et al.* Improved Clinical Outcome in Indolent B-Cell Lymphoma Patients Vaccinated with Autologous Tumor Cells Experiencing Immunogenic Death. *Cancer Research* **70**, 9062–9072 (2010).
296. Murao, A., Aziz, M., Wang, H., Brenner, M. & Wang, P. Release mechanisms of major DAMPs. *Apoptosis* **26**, 152–162 (2021).
297. Berghe, T. V. *et al.* Necroptosis, necrosis and secondary necrosis converge on similar cellular disintegration features. *Cell Death Differ* **17**, 922–930 (2010).

298. Jahr, S. *et al.* DNA fragments in the blood plasma of cancer patients: quantitations and evidence for their origin from apoptotic and necrotic cells. *Cancer Res* **61**, 1659–1665 (2001).
299. Choi, J.-J., Reich III, C. F. & Pisetsky, D. S. Release of DNA from Dead and Dying Lymphocyte and Monocyte Cell Lines In Vitro. *Scandinavian Journal of Immunology* **60**, 159–166 (2004).
300. Lüthi, A. U. *et al.* Suppression of Interleukin-33 Bioactivity through Proteolysis by Apoptotic Caspases. *Immunity* **31**, 84–98 (2009).
301. Kazama, H. *et al.* Induction of Immunological Tolerance by Apoptotic Cells Requires Caspase-Dependent Oxidation of High-Mobility Group Box-1 Protein. *Immunity* **29**, 21–32 (2008).
302. Garg, A. D. *et al.* A novel pathway combining calreticulin exposure and ATP secretion in immunogenic cancer cell death. *The EMBO Journal* **31**, 1062–1079 (2012).
303. Michaud, M. *et al.* Autophagy-Dependent Anticancer Immune Responses Induced by Chemotherapeutic Agents in Mice. *Science* **334**, 1573–1577 (2011).
304. Martins, I. *et al.* Chemotherapy induces ATP release from tumor cells. *Cell Cycle* **8**, 3723–3728 (2009).
305. Elliott, M. R. *et al.* Nucleotides released by apoptotic cells act as a find-me signal to promote phagocytic clearance. *Nature* **461**, 282–286 (2009).
306. Kearney, C. J. *et al.* Necroptosis suppresses inflammation via termination of TNF- or LPS-induced cytokine and chemokine production. *Cell Death Differ* **22**, 1313–1327 (2015).
307. Orozco, S. L. *et al.* RIPK3 Activation Leads to Cytokine Synthesis that Continues after Loss of Cell Membrane Integrity. *Cell Reports* **28**, 2275–2287.e5 (2019).
308. Zhu, K. *et al.* Necroptosis promotes cell-autonomous activation of proinflammatory cytokine gene expression. *Cell Death Dis* **9**, 500 (2018).
309. Vanden Berghe, T. *et al.* Necrosis is associated with IL-6 production but apoptosis is not. *Cellular Signalling* **18**, 328–335 (2006).
310. Aaes, T. L. *et al.* Vaccination with Necroptotic Cancer Cells Induces Efficient Anti-tumor Immunity. *Cell Reports* **15**, 274–287 (2016).
311. Hartwig, T. *et al.* The TRAIL-Induced Cancer Secretome Promotes a Tumor-Supportive Immune Microenvironment via CCR2. *Molecular Cell* **65**, 730–742.e5 (2017).
312. Lamkanfi, M. *et al.* Inflammasome-Dependent Release of the Alarmin HMGB1 in Endotoxemia. *The Journal of Immunology* **185**, 4385–4392 (2010).
313. Wang, Q. *et al.* Pyroptotic cells externalize eat-me and release find-me signals and are efficiently engulfed by macrophages. *International Immunology* **25**, 363–372 (2013).
314. Heilig, R. *et al.* The Gasdermin-D pore acts as a conduit for IL-1 β secretion in mice. *European Journal of Immunology* **48**, 584–592 (2018).
315. Hu, B. *et al.* Inflammation-induced tumorigenesis in the colon is regulated by caspase-1 and NLRC4. *Proceedings of the National Academy of Sciences* **107**, 21635–21640 (2010).
316. von Moltke, J. *et al.* Rapid induction of inflammatory lipid mediators by the inflammasome in vivo. *Nature* **490**, 107–111 (2012).

317. Hangai, S. *et al.* PGE2 induced in and released by dying cells functions as an inhibitory DAMP. *Proc. Natl. Acad. Sci. U.S.A.* **113**, 3844–3849 (2016).
318. Kayagaki, N. *et al.* NINJ1 mediates plasma membrane rupture during lytic cell death. *Nature* **591**, 131–136 (2021).
319. Dondelinger, Y. *et al.* NINJ1 is activated by cell swelling to regulate plasma membrane permeabilization during regulated necrosis. *Cell Death Dis* **14**, 755 (2023).
320. Hirt, U. A. & Leist, M. Rapid, noninflammatory and PS-dependent phagocytic clearance of necrotic cells. *Cell Death Differ* **10**, 1156–1164 (2003).
321. Brouckaert, G. *et al.* Phagocytosis of Necrotic Cells by Macrophages Is Phosphatidylserine Dependent and Does Not Induce Inflammatory Cytokine Production. *MBoC* **15**, 1089–1100 (2004).
322. Koncz, G. *et al.* Damage-mediated macrophage polarization in sterile inflammation. *Front. Immunol.* **14**, (2023).
323. Zhang, X., Ma, Y., Lv, G. & Wang, H. Ferroptosis as a therapeutic target for inflammation-related intestinal diseases. *Front. Pharmacol.* **14**, 1095366 (2023).
324. Wen, Q., Liu, J., Kang, R., Zhou, B. & Tang, D. The release and activity of HMGB1 in ferroptosis. *Biochemical and Biophysical Research Communications* **510**, 278–283 (2019).
325. Jia, M. *et al.* Redox homeostasis maintained by GPX4 facilitates STING activation. *Nat Immunol* **21**, 727–735 (2020).
326. Dai, E. *et al.* Ferroptotic damage promotes pancreatic tumorigenesis through a TMEM173/STING-dependent DNA sensor pathway. *Nat Commun* **11**, 6339 (2020).
327. Dai, E. *et al.* Autophagy-dependent ferroptosis drives tumor-associated macrophage polarization via release and uptake of oncogenic KRAS protein. *Autophagy* **16**, 2069–2083 (2020).
328. Wang, Y. *et al.* Quercetin alleviates acute kidney injury by inhibiting ferroptosis. *Journal of Advanced Research* **28**, 231–243 (2021).
329. Martin-Sanchez, D. *et al.* Ferroptosis, but Not Necroptosis, Is Important in Nephrotoxic Folic Acid-Induced AKI. *JASN* **28**, 218–229 (2017).
330. O’Donnell, V. B., Aldrovandi, M., Murphy, R. C. & Krönke, G. Enzymatically oxidized phospholipids assume center stage as essential regulators of innate immunity and cell death. *Sci. Signal.* **12**, eaau2293 (2019).
331. Luo, X. *et al.* Oxygenated phosphatidylethanolamine navigates phagocytosis of ferroptotic cells by interacting with TLR2. *Cell Death Differ* **28**, 1971–1989 (2021).
332. Rothe, T. *et al.* 12/15-lipoxygenase-mediated enzymatic lipid oxidation regulates DC maturation and function. *J. Clin. Invest.* **125**, 1944–1954 (2015).
333. Musee, J. & Marnett, L. J. Prostaglandin H Synthase-2-catalyzed Oxygenation of 2-Arachidonoylglycerol Is More Sensitive to Peroxide Tone than Oxygenation of Arachidonic Acid. *Journal of Biological Chemistry* **287**, 37383–37394 (2012).
334. Sengupta, A. *et al.* Targeted Disruption of Glutathione Peroxidase 4 in Mouse Skin Epithelial Cells Impairs Postnatal Hair Follicle Morphogenesis that Is Partially Rescued

- through Inhibition of COX-2. *Journal of Investigative Dermatology* **133**, 1731–1741 (2013).
335. Efimova, I. *et al.* Vaccination with early ferroptotic cancer cells induces efficient antitumor immunity. *J Immunother Cancer* **8**, e001369 (2020).
336. Wiernicki, B. *et al.* Cancer cells dying from ferroptosis impede dendritic cell-mediated anti-tumor immunity. *Nat Commun* **13**, 3676 (2022).
337. Wang, W. *et al.* CD8+ T cells regulate tumour ferroptosis during cancer immunotherapy. *Nature* **569**, 270–274 (2019).
338. Liao, P. *et al.* CD8+ T cells and fatty acids orchestrate tumor ferroptosis and immunity via ACSL4. *Cancer Cell* **40**, 365-378.e6 (2022).
339. Kapralov, A. A. *et al.* Redox lipid reprogramming commands susceptibility of macrophages and microglia to ferroptotic death. *Nat Chem Biol* **16**, 278–290 (2020).
340. Canli, Ö. *et al.* Myeloid Cell-Derived Reactive Oxygen Species Induce Epithelial Mutagenesis. *Cancer Cell* **32**, 869-883.e5 (2017).
341. Kim, R. *et al.* Ferroptosis of tumour neutrophils causes immune suppression in cancer. *Nature* **612**, 338–346 (2022).
342. Veglia, F. *et al.* Lipid bodies containing oxidatively truncated lipids block antigen cross-presentation by dendritic cells in cancer. *Nat Commun* **8**, 2122 (2017).
343. Cao, W. *et al.* Oxidized Lipids Block Antigen Cross-Presentation by Dendritic Cells in Cancer. *The Journal of Immunology* **192**, 2920–2931 (2014).
344. Ma, X. *et al.* CD36-mediated ferroptosis dampens intratumoral CD8+ T cell effector function and impairs their antitumor ability. *Cell Metabolism* **33**, 1001-1012.e5 (2021).
345. Xu, S. *et al.* Uptake of oxidized lipids by the scavenger receptor CD36 promotes lipid peroxidation and dysfunction in CD8+ T cells in tumors. *Immunity* **54**, 1561-1577.e7 (2021).
346. Xu, C. *et al.* The glutathione peroxidase Gpx4 prevents lipid peroxidation and ferroptosis to sustain Treg cell activation and suppression of antitumor immunity. *Cell Reports* **35**, 109235 (2021).
347. Cowled, P. & Fitridge, R. Pathophysiology of Reperfusion Injury. in *Mechanisms of Vascular Disease: A Reference Book for Vascular Specialists* (eds. Fitridge, R. & Thompson, M.) (University of Adelaide Press, Adelaide (AU), 2011).
348. Linkermann, A. *et al.* Synchronized renal tubular cell death involves ferroptosis. *Proc. Natl. Acad. Sci. U.S.A.* **111**, 16836–16841 (2014).
349. Li, Q. *et al.* Inhibition of neuronal ferroptosis protects hemorrhagic brain. *JCI Insight* **2**, (2017).
350. Li, W. *et al.* Ferroptotic cell death and TLR4/Trif signaling initiate neutrophil recruitment after heart transplantation. *Journal of Clinical Investigation* **129**, 2293–2304 (2019).
351. Tsurusaki, S. *et al.* Hepatic ferroptosis plays an important role as the trigger for initiating inflammation in nonalcoholic steatohepatitis. *Cell Death Dis* **10**, 449 (2019).
352. Qi, J., Kim, J.-W., Zhou, Z., Lim, C.-W. & Kim, B. Ferroptosis Affects the Progression of Nonalcoholic Steatohepatitis via the Modulation of Lipid Peroxidation–Mediated Cell Death in Mice. *The American Journal of Pathology* **190**, 68–81 (2020).

353. Mayr, L. *et al.* Dietary lipids fuel GPX4-restricted enteritis resembling Crohn's disease. *Nat Commun* **11**, 1775 (2020).
354. Liu, P. *et al.* Ferrostatin-1 alleviates lipopolysaccharide-induced acute lung injury via inhibiting ferroptosis. *Cell Mol Biol Lett* **25**, 10 (2020).
355. Yoshida, M. *et al.* Involvement of cigarette smoke-induced epithelial cell ferroptosis in COPD pathogenesis. *Nat Commun* **10**, 3145 (2019).
356. Li, X. *et al.* Ferroptosis inhibitor alleviates Radiation-induced lung fibrosis (RILF) via down-regulation of TGF- β 1. *J Inflamm* **16**, 11 (2019).
357. Yang, W. S. & Stockwell, B. R. Ferroptosis: Death by Lipid Peroxidation. *Trends in Cell Biology* **26**, 165–176 (2016).
358. Pasparakis, M. & Vandenabeele, P. Necroptosis and its role in inflammation. *Nature* **517**, 311–320 (2015).
359. Tanzer, M. C. *et al.* Quantitative and Dynamic Catalogs of Proteins Released during Apoptotic and Necroptotic Cell Death. *Cell Reports* **30**, 1260-1270.e5 (2020).
360. Phulphagar, K. *et al.* Proteomics reveals distinct mechanisms regulating the release of cytokines and alarmins during pyroptosis. *Cell Reports* **34**, 108826 (2021).
361. Seiler, A. *et al.* Glutathione Peroxidase 4 Senses and Translates Oxidative Stress into 12/15-Lipoxygenase Dependent- and AIF-Mediated Cell Death. *Cell Metabolism* **8**, 237–248 (2008).
362. Bebbler, C. M. *et al.* Ferroptosis response segregates small cell lung cancer (SCLC) neuroendocrine subtypes. *Nat Commun* **12**, 2048 (2021).
363. Eichelbaum, K. & Krijgsveld, J. Combining Pulsed SILAC Labeling and Click-Chemistry for Quantitative Secretome Analysis. in *Exocytosis and Endocytosis* (ed. Ivanov, A. I.) vol. 1174 101–114 (Springer New York, New York, NY, 2014).
364. Ong, S.-E. & Mann, M. A practical recipe for stable isotope labeling by amino acids in cell culture (SILAC). *Nat Protoc* **1**, 2650–2660 (2006).
365. Calandra, T. & Roger, T. Macrophage migration inhibitory factor: a regulator of innate immunity. *Nat Rev Immunol* **3**, 791–800 (2003).
366. Castro, B. A. *et al.* Macrophage migration inhibitory factor downregulation: a novel mechanism of resistance to anti-angiogenic therapy. *Oncogene* **36**, 3749–3759 (2017).
367. Stoppe, C. *et al.* The protective role of macrophage migration inhibitory factor in acute kidney injury after cardiac surgery. *Sci. Transl. Med.* **10**, eaan4886 (2018).
368. Wang, Y., Armando, A. M., Quehenberger, O., Yan, C. & Dennis, E. A. Comprehensive ultra-performance liquid chromatographic separation and mass spectrometric analysis of eicosanoid metabolites in human samples. *Journal of Chromatography A* **1359**, 60–69 (2014).
369. Yamaguchi, A., Botta, E. & Holinstat, M. Eicosanoids in inflammation in the blood and the vessel. *Front. Pharmacol.* **13**, 997403 (2022).
370. Eliopoulos, A. G. Induction of COX-2 by LPS in macrophages is regulated by Tpl2-dependent CREB activation signals. *The EMBO Journal* **21**, 4831–4840 (2002).
371. Mills, E. L. *et al.* Itaconate is an anti-inflammatory metabolite that activates Nrf2 via alkylation of KEAP1. *Nature* **556**, 113–117 (2018).

372. Tannahill, G. M. *et al.* Succinate is an inflammatory signal that induces IL-1 β through HIF-1 α . *Nature* **496**, 238–242 (2013).
373. Medina, C. B. *et al.* Metabolites released from apoptotic cells act as tissue messengers. *Nature* **580**, 130–135 (2020).
374. Pang, Z. *et al.* MetaboAnalyst 6.0: towards a unified platform for metabolomics data processing, analysis and interpretation. *Nucleic Acids Research* gkae253 (2024) doi:10.1093/nar/gkae253.
375. Toda, G., Yamauchi, T., Kadowaki, T. & Ueki, K. Preparation and culture of bone marrow-derived macrophages from mice for functional analysis. *STAR Protocols* **2**, 100246 (2021).
376. Jiao, H. *et al.* Z-nucleic-acid sensing triggers ZBP1-dependent necroptosis and inflammation. *Nature* **580**, 391–395 (2020).
377. Zhang, B. *et al.* Single-cell RNA sequencing reveals induction of distinct trained-immunity programs in human monocytes. *Journal of Clinical Investigation* **132**, e147719 (2022).
378. Yoo, S.-E. *et al.* Gpx4 ablation in adult mice results in a lethal phenotype accompanied by neuronal loss in brain. *Free Radical Biology and Medicine* **52**, 1820–1827 (2012).
379. Proneth, B. & Conrad, M. Ferroptosis and necroinflammation, a yet poorly explored link. *Cell Death Differ* **26**, 14–24 (2019).
380. Seifert, L. *et al.* The necrosome promotes pancreatic oncogenesis via CXCL1 and Mincle-induced immune suppression. *Nature* **532**, 245–249 (2016).
381. MacKenzie, K. F. *et al.* PGE₂ Induces Macrophage IL-10 Production and a Regulatory-like Phenotype via a Protein Kinase A–SIK–CR3 Pathway. *The Journal of Immunology* **190**, 565–577 (2013).
382. Mehrotra, P. *et al.* Oxylipins and metabolites from pyroptotic cells act as promoters of tissue repair. *Nature* 1–9 (2024) doi:10.1038/s41586-024-07585-9.
383. Hemler, M. E., Cook, H. W. & Lands, W. E. M. Prostaglandin biosynthesis can be triggered by lipid peroxides. *Archives of Biochemistry and Biophysics* **193**, 340–345 (1979).
384. Kulmacz, R. J. & Lands, W. E. M. Requirements for hydroperoxide by the cyclooxygenase and peroxidase activities of prostaglandin H synthase. *Prostaglandins* **25**, 531–540 (1983).
385. Riganti, C., Gazzano, E., Polimeni, M., Aldieri, E. & Ghigo, D. The pentose phosphate pathway: An antioxidant defense and a crossroad in tumor cell fate. *Free Radical Biology and Medicine* **53**, 421–436 (2012).
386. Kuehne, A. *et al.* Acute Activation of Oxidative Pentose Phosphate Pathway as First-Line Response to Oxidative Stress in Human Skin Cells. *Molecular Cell* **59**, 359–371 (2015).
387. Schwartzman, J. M., Thompson, C. B. & Finley, L. W. S. Metabolic regulation of chromatin modifications and gene expression. *Journal of Cell Biology* **217**, 2247–2259 (2018).
388. Roy, D. G. *et al.* Methionine Metabolism Shapes T Helper Cell Responses through Regulation of Epigenetic Reprogramming. *Cell Metabolism* **31**, 250-266.e9 (2020).

389. Yu, W. *et al.* One-Carbon Metabolism Supports S-Adenosylmethionine and Histone Methylation to Drive Inflammatory Macrophages. *Mol Cell* **75**, 1147–1160.e5 (2019).
390. Sánchez-Fernández, E. M. *et al.* Investigations on the oxygen dependence of a 2-oxoglutarate histone demethylase. *Biochemical Journal* **449**, 491–496 (2012).
391. Shiraki, N. *et al.* Methionine Metabolism Regulates Maintenance and Differentiation of Human Pluripotent Stem Cells. *Cell Metabolism* **19**, 780–794 (2014).
392. Ó Maoldomhnaigh, C. *et al.* Lactate Alters Metabolism in Human Macrophages and Improves Their Ability to Kill Mycobacterium tuberculosis. *Front. Immunol.* **12**, (2021).
393. Martínez-Reyes, C. P. *et al.* Uric Acid Has Direct Proinflammatory Effects on Human Macrophages by Increasing Proinflammatory Mediators and Bacterial Phagocytosis Probably via URAT1. *Biomolecules* **10**, 576 (2020).
394. Arts, R. J. W. *et al.* Glutaminolysis and Fumarate Accumulation Integrate Immunometabolic and Epigenetic Programs in Trained Immunity. *Cell Metabolism* **24**, 807–819 (2016).
395. Van Der Heijden, C. D. C. C. *et al.* Aldosterone induces trained immunity: the role of fatty acid synthesis. *Cardiovascular Research* cvz137 (2019) doi:10.1093/cvr/cvz137.
396. Yang, C. Y. *et al.* The transcriptional regulators Id2 and Id3 control the formation of distinct memory CD8⁺ T cell subsets. *Nat Immunol* **12**, 1221–1229 (2011).
397. Müller, I. *et al.* Gremlin-1 Is an Inhibitor of Macrophage Migration Inhibitory Factor and Attenuates Atherosclerotic Plaque Growth in ApoE^{-/-} Mice*. *Journal of Biological Chemistry* **288**, 31635–31645 (2013).
398. Müller, I. I. *et al.* Gremlin-1 inhibits macrophage migration inhibitory factor-dependent monocyte function and survival. *International Journal of Cardiology* **176**, 923–929 (2014).
399. Davis, J. M. *et al.* Pancreatic stromal Gremlin 1 expression during pancreatic tumorigenesis. *Genes & Diseases* **9**, 108–115 (2022).
400. Dorward, D. A. *et al.* The Role of Formylated Peptides and Formyl Peptide Receptor 1 in Governing Neutrophil Function during Acute Inflammation. *The American Journal of Pathology* **185**, 1172–1184 (2015).
401. Mandal, P., Novotny, M. & Hamilton, T. A. Lipopolysaccharide Induces Formyl Peptide Receptor 1 Gene Expression in Macrophages and Neutrophils via Transcriptional and Posttranscriptional Mechanisms¹. *The Journal of Immunology* **175**, 6085–6091 (2005).
402. Carp, H. Mitochondrial N-formylmethionyl proteins as chemoattractants for neutrophils. *Journal of Experimental Medicine* **155**, 264–275 (1982).
403. Rabiet, M.-J., Huet, E. & Boulay, F. Human mitochondria-derived N-formylated peptides are novel agonists equally active on FPR and FPRL1, while Listeria monocytogenes-derived peptides preferentially activate FPR. *European Journal of Immunology* **35**, 2486–2495 (2005).
404. Crouser, E. D. *et al.* Monocyte activation by necrotic cells is promoted by mitochondrial proteins and formyl peptide receptors. *Critical Care Medicine* **37**, 2000 (2009).

405. Mukhopadhyay, S. *et al.* SR-A/MARCO-mediated ligand delivery enhances intracellular TLR and NLR function, but ligand scavenging from cell surface limits TLR4 response to pathogens. *Blood* **117**, 1319–1328 (2011).
406. Elomaa, O. *et al.* Cloning of a novel bacteria-binding receptor structurally related to scavenger receptors and expressed in a subset of macrophages. *Cell* **80**, 603–609 (1995).
407. Doi, T. *et al.* Charged collagen structure mediates the recognition of negatively charged macromolecules by macrophage scavenger receptors. *Journal of Biological Chemistry* **268**, 2126–2133 (1993).
408. Wermeling, F. *et al.* Class A scavenger receptors regulate tolerance against apoptotic cells, and autoantibodies against these receptors are predictive of systemic lupus. *Journal of Experimental Medicine* **204**, 2259–2265 (2007).
409. La Fleur, L. *et al.* Targeting MARCO and IL37R on Immunosuppressive Macrophages in Lung Cancer Blocks Regulatory T Cells and Supports Cytotoxic Lymphocyte Function. *Cancer Research* **81**, 956–967 (2021).
410. Georgoudaki, A.-M. *et al.* Reprogramming Tumor-Associated Macrophages by Antibody Targeting Inhibits Cancer Progression and Metastasis. *Cell Reports* **15**, 2000–2011 (2016).
411. Li, D. *et al.* Tumor-Produced Versican V1 Enhances hCAP18/LL-37 Expression in Macrophages through Activation of TLR2 and Vitamin D3 Signaling to Promote Ovarian Cancer Progression In Vitro. *PLOS ONE* **8**, e56616 (2013).
412. Kim, S. *et al.* Carcinoma-produced factors activate myeloid cells through TLR2 to stimulate metastasis. *Nature* **457**, 102–106 (2009).
413. Gao, D. *et al.* Myeloid Progenitor Cells in the Premetastatic Lung Promote Metastases by Inducing Mesenchymal to Epithelial Transition. *Cancer Research* **72**, 1384–1394 (2012).
414. Mills, C. D., Shearer, J., Evans, R. & Caldwell, M. D. Macrophage arginine metabolism and the inhibition or stimulation of cancer. *J Immunol* **149**, 2709–2714 (1992).
415. Nucera, S., Biziato, D. & De Palma, M. The interplay between macrophages and angiogenesis in development, tissue injury and regeneration. *The International Journal of Developmental Biology* **55**, 495–503 (2011).
416. Galluzzi, L. *et al.* Consensus guidelines for the definition, detection and interpretation of immunogenic cell death. *J Immunother Cancer* **8**, e000337 (2020).
417. Luoqian, J. *et al.* Ferroptosis promotes T-cell activation-induced neurodegeneration in multiple sclerosis. *Cell Mol Immunol* **19**, 913–924 (2022).
418. Hang, Z. *et al.* Ferroptosis was involved in the oleic acid-induced acute lung injury in mice. (2019).
419. Dong, H. *et al.* Nrf2 inhibits ferroptosis and protects against acute lung injury due to intestinal ischemia reperfusion via regulating SLC7A11 and HO-1. *Aging* **12**, 12943–12959 (2020).

420. Li, Y. *et al.* Inhibitor of apoptosis-stimulating protein of p53 inhibits ferroptosis and alleviates intestinal ischemia/reperfusion-induced acute lung injury. *Cell Death Differ* **27**, 2635–2650 (2020).
421. Li, J. *et al.* Panaxydol attenuates ferroptosis against LPS-induced acute lung injury in mice by Keap1-Nrf2/HO-1 pathway. *J Transl Med* **19**, 96 (2021).
422. Li, X., Zhuang, X. & Qiao, T. Role of ferroptosis in the process of acute radiation-induced lung injury in mice. *Biochemical and Biophysical Research Communications* **519**, 240–245 (2019).
423. Lian, N. *et al.* The Role of Ferroptosis in Bronchoalveolar Epithelial Cell Injury Induced by Cigarette Smoke Extract. *Front. Physiol.* **12**, (2021).
424. Zhao, J. *et al.* 15-Lipoxygenase 1 interacts with phosphatidylethanolamine-binding protein to regulate MAPK signaling in human airway epithelial cells. *Proc. Natl. Acad. Sci. U.S.A.* **108**, 14246–14251 (2011).
425. Tang, W. *et al.* Environmental allergens house dust mite-induced asthma is associated with ferroptosis in the lungs. *Exp Ther Med* **22**, 1483 (2021).
426. Wu, Y. *et al.* Induction of ferroptosis-like cell death of eosinophils exerts synergistic effects with glucocorticoids in allergic airway inflammation. *Thorax* **75**, 918–927 (2020).
427. Dar, H. H. *et al.* *Pseudomonas aeruginosa* utilizes host polyunsaturated phosphatidylethanolamines to trigger theft-ferroptosis in bronchial epithelium. *J Clin Invest* **128**, 4639–4653 (2019).
428. Amaral, E. P. *et al.* A major role for ferroptosis in Mycobacterium tuberculosis-induced cell death and tissue necrosis. *Journal of Experimental Medicine* **216**, 556–570 (2019).
429. Qiu, B. *et al.* Fatal COVID-19 pulmonary disease involves ferroptosis. *Nat Commun* **15**, 3816 (2024).
430. Hu, K. *et al.* Suppression of the SLC7A11/glutathione axis causes synthetic lethality in KRAS-mutant lung adenocarcinoma. *J Clin Invest* **130**, 1752–1766 (2020).
431. Ji, X. *et al.* xCT (SLC7A11)-mediated metabolic reprogramming promotes non-small cell lung cancer progression. *Oncogene* **37**, 5007–5019 (2018).
432. Wang, Z. *et al.* CREB stimulates GPX4 transcription to inhibit ferroptosis in lung adenocarcinoma. *Oncology Reports* **45**, 1–12 (2021).
433. Huang, C. *et al.* Upregulation and activation of p53 by erastin-induced reactive oxygen species contribute to cytotoxic and cytostatic effects in A549 lung cancer cells. *Oncology Reports* **40**, 2363–2370 (2018).
434. Xu, W. *et al.* Role of Ferroptosis in Lung Diseases. *JIR Volume* **14**, 2079–2090 (2021).
435. Guilliams, M. *et al.* Alveolar macrophages develop from fetal monocytes that differentiate into long-lived cells in the first week of life via GM-CSF. *Journal of Experimental Medicine* **210**, 1977–1992 (2013).
436. Mitsi, E. *et al.* Human alveolar macrophages predominately express combined classical M1 and M2 surface markers in steady state. *Respiratory Research* **19**, 66 (2018).
437. Fuentes-Mateos, R., Santos, E. & Fernández-Medarde, A. Optimized Protocol for Isolation and Culture of Murine Neonatal Primary Lung Fibroblasts. *Methods and Protocols* **6**, 14 (2023).

438. Kupka, S. *et al.* SPATA2-Mediated Binding of CYLD to HOIP Enables CYLD Recruitment to Signaling Complexes. *Cell Rep* **16**, 2271–2280 (2016).
439. Nardo, D. D. *et al.* Interleukin-1 receptor–associated kinase 4 (IRAK4) plays a dual role in myddosome formation and Toll-like receptor signaling. *Journal of Biological Chemistry* **293**, 15195–15207 (2018).
440. Tyanova, S., Temu, T. & Cox, J. The MaxQuant computational platform for mass spectrometry-based shotgun proteomics. *Nat Protoc* **11**, 2301–2319 (2016).
441. Tyanova, S. *et al.* The Perseus computational platform for comprehensive analysis of (prote)omics data. *Nat Methods* **13**, 731–740 (2016).
442. Wei, R. *et al.* Missing Value Imputation Approach for Mass Spectrometry-based Metabolomics Data. *Sci Rep* **8**, 663 (2018).
443. Hotelling, H. The Generalization of Student’s Ratio. *The Annals of Mathematical Statistics* **2**, 360–378 (1931).
444. EnhancedVolcano. *Bioconductor* <http://bioconductor.org/packages/EnhancedVolcano/>.
445. Ewels, P. A. *et al.* The nf-core framework for community-curated bioinformatics pipelines. *Nat Biotechnol* **38**, 276–278 (2020).
446. Dobin, A. *et al.* STAR: ultrafast universal RNA-seq aligner. *Bioinformatics* **29**, 15–21 (2013).
447. Patro, R., Duggal, G., Love, M. I., Irizarry, R. A. & Kingsford, C. Salmon provides fast and bias-aware quantification of transcript expression. *Nat Methods* **14**, 417–419 (2017).
448. Love, M. I., Huber, W. & Anders, S. Moderated estimation of fold change and dispersion for RNA-seq data with DESeq2. *Genome Biology* **15**, 550 (2014).
449. Strimmer, K. fdrtool: a versatile R package for estimating local and tail area-based false discovery rates. *Bioinformatics* **24**, 1461–1462 (2008).
450. Kolberg, L., Raudvere, U., Kuzmin, I., Vilo, J. & Peterson, H. gprofiler2 -- an R package for gene list functional enrichment analysis and namespace conversion toolset g:Profiler. Preprint at <https://doi.org/10.12688/f1000research.24956.2> (2020).
451. Ritchie, M. E. *et al.* limma powers differential expression analyses for RNA-sequencing and microarray studies. *Nucleic Acids Research* **43**, e47 (2015).

6. Publications

Teilpublikation:

- **Yapici FI**, Seidel E, Dahlhaus A, Weber J, Schmidt C, Chaves Filho AB, Yang M, Nenchova M, GÜngör E, Kotouza I, Beck J, Stroh J, Abdallah AT, Lackmann JW, Bebbler CM, Androulidaki A, Kreuzalar P, Schulze A, Frezza C & von Karstedt S.
An Atlas of Ferroptosis-induced Secretomes (*submitted*)
- **Yapici FI**, Bebbler CM & von Karstedt S. (2024) 'A guide to ferroptosis in cancer', *Molecular Oncology*, 18(6), pp. 1378–1396. doi:10.1002/1878-0261.13649.
- Müller F, Lim JKM, Bebbler CM, Seidel E, Tishina S, Dahlhaus A, Stroh J, Beck J, **Yapici FI**, Nakayama K, Torres Fernández L, Brägelmann J, Leprivier G & von Karstedt S. 'Elevated FSP1 protects KRAS-mutated cells from ferroptosis during tumor initiation', *Cell Death & Differentiation*, 30(2), pp. 442–456. doi:10.1038/s41418-022-01096-8.

7. Acknowledgments

First of all, I would like to thank my supervisor Prof. Dr. Silvia von Karstedt who gave me the opportunity to do my PhD in her lab and for trusting me with this amazing project. She has given me an excellent guidance and motivational support, and taught me how to be a better scientist. Thank you for your big support over the years, for the excellent guidance, the motivational support and the constant encouragement.

I want to thank Prof. Dr. Günther Schwarz and Prof. Dr. Hamid Kashkar for your invaluable support and scientific guidance during my PhD thesis as my Thesis Advisory Committee. Moreover, I would like to thank Prof. Dr. Kay Hofmann who kindly agreed to take part in my dissertation defence committee.

Mostly, I would like to thank the whole von Karstedt lab who supported me over all these years. Especially, I want to thank Alina Dahlhaus, Christina Bebbler, Ariadne Androulidaki, Eric Seidel, Sofya Tishina and Fanyu Liu for fruitful discussions and a great fun atmosphere. But mostly to Alina Dahlhaus who helped me with the experiments in and out of the lab especially in times when I felt overwhelmed and stressed. Also, special thanks to old von Karstedt lab members Laura Prieto Clemente and Fabienne Müller for their friendship and support. In addition, I would like to thank my students Maria Nenchova, Emre Güngör, Julia Beck and Ioanna Kotouza for their contribution to this project.

Son olarak da aileme ve arkadaşlarıma teşekkür etmek istiyorum. Üniversite sonrası yüksek lisans ve doktora maceramı desteklediğiniz için bu noktaya gelebildim. Bu zorlu ve uzun süreçte beni desteklediğiniz, dinlediğiniz, tavsiyelerde bulunduğunuz ve benimle ilgilendiğiniz için hepinize çok teşekkür ederim sizi çok seviyorum.

8. Erklärung zur Dissertation

gemäß der Promotionsordnung vom 12 März 2020

Hiermit versichere ich an Eides statt, dass ich die vorliegende Dissertation selbstständig und ohne die Benutzung anderer als der angegebenen Hilfsmittel und Literatur angefertigt habe. Alle Stellen, die wörtlich oder sinngemäß aus veröffentlichten und nicht veröffentlichten Werken dem Wortlaut oder dem Sinn nach entnommen wurden, sind als solche kenntlich gemacht. Ich versichere an Eides statt, dass diese Dissertation noch keiner anderen Fakultät oder Universität zur Prüfung vorgelegen hat; dass sie - abgesehen von unten angegebenen Teilpublikationen und eingebundenen Artikeln und Manuskripten - noch nicht veröffentlicht worden ist sowie, dass ich eine Veröffentlichung der Dissertation vor Abschluss der Promotion nicht ohne Genehmigung des Promotionsausschusses vornehmen werde. Die Bestimmungen dieser Ordnung sind mir bekannt. Darüber hinaus erkläre ich hiermit, dass ich die Ordnung zur Sicherung guter wissenschaftlicher Praxis und zum Umgang mit wissenschaftlichem Fehlverhalten der Universität zu Köln gelesen und sie bei der Durchführung der Dissertation zugrundeliegenden Arbeiten und der schriftlich verfassten Dissertation beachtet habe und verpflichte mich hiermit, die dort genannten Vorgaben bei allen wissenschaftlichen Tätigkeiten zu beachten und umzusetzen. Ich versichere, dass die eingereichte elektronische Fassung der eingereichten Druckfassung vollständig entspricht.

Teilpublikationen:

Yapici FI, Seidel E, Dahlhaus A, Weber J, Schmidt C, Chaves Filho AB, Yang M, Nenchova M, Güngör E, Kotouza I, Beck J, Stroh J, Abdallah AT, Lackmann JW, Bebbler CM, Androulidaki A, Kreuzalar P, Schulze A, Frezza C & von Karstedt S.

An Atlas of Ferroptosis-induced Secretomes (*submitted*)

Datum, Name und Unterschrift

01.07.2024, Fatma Isil Yapici

